Deutsche Geophysikalische Gesellschaft e.V.

Inhalt

MITTEILUNGEN

DGG-Kolloquium

Geohazards – Landslides

Karlsruhe,
12. März 2014

Sonderband I/2014
ISSN 0947-1944

Herausgeber:
Deutsche Geophysikalische Gesellschaft e.V.

IMPRESSUM

Herausgeber: Deutsche Geophysikalische Gesellschaft e.V.
Telegrafenberg, 14473 Potsdam

Redaktion: Arbeitskreis „Angewandte Geophysik“

Dr. T. Fechner, Neuwied
Dr. T. Litwinska-Kemperink, Oldenzaal
Prof. Dr. M. Joswig, Stuttgart
Dr. D. Orlowsky, Essen
Dr. A. Schuck, Leipzig (Sprecher)
Prof. Dr. U. Yaramanci, Hannover

Kontakt:

Dr. A. Schuck
GGL Geophysik und Geotechnik Leipzig GmbH
Bautzner Str. 67, 04347 Leipzig
Tel. 0341/2421-310, andreas.schuck@ggl-gmbh.de

DGG-Kolloquium

Geohazards - Landslides

74. Jahrestagung der Deutschen Geophysikalischen Gesellschaft e.V.

Karlsruhe, 12. März 2014

Large Landslides in Computational Geomechanics – Model Validation and Mitigation

Tom Schanz[(a)], Lisa Borgatti[(b)] and Long Nguyen Tuan[(a)]

[(a)] Chair for Foundation Engineering, Soil and Rock Mechanics, Ruhr-Universität Bochum, Germany
[(b)] Department of Civil, Chemical, Environmental and Materials Engineering DICAM, Alma Mater Studiorum Università di Bologna, Italy
Email: tom.schanz and long.nguyentuan@rub.de, lisa.borgatti@unibo.it

1. Introduction

In northern Italy, landslide hazard is high, mainly due to its geological and tectonic context. Therefore, landslide phenomena have to be analysed in order to propose proper mitigation actions. Modelling and numerical simulation in Geomechanics provides the ability to make predictions and propose mitigation actions based on the information collected on material behaviour, topography, geology etc.. The results allow land sliding phenomena to be described by calibrated geotechnical models and eventually mitigated with properly designed countermeasure works. In this paper, two large landslide examples are analysed: the slope instability processes in San Leo (northern Apennines, Italy) and the large landslide of Corvara (Dolomites, Italy).

Firstly, slope instability processes in San Leo town are analysed. This town was built on a calcarenite and sandstone slab, which is crossed by several joint sets and faults. The calcarenite rock slab, on which the medieval town of San Leo is situated, is intensively tectonised and crossed by a number of joint sets and faults. It is affected by lateral spreading instability processes associated with rock falls and topples (D'Ambra et al., 2004). The clayey substratum is involved in slow movements, like earth flows and slides. In the present work these phenomena are analysed within the framework of unsaturated soil mechanics. A coupled hydro-mechanical model employing viscoplasticity (BBM-VP) is adopted herein to numerically simulate the landslide processes in San Leo. The model allows simulating the hardening and softening processes in the rock material due to hydraulic loading and unloading, and the shear strength change with degree of saturation. The results are then compared with those obtained for the same problem but employing different constitutive model for explaining the viscoplastic behaviour that is independent on suction and based on Drucker-Prager plasticity (DP-VP). The differences of these two material model approaches are analysed in the geotechnical modelling context (Nguyen-Tuan et al., 2014).

Secondly, the large earthflow of Corvara is analysed because of its socio-economic relevance and for the availability of an extensive dataset of field investigation and monitoring data.The landslide area extends from the Col Alto to Pralongià, stretching in altitude from about 1600 m to around 2100 m a.s.l. The landslide can be described as an active slow-moving earthflow affecting flysch rock masses with an estimated volume 50 million cubic metres. It damages a national road and a set of facilities including ski infrastructures, electricity lines and a golf-course. Moreover, in the worst case scenarios, the landslide might affect some buildings located in front of its toe and possibly endanger the downstream settlements by damming the streams running at its flanks.

The Corara landslide has been modelled and numerically simulated. The soft soil creep model, which was developed by Vermeer and Neher (1999) is adopted to account particularly for slow-moving earthflows. Moreover, we present a back analysis to identify parameter for the material model. This method is based on statistical analyses and a particle swarm optimization algorithm for calibrating the constitutive model parameters. Afterwards, different remediation methods have been analysed and assessed. The results in this section are a summary of the series of the studies carried out by Meier and Schanz (2007), Meier et al. (2008), Knabe et al. (2009), and Schanz (2011).

2. Geotechnical modelling of San Leo slope instability processes

2.1. Slope instability phenomena

San Leo is located on the Val Marecchia thrust sheet, where the most ancient Ligurian Units and the younger Epiligurian Units over-thrusted the autochthonous Units of the Umbro-marchean-romagnan domain. The Epiligurian Units (mainly hard rocks) rest unconformably on the Ligurian Units (varicoloured clays, marly and limestones), forming plates or slabs. The town of San Leo was built on one of these slabs, which is crossed by several joint sets and faults. It is affected by lateral spreading with associated rock falls and topples, partly developing along pre-existing discontinuities. Moreover, clay-shale and loose superficial deposits are involved in earthflows.

The high deformability contrast between the slab and the underlying clay-shale drives the instability of the whole area (Casagli, 1994;D'Ambra et al., 2004). Together with the structural setting of the slab, a further predisposing factor is the groundwater flow path developing inside the plate (Fig. 1). The groundwater flow is driven by discontinuity network, which induce a rather high secondary permeability within the calcarenite slab. This leads to the formation of ephemeral springs at the base of the cliffs, near the contact with the almost impermeable substratum. The springs promote the remoulding of the basal clay-shale, leading, together with creep and subsequent flows, to the undermining of the foot of the rock slab. These processes can cause the progressive opening and widening of fractures in the rock masses which, in turn lead to higher discharge rates in the springs.

During the most recent and notable landslide event, occurred in May 2006, a rock fall affected the northern side of the slab, suddenly detaching from the vertical cliff. The undrained loading at the top of the clay-shale slope triggered an earthflow which reached velocities in the order of 4.2 cm/h.

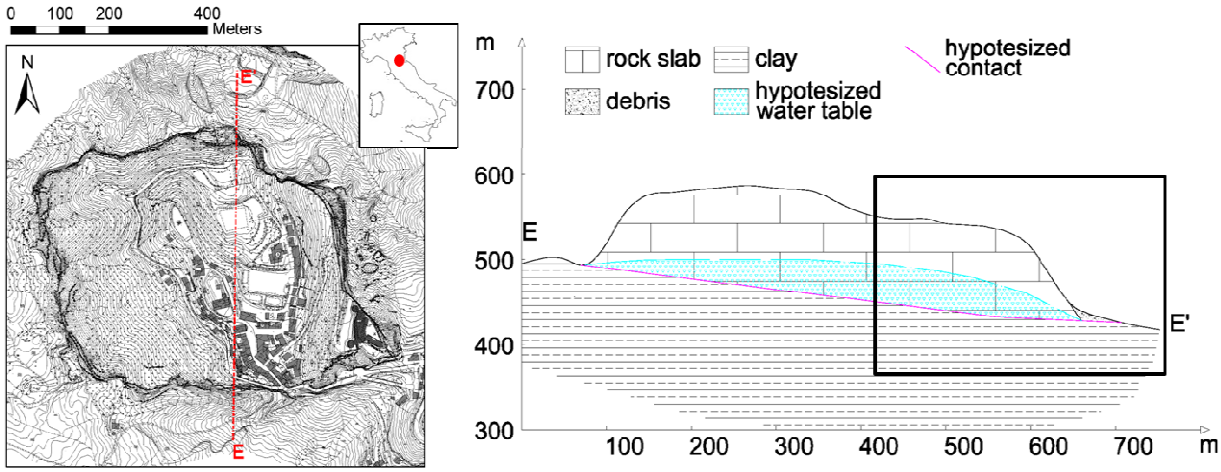

(a) (b)

Fig. 1: (a) South-North EE' section of San Leo slab; (b) location of the studied area (red point) and trace of the EE' section (Nguyen-Tuan et. al., 2014).

2.2. Coupled modelling analysis

2.2.1. Mechanical constitutive model

The models considered here are elasto-viscoplastic models for unsaturated soil based on the Perzyna viscoplasticity (Perzyna, 1966). The formulation for the constitutive modelling is based on the use of pair stress state variables, namely net stress and suction. Suction *(s)* is the difference between gas pressure P_g and liquid pressure P_l. Suction is zero when the soil pore system is filled with only one fluid. Therefore, the stress variables are suction and net stress for unsaturated condition and effective stress in saturated state. The definition of the stress variables in both saturated and unsaturated state is given via Eq. (1):

$$\begin{aligned} s &= \max\left[\left(P_g - P_l\right); 0\right] \\ \boldsymbol{\sigma}' &= \boldsymbol{\sigma}^{total} - \max(P_g; P_l)\mathbf{I} \\ p' &= p^{total} - \max(P_g; P_l) \end{aligned} \tag{1}$$

where $\boldsymbol{\sigma}^{total}$ is the tensor of the total stress, I is identity matrix, p^{total} is the total mean stress, σ' and p' are correspondingly the net stress and the mean net stress in unsaturated case or the effective stress and the effective mean stress in saturated case.

The two viscoplastic models considered here are implemented in the FE program CODE_BRIGHT (Olivella and Gens, 2000, DIT-UPC, 2009). The first one is a linear elastic viscoplastic model for unsaturated soil based on the BBM (Alonso et al., 2005). The second model is a linear elastic viscoplastic model based on the Drücker-Prager failure criterion (Drucker and Prager, 1952). Following the Perzyna visco-plastic concept, the total strain rate is assumed to be a sum of the elastic ($\dot{\boldsymbol{\varepsilon}}^e$) and viscoplastic ($\dot{\boldsymbol{\varepsilon}}^{vp}$) strain rates:

$$\dot{\boldsymbol{\varepsilon}} = \dot{\boldsymbol{\varepsilon}}^e + \dot{\boldsymbol{\varepsilon}}^{vp} \tag{2}$$

The elastic part is related to the net stress $\dot{\boldsymbol{\sigma}}'$ through the generalized Hooke's law:

$$\dot{\boldsymbol{\sigma}}' = \boldsymbol{C}^e \dot{\boldsymbol{\varepsilon}}^e \tag{3}$$

where $\boldsymbol{C}^e$ is the elastic stiffness tensor. As proposed in Perzyna (1966), the visco-plastic strain rate is defined as:

$$\begin{aligned} \dot{\boldsymbol{\varepsilon}}^{vp} &= \Gamma\left\langle\Phi(F)\right\rangle \frac{\partial G}{\partial \boldsymbol{\sigma}'} \\ \Phi(F) &= \begin{cases} (F/F_0)^N, & if \quad F > 0 \\ 0, & if \quad F \le 0 \end{cases} \end{aligned} \tag{4}$$

where Γ is the viscosity parameter, $\Phi(F)$ is a flow function, F is the yield function, F_0 is a normalizing constant in the same units as F. Finally, *G* is the viscoplastic potential.

a) BBM-VP model

In BBM-VP model *F* in Eq. (4) are given according to Eq. (5) (Alonso et al., 2005):

$$F(q, p, s) = a\frac{1}{3}q^2 - M^2\gamma\left(p' + p_s\right)\left(p_o - p'\right) \tag{5}$$

where *M* is the slope of the critical state line and may depend on suction, p_s is the tensile stress limit that follows a linear relationship with suction, p_o is the pre-consolidation pressure depending on suction according to Eq. (6), *q* is the deviatoric stress, γ and a are model parameters. The viscoplastic potential in this case is similar with yield surface equation with a non-associativity parameter. Parameter p_s is a tensile strength, it depends on suction. According to Alonso (1990) the pre-consolidation pressure depends on suction in the following way:

$$p_o = p^c \left(\frac{p_o^*}{p^c} \right)^{\frac{\lambda(0)-\kappa}{\lambda(s)-\kappa}} \tag{6}$$

where p^c is a reference pressure, p_o^* is the pre-consolidation pressure for a saturated state, κ and $\lambda(0)$ are model parameters, $\lambda(s)$ is the stiffness parameter for changes in the net mean stress at a given suction (*s*).

M determines the slope of the critical state line and it depends on suction according to (Alonso et al., 2005):

$$M(s) = M_{dry} - \left(M_{dry} - M_{sat} \right) \left(\frac{M_{sat}}{M_{dry}} \right)^s ; \quad \left(M_{sat} < M_{dry} \right) \tag{7}$$

where M_{dry} and M_{sat} are critical state line slopes at dry state and saturated state correspondingly.

b) DP-VP model

In DP-VP model, *F* and *G* in Eq. (4) are given by Eq. (8):

$$G = F = q - Mp' - c'\beta_c \tag{8}$$

In this case *M* and β_c are calculated by Eq. (9) to provide the best fit to the Mohr-Coulomb hexagon and φ' and c' are the effective angle of friction and the cohesion defining the Mohr-Coulomb failure envelope at saturated condition.

$$M = \frac{6\sin\varphi'}{3-\sin\varphi'} \qquad \beta_c = \frac{6\cos\varphi'}{3-\sin\varphi'} \tag{9}$$

2.2.2. Hydraulic equations

The advective flow of the water phase is described via the generalized Darcy's law:

$$\mathbf{q}_l = -\frac{\mathbf{k} k_{rl}}{\mu_l} \left(\nabla P_l - \rho_l \mathbf{g} \right) \tag{10}$$

where μ_l is the dynamic viscosity of the pore liquid, *g* is the gravity acceleration, ρ_l is the liquid density. The tensor of intrinsic permeability **k** is defined by the Kozeny's model. The relative permeability k_{rl}, is derived from the Mualem-van Genuchten model:

$$k_{rl} = \sqrt{S_e}\left(1-\left(1-S_e^{1/\lambda}\right)^{\lambda}\right)^2 \tag{11}$$

where λ is a shape parameter for retention curve. The effective degree of saturation S_e is calculated as two parameters model of van Genucten model (van Genuchten, 1980)

$$S_e = \frac{S_l - S_{rl}}{S_{ls} - S_{rl}} = \left(1+\left(\frac{P_g - P_l}{P_0}\right)^{\frac{1}{1-\lambda}}\right) \tag{12}$$

where S_{ls} and S_{rl} are the maximum and the residual degree of saturation, P_0 is a model parameter.

2.3. Numerical model of San Leo landslide

The slope instability phenomena in San Leo are simplified and the geometry of the adopted geotechnical model is shown in Fig. 2. The model in Fig. 2 is based on the description of the test site given in section 2. The problem is analysed in two phases. In the first phase, the infiltration is analysed considering water flow through non-deformable porous media – the unsaturated rock and the clay-shale material. In the second phase the coupled hydro-mechanical approach is used to analyse the stress-strain behaviour during the infiltration process. For the second phase, the hydraulic boundary conditions correspond to the water pressure obtained in the first phase. The whole slope is subjected to consolidation in order to simulate closely the initial conditions of the clay-shale formation in the first stage. Afterwards the infiltration step is simulated in the second stage.

In the first phase, the numerical model of San Leo is computed solving only an equation of mass balance of water with hydraulic constitutive equations. This phase aims to simulate the rain water infiltration from the surface of the rock slab. Due to the large difference in the permeability of the rock and the clay-shale formation, the groundwater table develops in the rock slab (Fig. 3). The water is assumed to drain beneath the rock slab and to flow out at the foot of the rock wall as a spring. The numerical simulation shows that the rain falling on the top of the rock slab permeates into the rock slab due to its weight and the capillary force. The ground water table is formed as in Fig. 3.

In the second phase, the numerical model is computed by solving two balance equations simultaneously: an equation of mass balance of water hydraulic constitutive equations and a equation of momentum balance for the medium with stress-strain relations. Two difference constitutive models for the stress-strain relations are used for two computational cases: BBM-VP model and DP-VP model. The same hydraulic constitutive equations and boundary conditions are the used for both cases. The main result obtained is discussed as follows. When analysed by BBM-VP model during water infiltration, the model shows differential displacements between the area beneath the rock slab (point A) and the region on the clay-shale slope close to the rock slab (point B). On the contrary, there is no significant change of vertical displacements during water infiltration when analysed by DP-VP model (Fig. 4). The small displacements observed by computing with DP-VP model are due to the increase of water content that causes an increase of the soil weight and thus increase of a body load. Stress distribution obtained by BBM-VP model demonstrates that the distribution of vertical pressure is influenced by infiltration processes (Fig. 5). The comparison of the vertical stress distribution along the interface between rock slab and clay-shale shows that after infiltration process the vertical stress increases significantly at the location close to point A if compared to the vertical stress before infiltration process. The differential stress distribution along the slab (Fig. 5) induces high shear force which may damage the rock mass when the shear force exceeds its shear strength.

From the above discussion it can be concluded that the instability phenomena in San Leo should be analysed via a coupled problem formulation. It is also demonstrated that the coupled hydro-mechanical viscoplastic model allows better explaining the mechanical behaviour of the clay-shale slope.

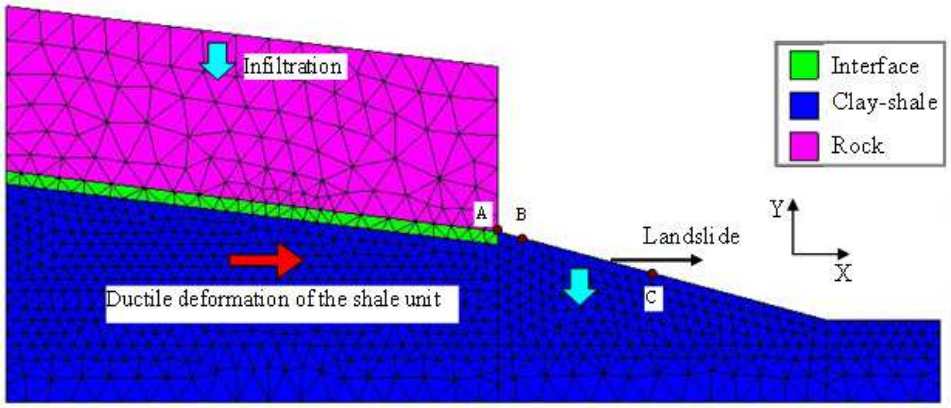

Fig. 2: A conceptual model of instability problems in San Leo (Nguyen-Tuan et. al., 2014).

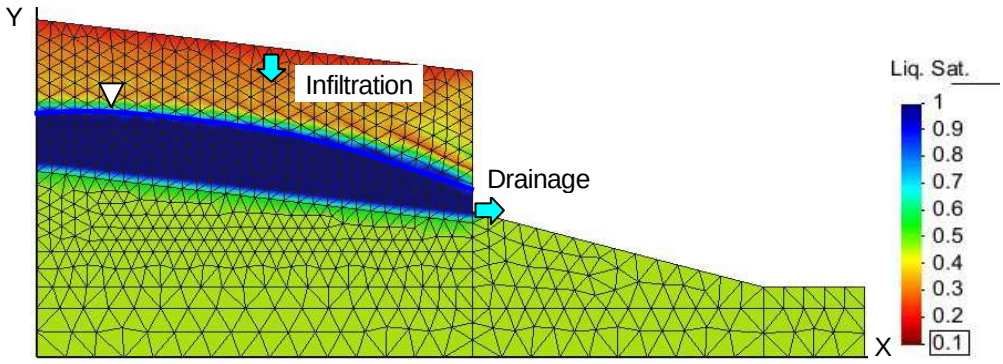

Fig. 3: Phase 1 - Degree of saturation at 4 days after a rainfall

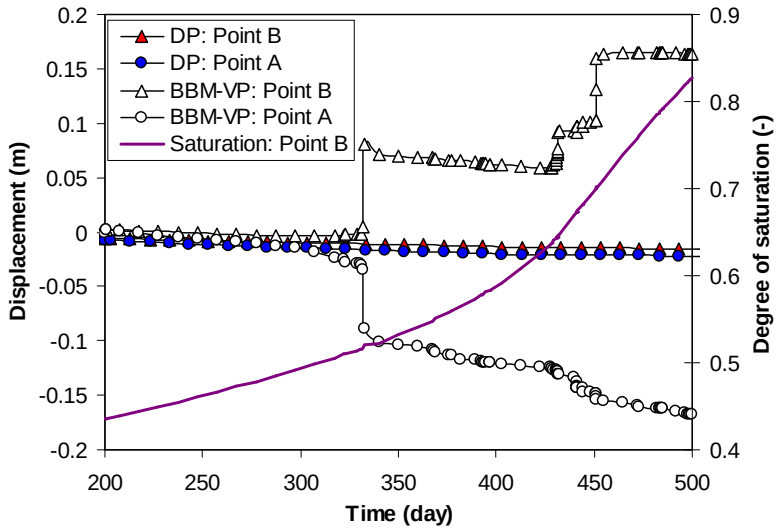

Fig. 4: Displacement and water saturation

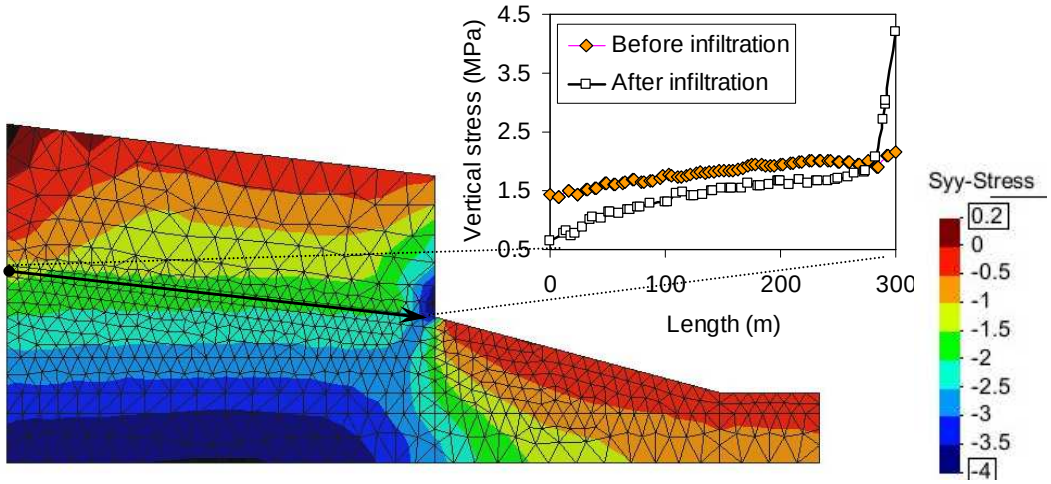

Fig. 5: Phase 2 - Vertical stress at the interface.

3. Corvara landslide (Dolomites, Italy)

3.1. Description of the phenomena

As illustrated in Fig. 6, the Corvara landslide lays upslope the village of Corvara in Badia (Province of Bolzano / South Tyrol). It has been active for thousands of years and has an extent of about 3 km². The volume of the landslide is of about 300 million m³, of which approximately 50 million m³ are currently active (Corsini et al. 2005). It can be describes as an earthflow.

The bedrock consists of alternating layers of marls, tuffite, shales, limestones, dolomites and sandstones. The landslide material consists of cohesive soils (silty clays) incorporating larger blocks and has a thickness of 10 - 50 m.

3.2. Geotechnical modelling and numerical simulation

Given the material involved , the mechanical behavior is expected to be very complex and therefore it is only possible to model some important aspects of this behavior. Like many soils with a high clay and silt content, the studied material is highly compressible and exhibits a significant amount of creep deformations, thus its behavior is strongly time-dependent. The soft soil creep model, which was developed by Vermeer and Neher (1999) is selected to account particularly for these phenomena. The model parameters for the soft soil creep model are summarised in Table 1.

The model adopted here does not take into account of influence of water pressures, which would be also possible but imply a considerable increase in calculation effort. The geometrical and geological profiles are presented in Fig. 7. The forward calculations are carried out applying the finite element method in the code PLAXIS.

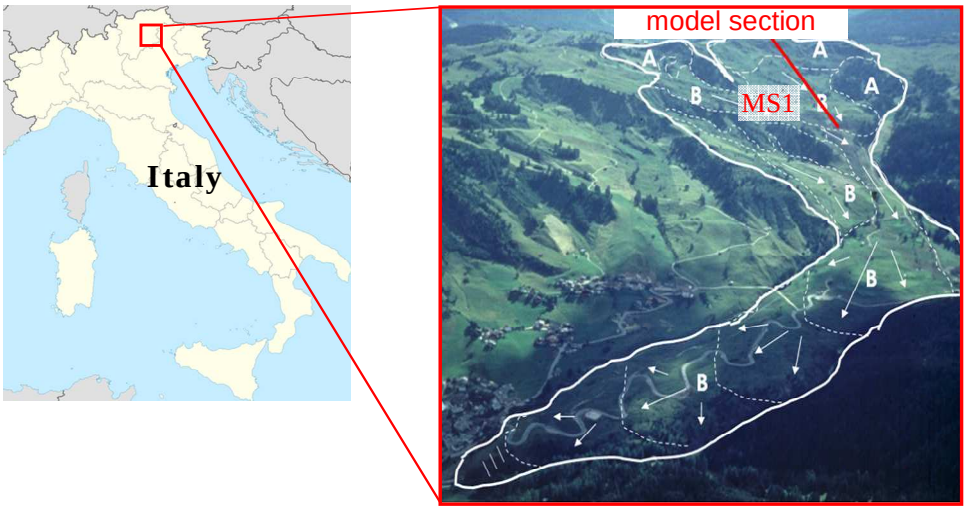

Fig. 6: Geographical location of Corvara in Badia,(Dolomites, Italy) and Corvara earthflow aerial view (after Borgatti et al. 2007)

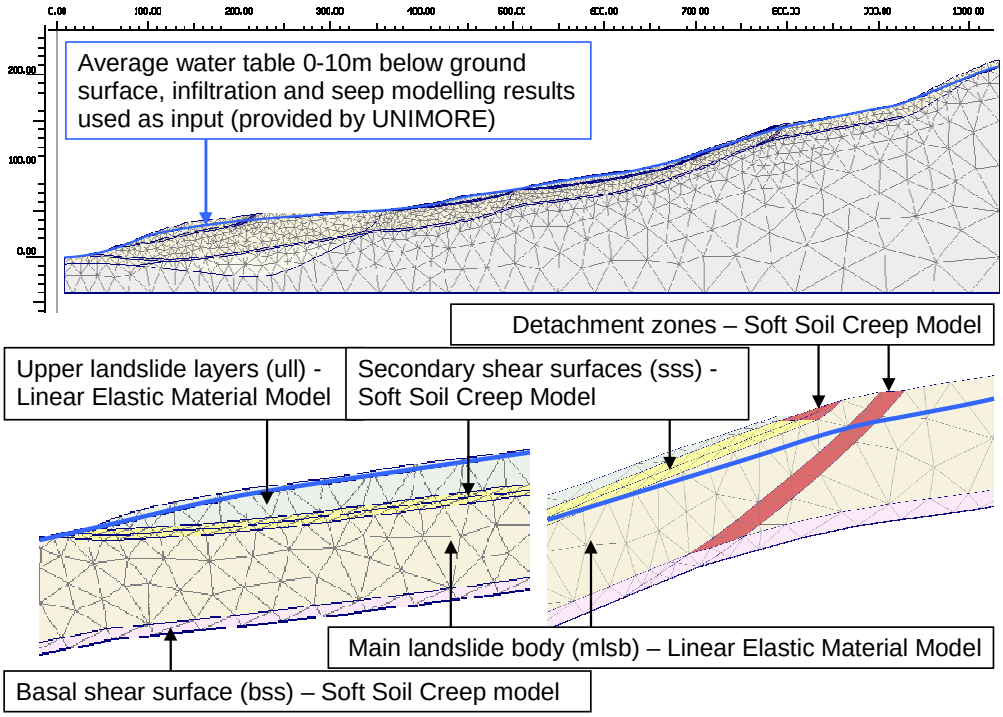

Fig. 7: Numerical model for the model section MS1 (Schanz, 2011)

Table 1: Parameters of the soft soil creep model.

Parameter	Symbol	Unit
Effective cohesion	c	kPa
Effective friction angle	φ	degree (°)
Dilatancy angle	ψ	degree (°)
Modified compression index	λ^*	-
Modified swelling index	κ^*	-
Modified creep index	μ^*	-

3.3. Back analysis

Back analysis is performed following a sequential process. Firstly, initial parameters for the soil model are determined, based on laboratory tests. Three types of tests have been carried out: oedometer tests, isotropic creep tests and deviatoric creep tests (in the triaxial apparatus). For the numerical model, an axisymmetric geometrical configuration was used with the exact dimensions of the test specimen. By fitting the experimental curves and numerical simulation curves, the parameters λ^*, κ^* and μ^* can be determined directly. The fitting algorithm used here is Particle Swarm Optimization (PSO) (Kennedy and Eberhart, 1995).

The parameters from calibrated lab test are used as initial forward calculation of Corvara earthflow. Based on the superficial displacementsmeasured in the field by GPS, the model parameters are calibrated through the optimization method. However, there are a large number of parameters for different soil layers; thus performing calibration for all parameters may lead to high uncertainty. A sensitivity analysis was performed in order to select the most sensitive parameters for the optimization process.

The parameters of constitutive model are used as variables in the optimization process. The parameters vary in order to fit with measured displacement in in-situ measurements by reducing error function (F). The error function is determined as:

$$F = \sqrt{\frac{1}{n}\sum_{i=1}^{n} w_i \left(y_{calc}^{i}(x) - y_{meas}^{i} \right)^2} \tag{13}$$

where y_{meas}^{i} is a measurement value and $y_{calc}^{i}(x)$ is a calculated value, w_i is weighting factor for each measurement point. The optimization method is a routine to minimise the error function (objective function). The PSO is also chosen for minimising error function. The optimization procedure is presented as in Fig. 8. As described in Fig. 8, the preset of parameter vector is derived from laboratory tests. The optimization algorithm attempts to minimize the objective function. When the objective function fulfills the criterion, the parameters obtained at the minimum of the objective function are optimized parameters. By this way, the parameters derived from laboratory tests are calibrated to adapt with reference data.

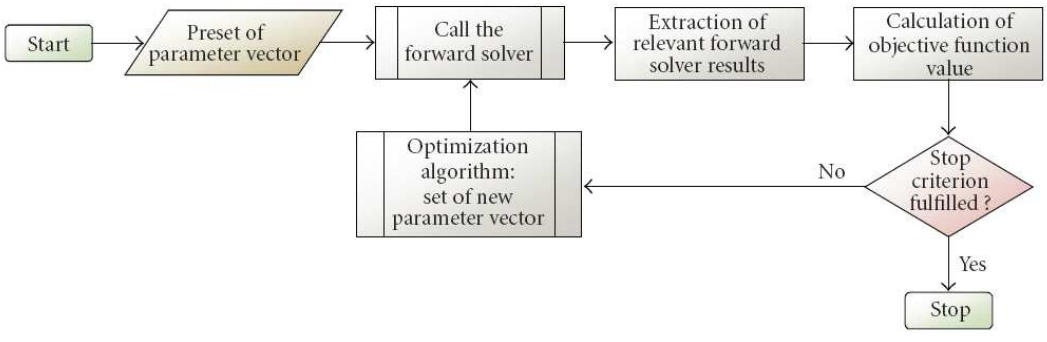

Fig. 8: Flowchart of PSO method (Meier et al., 2008)

3.4. Analysis for mitigation processes

Several remediation methods have been proposed. Retaining walls, such as slotted, stake, jet wall etc. are to be regarded as realistic remedial methods (see Fig. 9). Only pile walls are considered in the calculations. Drainage methods have also been considered, namely horizontal drainage and wells or drainage slots (see Fig. 10). This section introduces the numerical simulation for the different remediation methods i.e., bored pipe walls, anchored pile wall, drainage methods, and combination of these two methods. The numerical simulation is performed based on the set of calibrated parameters as shown in the previous section.

The numerical simulations for remediation methods are analysed in terms of annual creep rate and stability factor. The calculated annual creep rate is illustrated in Fig. 11. The results of creep rates are summed at different time step in a year. The results of different remediation methods are compared with the original state. It can be found that the calculated displacements without remediation remain constant over time, assuming constant boundary conditions. On the contrary, it is observed that the displacements decrease with time when using mediation methods. It is clear that the annual creep rate is minimized when using a combined remediation method.

Fig. 9: The construction of retaining walls with anchors (Schanz, 2011)

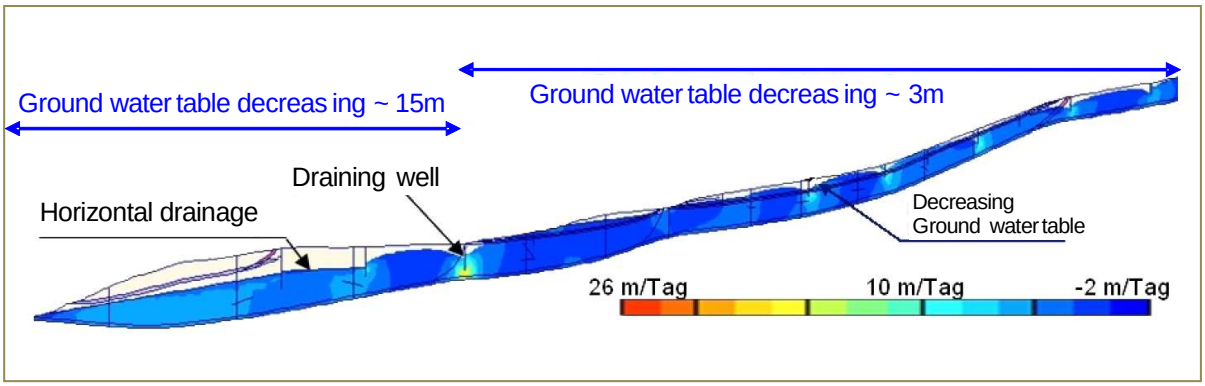

Fig. 10: Drainage methods (Schanz, 2011)

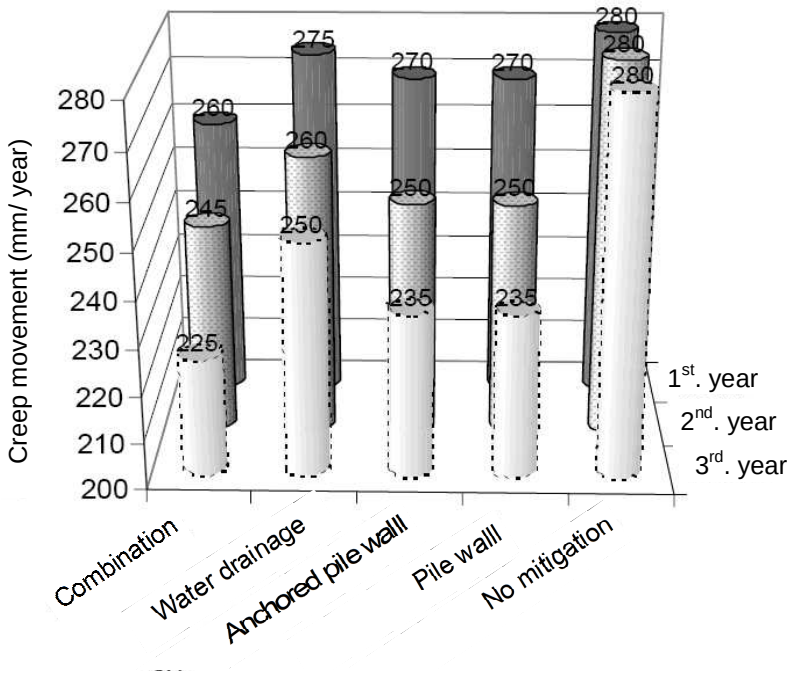

Fig. 11: Annual creep rate (after Knabe et al., 2009)

References

Alonso E. E., Olivella S. and Pinyol N. M. (2005) A review of Beliche Dam, *Géotechnique*, 55(4), pp. 267–285.

Alonso E., Gens A. and Josa A. (1990) A constitutive model for partially saturated soils. *Géotechnique*, 40(3), pp. 405-430.

Borgatti L., Corsini A., Marchetti M., Panizza M., Pellegrini M. and Soldati M. (2007) Relazioni tra Fenomeni franosi e cambiamenti climatici nel corso dell'Olocene. *Conferenza Nazionale*.

Casagli N. (1994) Fenomeni di instabilità in ammassi rocciosi sovrastanti un substrato deformabile: analisi di alcuni esempi nell' Appennino settentrionale. In "*II Convegno Nazionale dei Giovani ricercatori di Geologia Applicata", Viterbo*.

CODE_BRIGHT user's guide (2009), Universitat Politècnica de Catalunya, Barcelona, Spain.

Corsini A., Pasuto A., Soldati M., Zannoni A. (2005). Field monitoring of the Corvara landslide (Dolomites, Italy) and its relevance for hazard assessment. Geomorphology ,Vol. 66, 149-165.

D'Ambra S. and Giglio G. (2004) Lembo-Fazio A. Interventi di sistemazione e stabilizzazione della Rupe di San Leo. In "*10° Congress INTERPRAEVENT 2004", Riva del Garda*.

Drucker D. C. and Prager W. (1952). Soil mechanics and plastic analysis for limit design. *Quarterly of Applied Mathematics*, 10(2), pp. 157–165.

Kennedy J. and and Eberhart R (1995). Particle Swarm Optimization. *Proceedings of IEEE "International Conference on Neural Networks". IV*, 1942-1948

Knabe T., Schädler W., Corsini A., Mair V. and Schanz T. (2009). Geotechnische Bewertung der Hangbewegung Corvara (Dolomiten, Italien). In „*Stabilisierung von Rutschhängen, Böschungen und Einschnitten.*" Beiträge zum 24. Christian Veder Kolloquium, Graz, April 2009.

Kozeny J. (1927) Ueber kapillare Leitung des Wassers im Boden. *Wien, Akad. Wiss.*

Meier J. and Schanz T. (2007). Modellidentifikation für Geomechanische Fragestellungen – Chancen und Grenzen. In „*58. Berg- & Hüttenmännischer Tag*" Freiberg.

Meier J., Schaedler W., Borgatti L., Corsini A. and Schanz T. (2008) Inverse parameter identification technique using PSO algorithm applied to geotechnical modelling. *J. of Artificial Evolution and Applications* , Article ID 574613.

Nguyen-Tuan L., Spreafico M.C., Datcheva M., Borgatti L. and Schanz T. (2014) A Coupled Hydro-Mechanical Analysis OF Slope Instability Processes in San Leo (RN, Italy). In Proceedings of "*The 22nd UK Conference of the ACME*" 2 – 4 April 2014, University of Exeter, Exeter UK, (accepted).

Olivella S. and Gens A. (2000) Vapour Transport in Low Permeability Unsaturated Soils with Capillary Effects. *Transport in Porous Media*, 40, pp. 219–241.

Pasuto A. and Soldati M. (2013) 7.25 Lateral Spreading, In "*Treatise on Geomorphology*", edited by John F. Shroder, Academic Press, San Diego, pp. 239-248.

Perzyna P. (1966) Fundamental problems in viscoplasticity. *Advances in Applied Mechanics*, Academic Press, New York, 9, pp. 244-368.

Schanz T. (2011). Computational Geomechanics Applications to Slope Analysis. In "*Coupling of Flow and Deformation Processes for Modeling the Movement of Natural Slopes.*" December 2011, Bad Herrenalb, Germany.

van Genuchten M. T. (1980) A closed-form equation for predicting the hydraulic conductivity of unsaturated soils. *Soil Sci. Soc. Am. J.*, 44, pp. 892-898.

Vermeer P. A. and Neher H. P. (1999) A soft soil model that accounts for creep. In Proceedings of "*The International Symposium beyond 2000 in Computational Geotechnics*". 10 Years of PLAXIS Inetrnational, Balkema, Amsterdam, the Netherlands, March 1999, pp. 55–58.

Exploration of landslide geometry by seismics

Polom, U. and Krawczyk, C.M. (Leibniz-Institut für Angewandte Geophysik, Hannover)

Abstract

The expression „landslide“ is an unifying term for a series of more or less spontaneous movement of masses of soil, rock, artificial fill and others under the force of gravity. Landslides can also be triggered by a variety of incidents like earthquakes, volcano eruptions, heavy rain, natural or man-made destabilization processes, and others. They are not restricted to specific regions like, e.g., mountain ranges, which may be a first association. They also occur, e.g., in regions without significant topography, hidden in the subsurface (e.g., caused by mining) or submarine. In most of the cases such slide masses cannot be stopped once the sliding process has started. Even though devastating, landslides are not predictable in most cases. Therefore the important question today is: How can we detect suspicious slide masses, and how can we mitigate or reduce the risk of their impact? One approach is to learn more about and understand the processes of destabilization, and to explore the potential volume of slide masses to estimate their hazard potential. Seismic imaging methods are one applicable approach. The main challenges for this method are the required resolution and the shallow investigation depths. The state-of-the-art today still requires improvements towards a better understanding of the problem. In this paper, we show some examples of research and experience from LIAG and others made during the last years, which may be a starting point for further developments.

1 Introduction

Landslides are a strongly increasing natural hazard for communities, infrastructure, residents, and the environment all over the world. In general, increasing population and increasing land use lead to an upcoming spread of human settlements and activities towards vulnerable and less save areas, parallel attended with man-made environmental changes like non-controlled de-forestations and global warming processes that, e.g., amplify ground destabilization processes in former permafrost regions. Therefore, affected and vulnerable areas increasingly spread all over the world, from coastal regions up to the highest mountains, from tropical forest regions to ice shields. Depending on the ground stability itself, the hydraulic and geochemical regime, gravity forcing the movement processes, de-forestation, subrosion and erosion, and partly additional effects, the processes leading to mass movements vary in a broad manner. This includes long-term, slow slope processes over decades to suddenly occurring, catastrophic incidents within seconds, externally triggered by human or natural interference.

The growing impact of slope instability processes to human life, infrastructure, and economics is not only restricted to developing but also highly-developed countries. As an example, a repeated event like the Storregga submarine mega-slide of estimated 3,500 km^3 at the continental shelf along the Norwegian west coast would lead to a catastrophic impact to all coastal areas around the Norwegian Sea by a triggered tsunami, including the North Sea. Therefore, improved strategies for

onshore and offshore landslide risk mitigation and development of early recognition and warning systems are an increasing demand worldwide, also pushed into human awareness by the Sumatra Tsunami of 2004.

At a smaller scale, potential slide masses along the Norwegian fjords were detected to be of potential danger for human life and settlements along the shoreline of the fjords, because of repeated activity during the last century. Examples of such slide masses are the Åknes or Hegguraksla sites in western Norway (**Figure 1**), which are under sophisticated continuous remote monitoring by several geophysical methods initialized in 2004. Slide rates of these mass volumes typically range between 3-10 cm/y (source: Norwegian Geotechnical Institute, NGI).

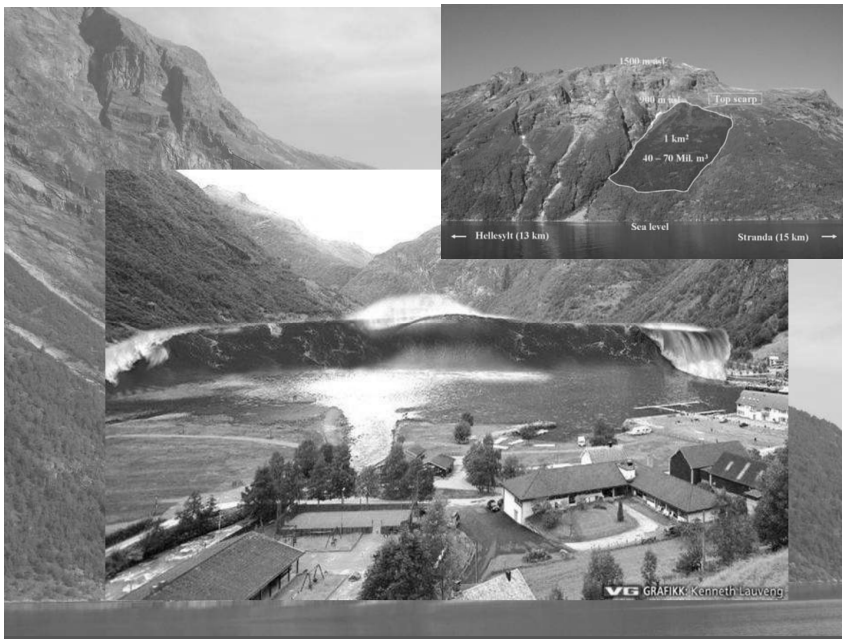

Fig. 1: Artistic illustration of a hypothetic tsunami which may probably be generated by the Åknes or Hegguraksla rock slide masses, county of Møre og Romsdal, western Norway. Due to the channel effect which prevents spherical spreading in the fjords, such waves are much more dangerous than those in an open ocean.

The artistic scenario in Figure 1 is not a complete fiction, because such geohazards are well known in the Norwegian history, causing severe damages and losses of human life. The Talfjorden tsunami in 1934 was generated by a massive landslide of two million cubic meters of rock dropped into the fjord, causing nearly fifty people's dead along the shoreline by waves up to 20 m high. **Figure 2** shows a modern artistic illustration of this incident.

Fig. 2: Artwork tracing the tsunami of ca. 20 m peak height, that was triggered 1934 by a massive landslide that dropped two million cubic meters of rock into the Tafjorden in Norway.

The artwork of these incidents may look like boosted news reports, but they are based on real incidents that occurred during the last century, even they mostly did not pass into the news in mid Europe. Only nearly two months prior to publication of this special issue, on January 29th 2014, a tsunami within a Norwegian fjord reported up to 15 m peak height caused by a submarine slide that hit the small village of Statland, 150 km northeast of the city of Trondheim, Norway (**Figure 3**). Several houses and factory buildings close to the shoreline were destroyed or badly damaged, and nearly all boats and ships in the marina sunk. 50 persons were reported to get homeless, one injured.

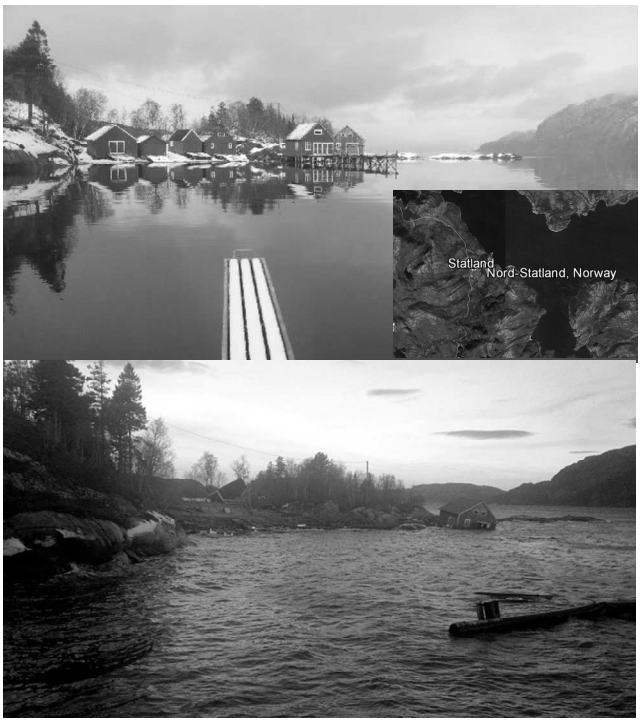

Fig. 3: 29th January 2014, 4.30 pm, Statland, province North Trondelag, Norway. A tsunami reported up to 15 m peak height supposedly caused by a submarine landslide that destroyed a small settlement at the coastline of the fjord. Top: view before tsunami impact; below: view after tsunami impact (source: AGU landslide blog).

Landslides occur when the shear stress at an interface within a mass volume forced by gravity exceeds the shear strain of the material. Therefore, the analysis of the shear strain within a mass volume suspected for sliding is an important parameter. Another important parameter is the fluid saturation, since it will also affect the shear strain within the mass volume. This context highlights the application of combined geophysical methods for investigation.

In most cases of a past or still ongoing landslide event, the internal structure of the moving masses is strongly changed compared to its original, more or less non-mobile situation, i.e. strong changes of the internal elastic parameter structure are suggested. In this case, all seismic methods strongly suffer due to the change to in-homogenous and anisotropic subsurface structures, non-linearly disturbing all calculations based on mathematical ray or wave propagation theories, thereby leading to strongly-disturbed wave propagation and recording behavior, followed by difficult data analysis. This requires careful interpretation of results applying commonly used methods, even if the results look promising.

If a landslide has happened, geophysical investigation methods are mostly of less interest, apart from detection of buried subjects. Most interesting for geophysical applications regarding landslides is the monitoring of potential slope instability in

terms of hazard mitigation and early warning systems. Especially for active seismic methods, ongoing sliding of masses is a difficult investigation task.

As an additional challenge for most geophysical investigations, steeply dipping slide masses that are present, e.g., in the Alps or along the Scandinavian fjords require adapted geophysical equipment and a sportive team for investigation. In most of those cases, the site access is difficult and the operation might be partly dangerous. Using explosives as seismic source should be urgently prevented to avoid triggering of a slide incident. Nowadays, most of the preferred investigation methods use small and lightweight equipment operated by hiking-trained persons, sometimes joking about 'steep rock slope seismics'. A promising and saver tool in recent years is to remotely control permanent monitoring systems via internet, that gain increased use.

2 Investigations by LIAG and partners

In 2007, LIAG tested in cooperation with a team of Stuttgart University and GEOSYM active seismic applications at Heumöser Hang, a multi-disciplinary landslide investigation site at Ebnit (Dornbirn)/Vorarlberg (Austria), where masses move very slowly with a rate of several cm/year (**Figure 4**).

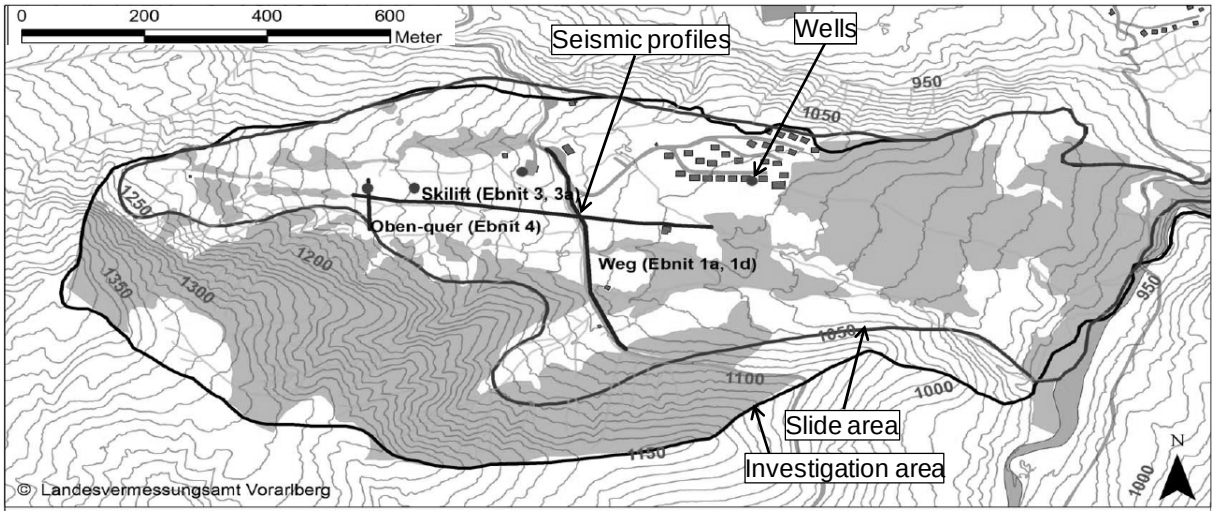

Fig. 4: Landslide investigation area Heumöser Hang in Ebnit (Dornbirn, Austria) (after Walser, 2007).

The site is under investigation since ca. 20 years, so that a lot of additional data, e.g., from wells are available to calibrate the results of active seismic measurements. Mostly P-wave operations were applied. Due to limited access to the terrain and missing dirt roads supporting S-wave operations, these were restricted to a test using commonly planted horizontal geophones along the main N-S profile, and to a small test area at its northern end, where a land streamer unit of 24 channels could be used. P-wave generation was carried out by hammer impacts and using the SISSY shotgun, for S-wave generation the ELVIS vibrator was used. The thickness of the slide mass was estimated between 4-15 m, so that reflection responses were not expected to be recorded with the P-wave configuration, but probably with the S-wave system assuming a soft slide mass over a stiffer basement as a simple subsurface model.

The overall result of these experiments shows a weak seismic response from the subsurface for both P- and S-wave recordings. **Figure 5** shows shot record examples using planted S-wave geophones, which indicate strongly inhomogeneous wave propagation in the subsurface, without any significant reflection response. Non-symmetric refractions without clear crossovers suggest strong variations at the base of the slide volume, which is also supported by the non-symmetric scattering of Love waves. A further reason for such wave field images may be the topographic variations at the base of the slide masses. After testing several processing strategies for these data without success, the final data processing was restricted to refraction analysis and refraction tomography inversion of P-wave recordings only (Walser, 2007) as a first step. More details about other seismic experiments at this location are published (Walter et al., 2011, Böniger et al., 2011).

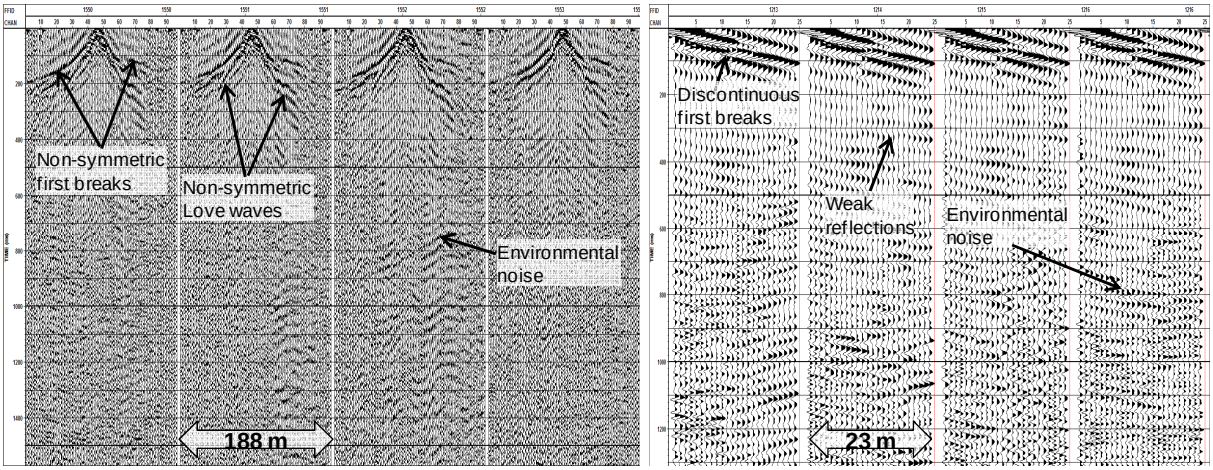

Fig. 5: Data examples from Heumöser Hang. Left: Raw records using planted horizontal geophones. Right: Raw recordings using a land streamer for tests at the northern end of the main N-S- profile. In both cases, the ELVIS source was used for shear wave generation.

The advantageous application of refraction methods is based on the simple model that more or less weak material slides on top of stiffer material, which is similar to the model of a weathering layer above the half space. The main disadvantage of applying P-wave-based refraction methods is the inhomogeneity within a sliding mass, a probably decreasing stiffness-to-depth function, which may strongly disturb the wave propagation and affect the inversion processes. Another problem is an often water saturated sliding plane or zone at the base, which may mask the slide interface. These problems focused our activities to the application of shear wave reflection seismics, to reduce the influence of velocity inversions and of the soil water content to the detection method.

In 2011, GEOSYM tested together with a team of Darmstadt University the application of land streamer-based shear wave reflection seismics on a slide mass near Susten in the Swiss Alps, providing the acquired data for inspection. Target of investigation was the base of the slide mass, which was estimated at ca. 60 m depth. This target is imaged in the data (**Figure 6**), but the imaging of internal structures within the mass volume is not easy to achieve. This work has not yet been continued or the data fully exhausted because of limited funds and capabilities.

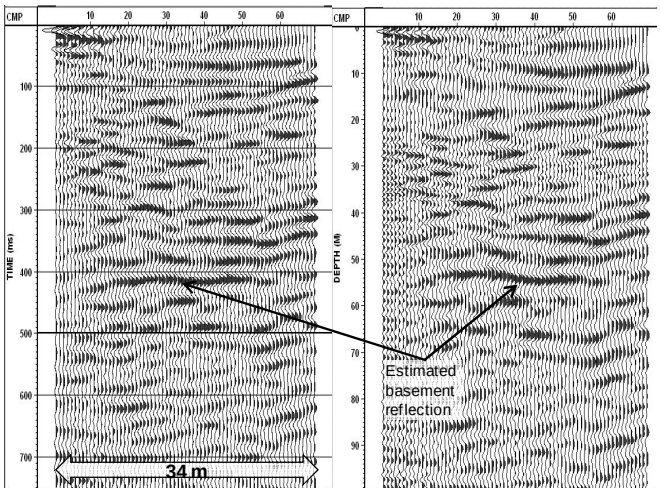

Fig. 6: Time and depth sections of a short shear wave test profile above the landslide mass near Susten, Swiss Alps, where the base of the slide mass was supposed to lie at ca. 60 m depth. While this interface could be imaged very well, internal structures within the slide mass are still difficult to interpret.

Successful imaging of internal structures of suspected slide masses was done with data gathered in Scandinavia, where the so called quick-clays (also called Leda clays) play an important role regarding landslide volumes. Even though these formerly marine deposited clays are mostly not under the influence of strong gravity gradients like most of the slide masses, e.g., in the Alps or in Norwegian fjords, they tend to spontaneous and fast liquefaction following an initial force, often spreading around in a chain reaction (**Figure 7**).

Fig. 7: Photos of recent quick-clay landslides in Norway, Sweden, and Canada, that caused severe destruction of infrastructure and housings within several minutes (top left and right after Sauvin et al., 2013; bottom left from Uppsala University; bottom right from AGU blog).

This type of slide masses is well known in the whole Nordic hemisphere and is typical for marine sediments which were uplifted above sea level after the last glaciation. Due to the wide distribution of this sediment type in Scandinavia, quick-clay slides have a strong influence regarding infrastructure safety and safe building foundation, and also in generating fjord tsunamis, often by destabilized submarine slide masses. The stiffness of these clays is directly connected to their salt content, which stabilizes the molecular structure. In their original condition, these clays have a very soft behavior with a N-value of below 5 (using penetration tests), and shear wave velocities of ca. 150 m/s or less. This requires special foundation methods for buildings. If the salt content is leached by sweet water inflow, e.g., due to rain, natural drainage, or man-made activities, the stiffness reduces further until the

material converts from a solid to a fluid. Of special interest are the internal structures within the clay bodies, for instance to detect pathways for sweet water intrusion, which can destabilize the clay around the water pathways by salt leaching. Such interfaces and included thin sand bodies can true up destabilized zones, which initialize slide planes. Another investigation target is the topography and the depth of the underlying bedrock, which can also cause sweet water intrusion, e.g., due to faults within the bedrock and along the bedrock surface.

In Norway, extended mapping and subsurface investigation is carried out in the Nidelva river valley south of the city of Trondheim, to analyze and verify the geohazard potential of the densely populated city, which increasingly expands in the whole area. The International Centre of Geohazards (ICG, Oslo) and the Norwegian Geological Survey (NGU, Trondheim) coordinate these investigations, supported by NORSAR (Kjeller). The river valley is mostly filled by marine clays, and landslide scars spread across the whole area. Several small quick-clay slides occurred in the past, but the estimated volume of some scars indicate catastrophic events, obviously (**Figure 8**).

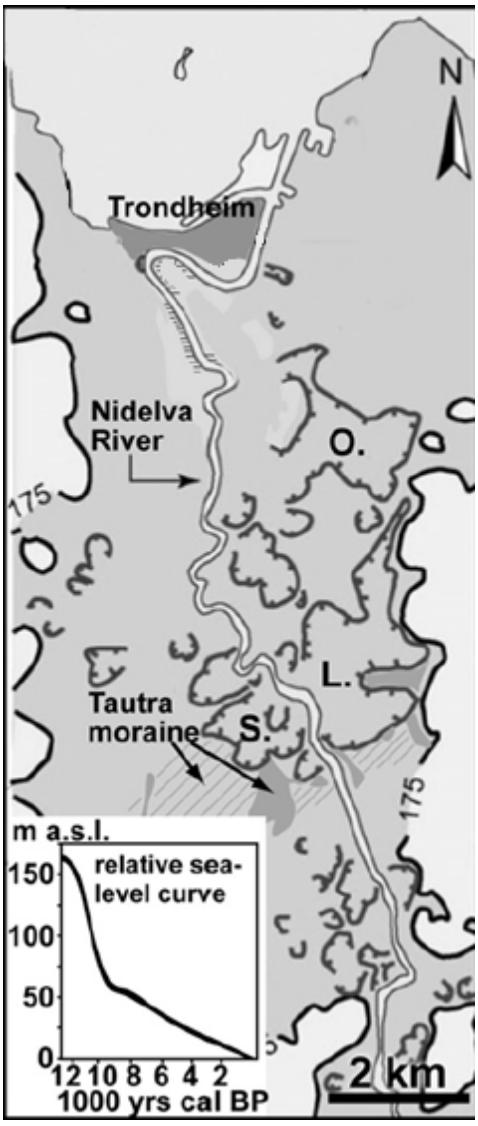

Fig. 8: Extension of thick soft marine clay deposits along the river Nidelva south of the city of Trondheim, Norway (light grey). In the North lies the Trondheimsfjorden with fluvio-deltaic sediments at its southern border (dark grey). The Brattora harbour area of Trondheim, build by land reclamation on the delta plane in front of the cost, is shown right above in light grey. In the whole area along the river Nidelva, bedrock outcrops and some peat bogs exist, but the subsurface structure and the depth to bedrock is widely unknown. Black lines denote the sea level 12000 years before present, now uplifted to 175 m a.s.l., dark grey lines denote scars caused by quick-clay landslides. Scars marked by S., L., and O. represent the Sjetnemarka, Leirfossen, and Othilienborg landslides of 30, 75, and 70 million m^3 respectively, which were estimated to cause catastrophic mass impacts into the fjord (graphics after Hansen et al., 2013).

In 2008, LIAG together with members of ICG, NGU, and NORSAR carried out shear wave reflection seismic using land streamer and S-wave vibrator in the Brattora harbour area of Trondheim (Polom et al., 2010). The experiment was initialized based on results from marine seismic investigations in the fjord, where a series of submarine slides was indicated along the delta plane north of Trondheim using very high-resolution offshore seismic methods (L'Heureux et al., 2010). It was the first time shear wave reflection seismic was applied in Norway, and the results showed the good applicability of this method for the investigation of the uplifted marine sediments onshore. **Figure 9** shows a structural interpretation of this shear wave seismic profiling by Hansen et al. (2013), with the intention to verify historic slide volumes by the deposit structures in the delta plane.

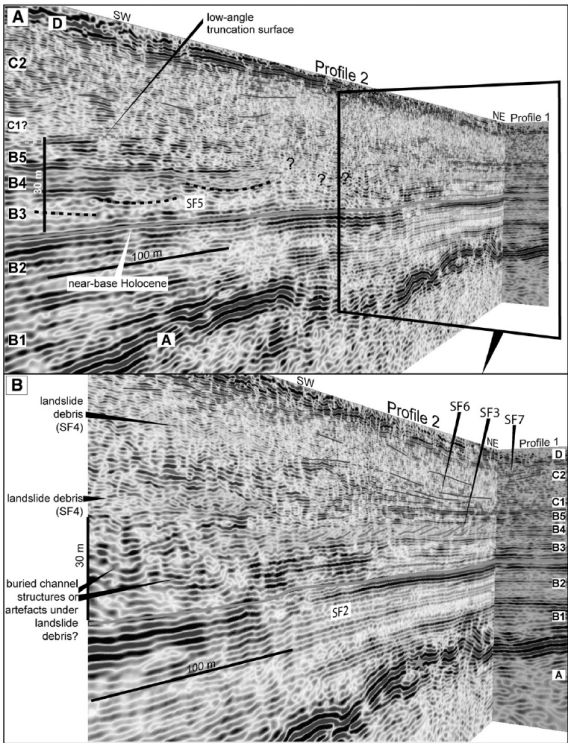

Fig. 9: Seismic profiling example of the Trondheim-Brattora shear wave reflection seismic experiment carried out in 2008. Interpretation of the seismic patterns was carried out to verify historic slide masses in the delta plane (after Hansen et al., 2013). Due to missing boreholes of sufficient depth in the area, the structures could not be calibrated until yet.

Further shallow shear wave seismic surveys in the Trondheim city area were carried out in 2012 by ICG together with a seismic team of University Pierre and Marie Curie (UPMC), Paris, to verify the application for the detection of quick-clay deposits and imaging of the bedrock topography. In contrast to the land streamer seismics used in 2008, planted horizontal geophones (14Hz) were used, combined with an ELVIS vibratory source to enable the operation in areas without surface pavement. **Figure 10** shows preliminary shear wave raw records (courtesy G. Sauvin, NGI) of these first experiments in excellent data quality. This is a result of the very low shear wave velocity of nearly 30 m/s (!) at the surface, which restricts the disturbing Love wave cone to the centre of the records. First breaks and reflection hyperbola move-out indicate shear wave velocities of nearly 150 m/s in deeper parts of the sediments above the bedrock. These investigations are ongoing.

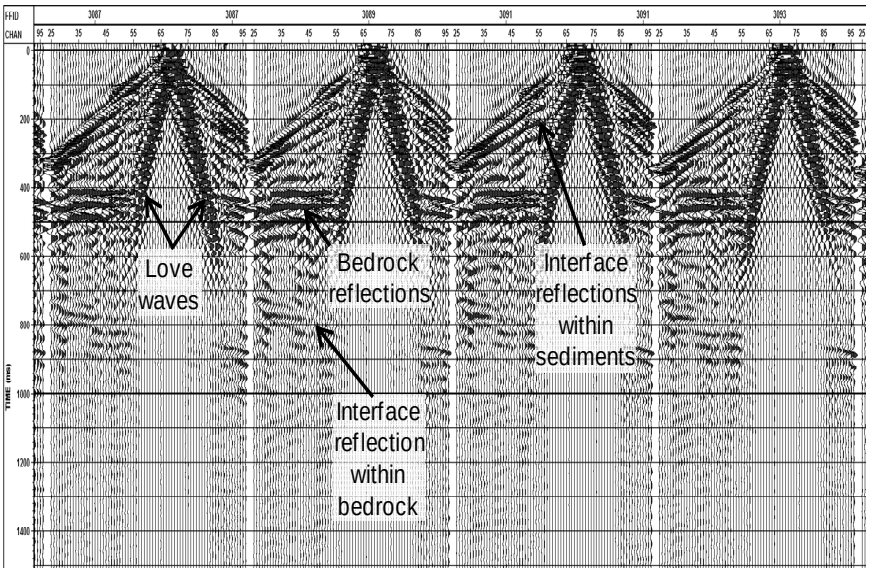

Fig. 10: Excellent quality raw shear wave reflection records gained in Trondheim city using planted horizontal geophones. The good separation of surface waves, direct waves and reflection response results from the very low shear wave velocity of nearly 30 m/s at the surface (data courtesy G. Sauvin, NGI).

Further investigations at quick-clay sites were carried out in 2011 in southwest Sweden in the framework of SEG's 'Geoscientists Without Borders' program. The investigation site Fråstad (**Figure 11**) north of the municipality Lilla Edet nearby the Göta river nearly 60 km north of Gothenburg was suggested by the Swedish Geological Survey as a typical quick-clay location, where a quick-clay landslide happened nearly 40 years ago (marked in **Figure 11** by the annotation "Landslide scar").

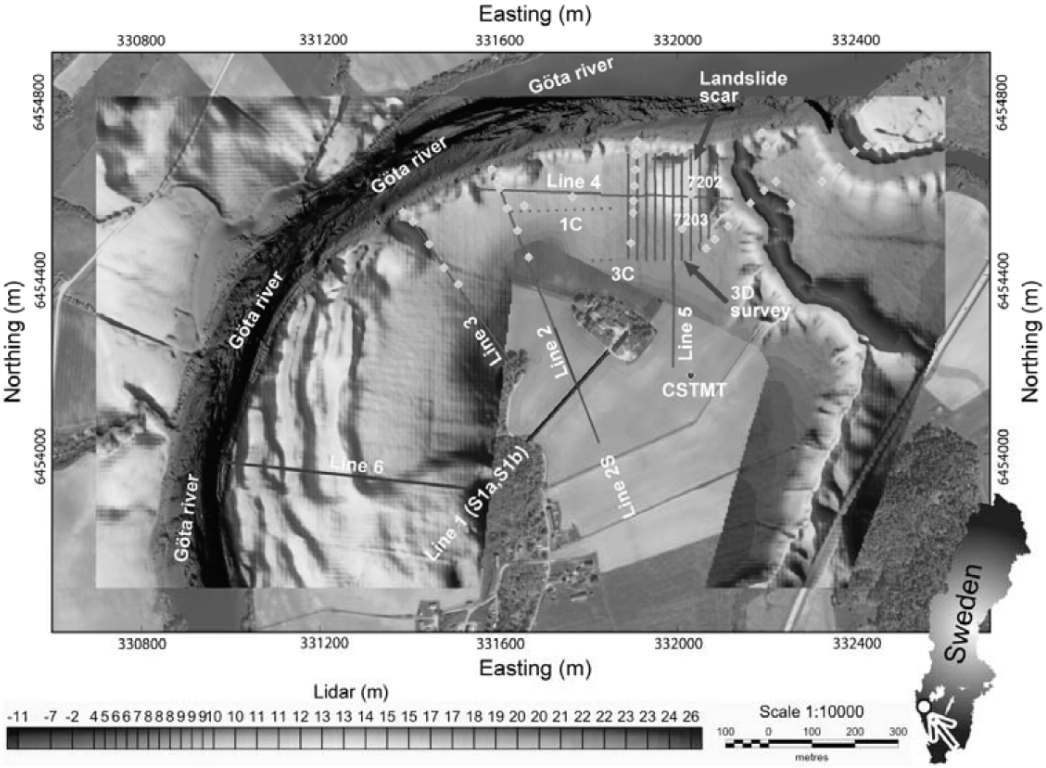

Fig. 11: Combined Lidar image and satellite photo of quick-clay investigation site Fråstad north of Lilla Edet, SW Sweden (from Malehmir et al., 2013a). This site is under investigation using multidisciplinary geophysical and geotechnical methods. In the centre of the area are the LIAG research profiles S1a, S1b, and S2, acquired 2011 using a land streamer combined with an ELVIS source.

Numerous scars along the Göta river (**Figure 11**) document further quick-clay landslides in this area. In 1957, a landslide area of 15 hectares was mobilized only some km south of the investigation area, resulting in 3 casualties and wide-spreading destruction. Furthermore the Göta river area north of Gothenburg is in general well known for a couple of quick-clay landslides during the past (Malehmir et al., 2013a).

The results from shear wave reflection profiling are shown in **Figure 12** for the profiles S1a (along a dirt road) and S2 on farmland (stubble field). The deposit structure above the bedrock could be imaged in excellent quality and in remarkable higher resolution than using P-waves (compare Krawczyk et al., 2013 and Malehmir et al., 2013a, 2013b), and fits the results from subsequent drilling very well. This also verifies the quality of the velocity analysis during shear wave data processing and the usability of the derived shear wave velocities for geotechnical soil stiffness indication. At the test location, the average velocity above bedrock was derived to nearly 130 m/s, indicating a very soft soil quality which prevents normal settlement for housings.

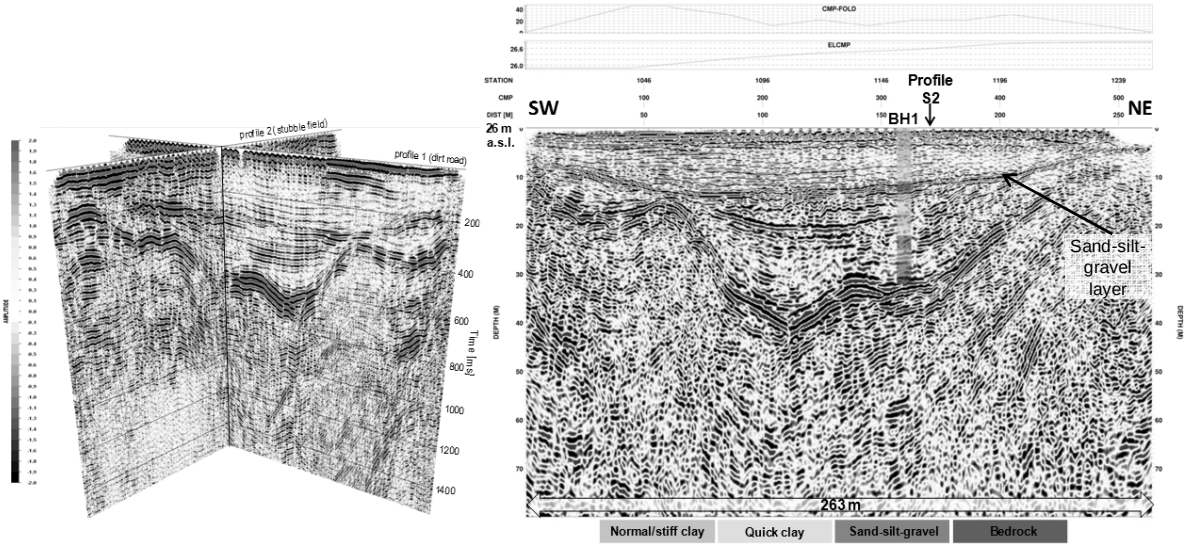

Fig. 12: Shear wave seismic imaging of an undisturbed quick-clay deposit in the Fråstad investigation area (after Polom et al., 2013). Left: time domain image (2.5-D combination of profiles 1a and 2), right: depth section of profile 1a. Depth conversion was carried out based on seismic velocity analysis only, well BH1 was drilled one year after seismic profiling. The depth section perfectly highlights the sand-silt-gravel layer within the quick-clay, which is suspected for sweet water transportation into the quick clay and salt leaching.

3 Conclusions

At the present state of research exploring the geometry of suspected land slide masses for risk assessment, or to detect historical events in the subsurface, seismic methods are still in the beginning of successful application, similar to other geophysical, geological or geotechnical methods. The methodical challenges and the variability of targets under investigation worldwide are much too complex to be solved by one method alone, enforcing multidisciplinary approaches and intensified international cooperation. Regarding strongly progressing land use, environmental changes due to global warming processes, de-forestation, and other factors, the pooling of worldwide expertise and scientific power will be the only key to provide better solutions for process understanding and early recognition of landslides.

4 References

Böniger U., Rumpf M., & Tronicke J. (2011) Refraction seismics to explore subsurface architecture of a creeping alpine hillslope. (EGU General Assembly), Vienna, Austria.

Hansen L., L'Heureux J.S., Sauvin G., Polom U., Lecomte I., Vanneste M., Longva O., Krawczyk C.M. (2013) Effects of mass-wasting on the stratigraphic architecture of a fjord-valley fill: correlation of onshore, shear-wave seismic and marine seismic data at Trondheim, Norway. Sedimentary Geology, 289, p.1-18.

L'Heureux J.-S.,Hansen L., Longva O., Emdal A., Grande L., (2010) A multidisciplinary study of submarine landslides at the Nidelva fjord delta, Central Norway — implications for geohazards assessments. Norwegian Journal of Geology 90, 1–20.

L'Heureux J.S., Long M., Vanneste M., Sauvin G., Hansen L., Polom U., Lecomte I., Dehls J., Janbu N. (2013) On the prediction of settlement from high-resolution shear-wave reflection seismic data: The Trondheim harbour case study, mid Norway. Engineering Geology 167, p. 72-83.

Krawczyk, C.M., Polom, U., Malehmir, A., Bastani, M. (2013) Quick-clay landslides in Sweden - insights from shear-wave reflection seismics and geotechnical integration. Proceedings Near Surface Geoscience 2013, 5 pp, www.earthdoc.org.

Malehmir A., Bastani M., Krawczyk C.M., Juhlin C., Gurk M., Ismail N., Polom U., Persson L. (2013a) Geophysical assessment and geotechnical investigation of quick-clay landslides - a Swedish case study. Near Surface Geophysics, 11, p. 341-350.

Malehmir A., Saalem M.U., Bastani M. (2013b) High-resolution reflection seismic investigations of quick-clay and associated formations at a landslide scar in southwest Sweden. Journal of Applied Geophysics, Volume 92, May 2013, p. 84–102.

Polom U., Hansen L., Sauvin G., L'Heureux J-S., Lecomte I., Krawczyk CM., Vanneste M and Longva, O. (2010). High-resolution SH-wave seismic reflection for characterization of onshore ground conditions in the Trondheim harbor, central Norway. In R.D. Miller, J.D. Bradford & K. Holliger (eds.), Advances in Near-Surface Seismology and Ground-Penetrating Radar, SEG, Tulsa, p. 297-312.

Polom U., Bagge M., Wadas S., Winsemann J., Brandes C., Binot F. & Krawczyk C.M. (2013) Surveying near-surface depocentres by means of shear wave seismics. First Break, 31, 8, p. 63-75.

Sauvin G., Lecomte I., Bazin S., L'Heureux J.S., Vanneste M., Solberg I.-L., and Dalsegg E. (2013) Towards geophysical and geotechnical integration for quick-clay mapping in Norway. Near Surface Geophysics, 2013, 11, p. 613-623

Walser M. (2007) Refraktionsseismik am Heumöser Hang. Diploma thesis, Stuttgart University (in German).

Walter M., Walser M. & Joswig M. (2011) Mapping Rainfall-Triggered Slidequakes and Seismic Landslide-Volume Estimation at Heumoes Slope. (10.2136/vzj2009.0147). Vadose Zone Journal, (10(2)), p. 487-495.

Discovery and interpretation of slidequake generation at softrock-landslides

Marco Walter[1,2] & Manfred Joswig[2]

[1] Seismic Solutions, Mettinger Strasse 103-105, 73728 Esslingen, Germany
E-Mail: Marco.Walter@seismicsolutions.de

[2] Institute for Geophysics, University of Stuttgart, Azenbergstrasse 16, 70174 Stuttgart, Germany

ABSTRACT

In this study, we describe conditions for slidequake generation at three different creeping softrock landslides: the Slumgullion landslide in the San Juan Mountains, Colorado, U.S., the Heumoes slope in the Austrian Alps, and the mudslide in Super-Sauze, French Alps. From a geomorphologic point of view, all three landslides are classified as creeping landslides with average velocities between several cm to m per year. Associating creep with viscous flow, and considering the largely saturated, clayey consistency of the slope body, one would not expect any brittle behaviour. Thus, it came as a surprise that impulsive seismic signals indicative of shear fracture could be discovered by sensitive passive monitoring methods at all three slopes. These fracture signals occur in episodes, have similar signatures as small earthquakes, and could be located within the slide bodies, i.e., are evidence of slidequakes.
Our investigations identified seismic and aseismic slip in each slide, with slidequakes focusing at significant bedrock structures or at lateral boundaries. Synoptic comparison of three scenarios underlines the importance of landslide-bedrock and landslide-lateral boundary interactions under gravitational loading and Mohr-Coulomb-type failure. Comparison to frictional and asperity models of crustal- and plate-scale boundaries may pave the way to a comprehensive understanding of slidequake generation, and future slope failure prediction.

INTRODUCTION

Slope-related failure by fracture processes with magnitudes of $M_L < 0.0$ has been observed on rockslides by classical seismological monitoring techniques. Gomberg et al. (1995) proposed the term ‘slidequake’, which describes the fracturing or stress relief of slope material by means of brittle failure. Slidequakes at rockslides were monitored by e.g. Roth et al. (2005) at the Aknes fjord in Norway, Brückl and Mertl (2006) in the Austrian Alps, Spillmann et al. (2007) in the Swiss Alps, for a rockslide by Helmstetter and Garambois (2010), and for a detaching rock column by Levy et al. (2011), both in the French Alps.
In contrast to the aforementioned studies, we present the analysis of slidequake generation at three landslides consisting of weak sediments: the Slumgullion landslide in Colorado, USA (Gomberg et al., 1995, 2011), the Heumoes slope in the Austrian Alps (Walter and Joswig, 2008, 2009; Walter et al., 2011), and the mudslide in Super-Sauze, French Alps (Walter et al., 2009, 2012). As softrock landslides are usually classified geomorphically as creeping, the existence of measurable slidequakes caused by brittle deformation could not been expected. Nevertheless, this study deals with the analysis of slidequakes observed at three different softrock landslides applying standard seismic instrumentation and signal processing tools, e.g. dense seismic networks typically used for monitoring rockslides. The apparent contradiction of viscous creep and the coexistence of slidequakes on softrock landslides has relevance to crustal-scale tectonics, where aseismic creep coexists with earthquake and other seismic phenomena (Peng and Gomberg, 2010).

Both the Slumgullion landslide and the Super-Sauze mudslide creep persistently at similar rates, have shallow and consistent groundwater levels, and have structures likely controlled by the basal topography. However, unlike the Slumgullion landslide that consists of volcanic deposits weathered to clayey sand and slides along bounding faults (Coe et al., 2009; Schulz et al., 2009a), the Super-Sauze mudslide is more like a granular flow (clayey schist that weathers to borderline coarse-fine soil), is younger (~50 years), and has some rockfalls and debris flows. The Heumoes slope also moves steadily but more slowly (generally < 10 cm/yr) and is comprised of silty, loose scree and over-consolidated glacial till that slides on glacial till and calcareous marl and thus likely exhibits more brittle behavior. In contrast to rockslides, the water content directly determines whether the material deforms as brittle failure or ductile-viscous deformation. Maquaire et al. (2003) investigated the shear strength properties of different black marls and determined the maximum moisture content for brittle deformation between 23% and 30% at different soil samples.
Gomberg et al. (1995, 2011) hypothesized that slidequake generation at the Slumgullion landslide might be analogous to that of tectonic faults with frictional behaviors ranging from stick-slip to steady creep. While most of the signals they observed originated outside the fastest-moving, monitored part of the slide, they inferred steady aseismic creep along the basal surface and stick-slip failure modulated by dilatancy along the slide-bounding strike-slip faults. In addition to impulsive slidequakes, Walter et al. (2009, 2012) observed energetic weaker signals with non-impulsive, reverberant, high frequency (relative to other signals on the slide) signatures clear at only one or a few sites at Super-Sauze. They inferred that these signals originated at the interfaces between the slide materials and bedrock where the latter formed crests, atop of which specific fissure structures often formed.

Slumgullion landslide

The Slumgullion landslide is located in the San Juan Mountains of Colorado, USA. It is composed of variably weathered Tertiary basalt, rhyolite and andesite units that have been highly modified by acid-sulfate hydrothermal alteration (Lipman, 1976; Diehl and Schuster, 1996) and weathered to clayey, silty sand. The landslide is situated within thicker landslide deposits comprised of similar material, although intact rock abuts the lateral margins of the active slide near its longitudinal center. The landslide is 3.9 km long, averages about 300 m wide, and has estimated average thickness of 13 m and volume of 20 x 10^6 m^3 (Parise and Guzzi, 1992).
The Slumgullion landslide moves persistently at rates of 0.5-2 cm/d (Fleming et al., 1999; Coe et al., 2003; Schulz et al., 2009a) and appears to have done so for at least the past 300 yrs (Varnes and Savage, 1996). Pore-water pressures control landslide speed (Varnes and Savage, 1996; Coe et al., 2003; Schulz et al., 2009a), with significant rainfall or snowmelt causing landslide acceleration within hours and elevated speeds lasting for weeks-months. Shear-zone dilation and consequent pore-water pressure decrease appear to retard acceleration (Schulz et al., 2009a) while onset of low atmospheric tides appears to trigger daily acceleration episodes (Schulz et al., 2009b). Movement of Slumgullion occurs by translational sliding along clayey bounding faults, while many internal faults bound individual kinematic elements comprising the slide.
The field experiment conducted August 18-26, 2009 involved deployment of a temporary seismic network and displacement measurement instrumentation spanning a ~450 m long section in the middle of the landslide where driving forces are greatest and surface velocities are the highest of anywhere on the landslide (see Gomberg et al., 2011 for details). An 88 short-period (2 Hz natural frequency) vertical seismometers array was deployed on a grid with inter-station spacings of 25-50 m extending across the entire slide width and just off it on both sides. Slow, aseismic deformation was monitored in a variety of ways and a weather station within our array measured barometric pressure, temperature, wind speed, and rainfall, augmenting other permanent environmental monitoring gear.

Heumoes slope

The creeping Heumoes slope is located in the northern Alpine Upland, in the Vorarlberg Alps, Austria, around 25 km south of Bregenz (Fig. 1). The landslide extends 1800 m in length and 600 m in width with elevations between 940 m (east) and 1360 m (west). The unstable slope material has an average thickness of ~20 m (Lindenmaier et al., 2005) and consists of very heterogeneous loamy scree and glacial till, which is mainly comprised of silty and clayey material as well as glacial components of varying size from the surrounding bedrock. The hard rock basement consists of layered Upper Cretaceous marls. The movement of the Heumoes slope has been observed since the 1990s with various approaches. These investigations were mainly focused on the determination of geotechnical, hydrological and hydraulic relationships that lead to measurable displacements at the surface of a few cm per year. The Heumoes slope can be divided in three areas where different movement rates at the slope's surface were observed. The eastern part of the slope is characterized by the highest displacement rates of more than 10 cm/yr while the western part of the landslide shows average displacements of up to 10 cm/yr. The most stable part of the Heumoes slope is located in the middle part where average rates of up to 5 cm/yr were observed (Dependahl and Schmitt, 2003; Lindenmaier et al., 2005; Fig. 1). A coupling of heavy rainfall and subsurface water dynamics was observed by e.g. Lindenmaier et al. (2005) and Wienhöfer et al. (2011) indicating that a rainfall-triggered movement of the Heumoes slope is most likely.

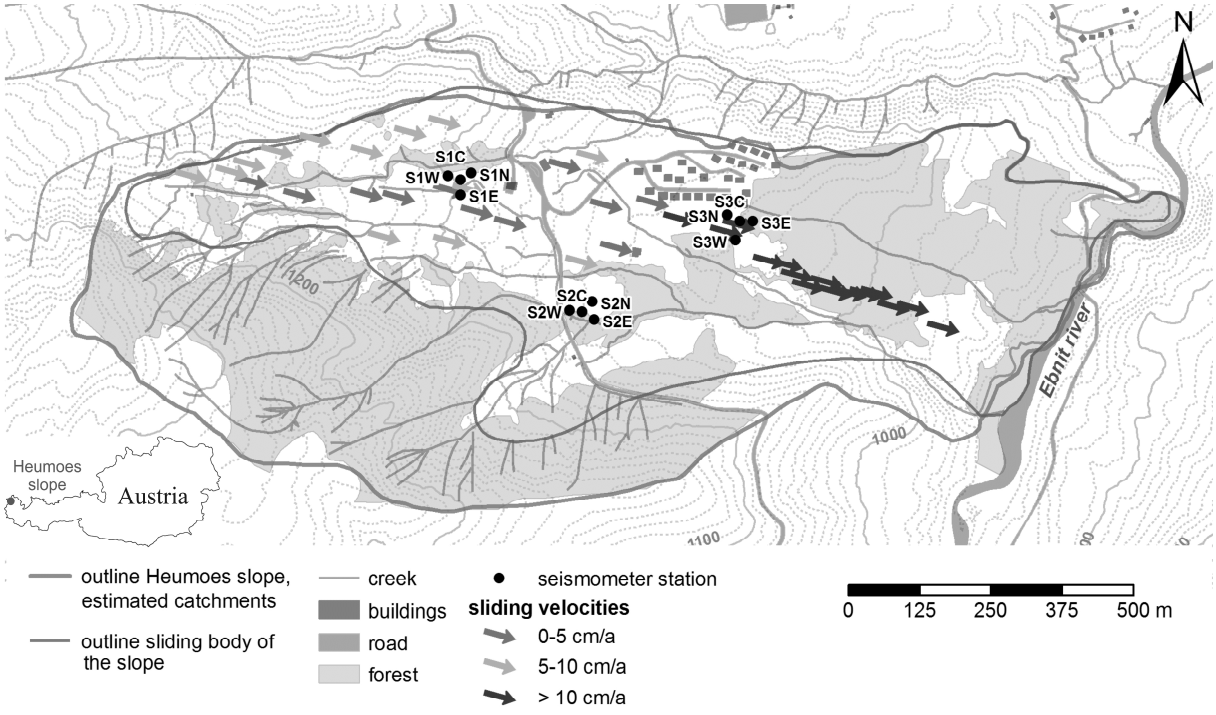

Figure 1. General set-up of the Heumoes slope, average sliding velocities (after Depenthal and Schmitt, 2003), and locations of installed seismometer stations of the permanent seismic network.

Several field campaigns were carried out between 2005 and 2008 in order to analyse slidequakes associated with the creeping movement of the Heumoes by deploying several small aperture seismic arrays. In these studies a total of 39 slidequakes with magnitudes of $-2.2 \leq M_L \leq -0.7$ were recorded and located (Walter and Joswig, 2008; Walter et al., 2011). The majority of events were located in the central section of the landslide that displays higher surface displacement rates compared to its eastern part (Fig. 1). Since the eastern part of

the slope shows the highest movement rates at the surface, one would expect to detect more events generated in this slope area. To understand and to investigate the spatio-temporal occurrence of slidequakes at the Heumoes slope, several permanent small-aperture seismic arrays were installed in July 2009 (Fig. 1). Each array consists of one 3-component and three 1-component short period seismometers with an aperture between 40 and 50 m. Data were recorded in continuous mode with a sampling rate of 400 Hz. The presented results are based on the data analysis between July 2009 and May 2011.

Super-Sauze mudslide

The mudslide in Super-Sauze is located in the Barcelonnette Basin in the Southern French Maritime Alps, approximately in the middle between the cities of Gap and Nice (Fig. 2). The mudslide started to form in the 1960's and today it measures 850 m long with an elevation between 2105 m (crown) and 1740 m (toe). The unstable slope with an estimated volume of 750000 m^3 mainly consists of heterogeneous soft Jurassic, black marls with a maximum thickness of ~20 m, and shows significant dynamic behavior with displacement velocities of more than 3 cm/day (Amitrano et al., 2007). The observed average displacement rates of the mudslide vary: the highest movements can be observed in the mid-part of the slope and decrease in the toe direction to less than 2 mm/day (Fig. 2). The influence of the bedrock topography to the stability of the slope was investigated by Maquaire et al. (2003). They inferred that heterogeneous movement of the entire mudslide is likely caused by stable buried in-situ crests at the bedrock of the mudslide, with gullies between the crests channelizing the unstable material. Deformations of the entire mudslide are also directly influenced by its lateral boundaries (Maquaire et al., 2003). Fissure patterns at the mudslide's surface were mapped by Niethammer et al. (2012) using UAV-based (Unmanned Aerial Vehicle) high-resolution remote sensing methods. They observed specific fissure patterns in slope areas that correlate with the locations of buried in-situ bedrock crests and at lateral boundaries of the landslide.

In Super-Sauze, a field-campaign was carried out between 14th and 24th July 2008, where four small-aperture arrays were installed to monitor possible slidequake generation (Fig. 2). The aperture of the seismic arrays was setup similar to the Heumoes slope between 40 and 50 m. Data were also recorded continuously with a sampling rate of 400 Hz.

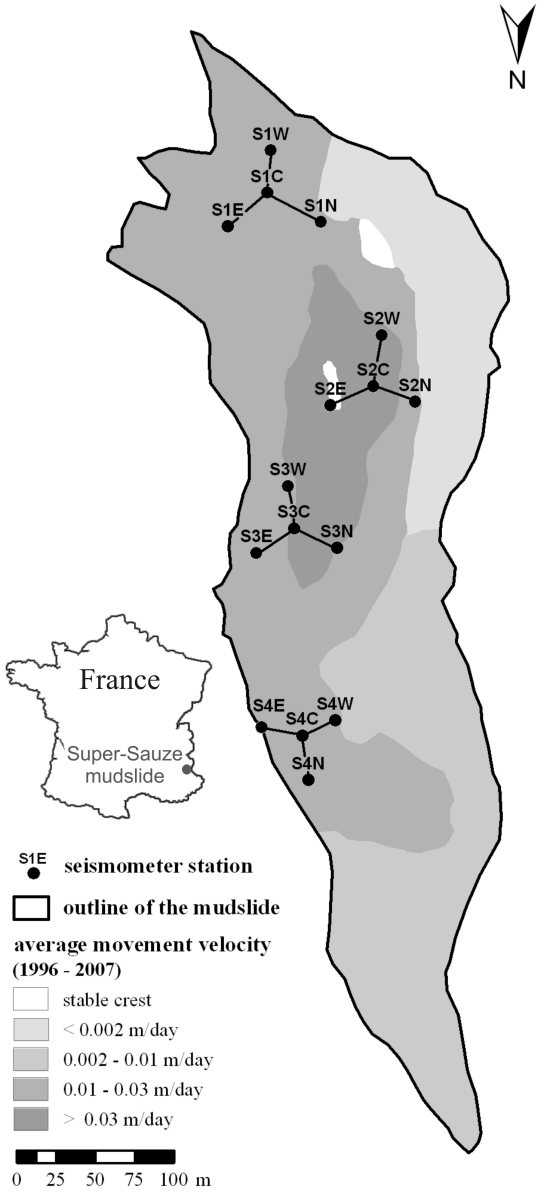

Figure 2. Location of the installed seismometer stations (black dots) and average movement velocity of the mudslide between 1997 and 2007 determined by Amitrano et al. (2007)

APPLIED METHODS

Despite its remoteness from obvious natural and unnatural noise sources, a tremendous richness of seismic signals was recorded on the Slumgullion landslide. Details about the deployments, analyses, and interpretations of these signals may be found in Gomberg et al. (2011). The density of seismic stations deployed permitted some simple, albeit qualitative, assessments of signal origins. Almost all the seismic data were scanned visually.
Many seismic signals were clearly not related to landslide deformation and based on arrival moveout times, no sources originated within the seismic network, although some could be attributed to sources along the edges of the seismic network.Location uncertainties for sources outside the network are inherently large, particularly because of the highly heterogeneous material and irregular topography of the Slumgullion landslide. For several event types we applied quantitative source detection and location algorithms and used a variety of signal characteristics to glean clues about source type and location. To detect and measure some of the repeating signals we employed a template cross-correlation approach. Event locations were estimated with two location algorithms, one using manually picked phase arrival times and a grid-search fitting between measured travel times and those calculated for a plane-layered medium (Gomberg et al., 1990). The other algorithm was a beam-forming approach developed for a landslide study elsewhere (see Lacroix and Helmstetter (2011)). Magnitudes were not estimated for any of the sources studied.
The recorded data at the Heumoes slope and at the mudslide in Super-Sauze were processed using the software HypoLine, an interactive, graphical jackknife tool which displays the most plausible solution for low-SNR (signal to noise ratio) signals, resolving the influence of individual parameters on the event-localization in real-time (Joswig, 2008). The raw-data was high-pass filtered above 5 Hz in order to eliminate anthropogenic noise and to increase the SNR. As it was assumed that brittle failure takes place within the soft rock sedimentary cover, a layer over a homogeneous half-space model was used for event location and delivered the highest location accuracy of calibration shots; a 3D-model was not used. Compared to the Slumgullion landslide, the recorded slidequakes at Heumoes slope and the mudslide in Super-Sauze could be located by the use of the software HypoLine. The source location allowed additionally the determination of their local magnitude M_L, which permitted inferences about source processes and the estimation of the dimension of rupture areas. Due to the sparse station distribution and the low thickness of the respective sediment body, the source depth could not be determined.

RESULTS

Characterization of the variety of recorded signals required significant qualitative and quantitative examination and analysis. Diagnostic parameters estimated included apparent phase velocities to constrain locations, signal coherency to detect families of repeating or similar sources, pattern recognition techniques to detect low-SNR slidequakes, and a variety of location algorithms. Many of the slidequake signals have properties that are remarkably similar to those of earthquakes and other local tectonic fault slip events: a high-frequency P-phase up to ~80 Hz and low frequency S-phase up to ~30 Hz (Walter and Joswig, 2008; Walter et al., 2009, 2012; Gomberg et al., 2011; Figure 3). Due to the shallow source depth of slidequakes, the signals show a prominent surface wave coda. Maximum signal amplitudes varied over two orders of magnitude and the dominant frequency contents ranged from 10 to more than 80 Hz on all three slides.
Figure 3 shows typical seismograms and sonograms of recorded slidequakes at Heumoes slope, Super-Sauze and Slumgullion landslide (Fig.3a – Fig. 3c). The lack of clear dispersion for the slidequake signals recorded at the Slumgullion landslide likely reflects propagation differences. Similar spectral characteristics (a decrease in frequency with time) can be observed in signals from local earthquakes (Fig.3d and Fig.3e).

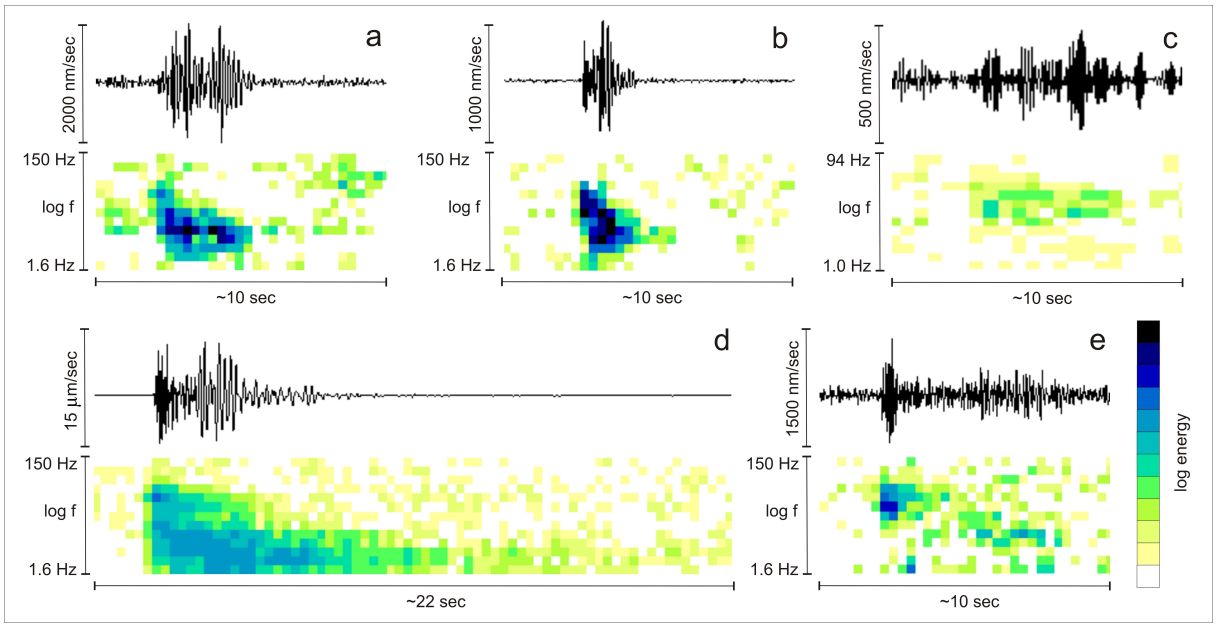

Figure 3. Comparison of typical seismograms and sonograms of observed slidequakes with local earthquakes. (a) slidequake observed at Heumoes slope (M_L = -1.4 in ~180 m distance). (b) slidequake observed in Super-Sauze (M_L = -2.4 in ~100 m distance). (c) slidequake observed at Slumgullion. (d) strong local earthquake (M_L = 2.3 in ~11 km distance). (e) weak local earthquake (M_L = 0.7 in ~22 km distance). Note the different amplitude and frequency scales.

Slumgullion landslide

Here we summarize the most well constrained class of seismic source studied on the Slumgullion landslide. Details may be found in Gomberg et al. (2011). The most thoroughly analyzed signals are ~3 sec duration, monochromatic wavepackets that repeated over 90 times during the monitoring period. We inferred that these are trapped waves generated by stick-slip events along the slide-bounding strike-slip faults (Fig.4; Walter et al., 2013), with occurrence rates that are highest in synch with daytime increases in the landslide slip rate.

Evidence supporting this source type includes energy focused at 11.9 Hz at all stations and without harmonics, amplitudes strongly peaked at the stations along the southern edge of the landslide, variable apparent velocities that increase with distance, and high stacked correlation coefficients for locations along the southern edge of the landslide.

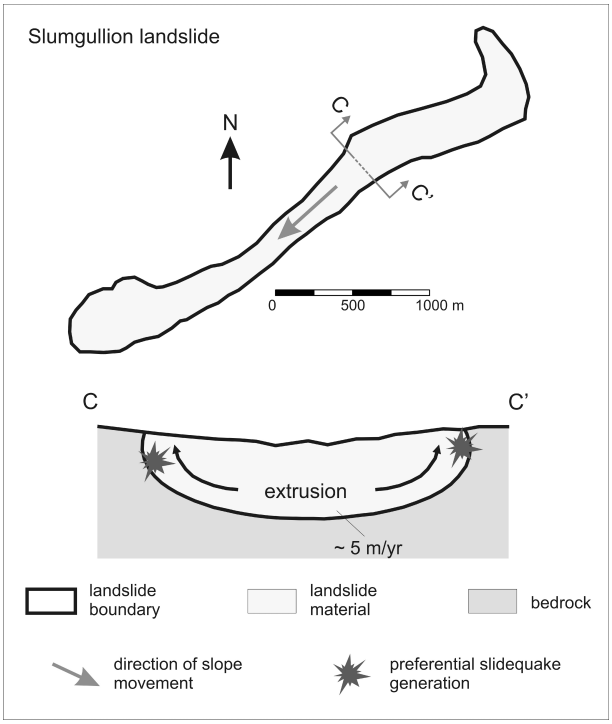

Figure 4. Schematic illustration of preferential slidequake generation at Slumgullion landslide (Walter et al., 2013; landslide and bedrock geometry modified after Fleming et al., 1999).

Gomberg et al. (2011) explained these events by appealing to a model proposed by Schulz et al. (2009b), in which slide-bounding strike-slip faults slip fastest during the daytime when atmospheric pressure is lowest. The daily modulation of surface pressures modulates fluid flow within the slide mass, decreasing its basal frictional strength when surface pressures are lowest and allowing the slide to speed up. Dilatant strengthening (Schulz et al., 2009a) along the lateral slide-bounding faults during more rapid shearing leads to increased rates of brittle failure events and effectively puts the brakes on the slip and the cycle repeats.

Heumoes slope

At Heumoes slope, a total of 121 slidequakes of magnitudes $-2.5 \leq M_L \leq -0.5$ were recorded and located during the field campaigns between 2005 and 2008 (39 events) and during the permanent seismic monitoring between July 2009 and May 2011 (82 events). The vast majority of events are clustered in the central section of the landslide, which is characterized by the lowest surface displacement rates (Fig. 5). Seismic refraction measurements across several profiles were carried out in 2006 in order to obtain detailed information about the bedrock geometry (Walter et al., 2011). The active seismics revealed a significant upwarping of the bedrock in the mid-part of the slope. This bedrock elevation is oriented perpendicularly to the movement direction of the entire slope, and likely acts as a barrier and slows the surface displacement rates.

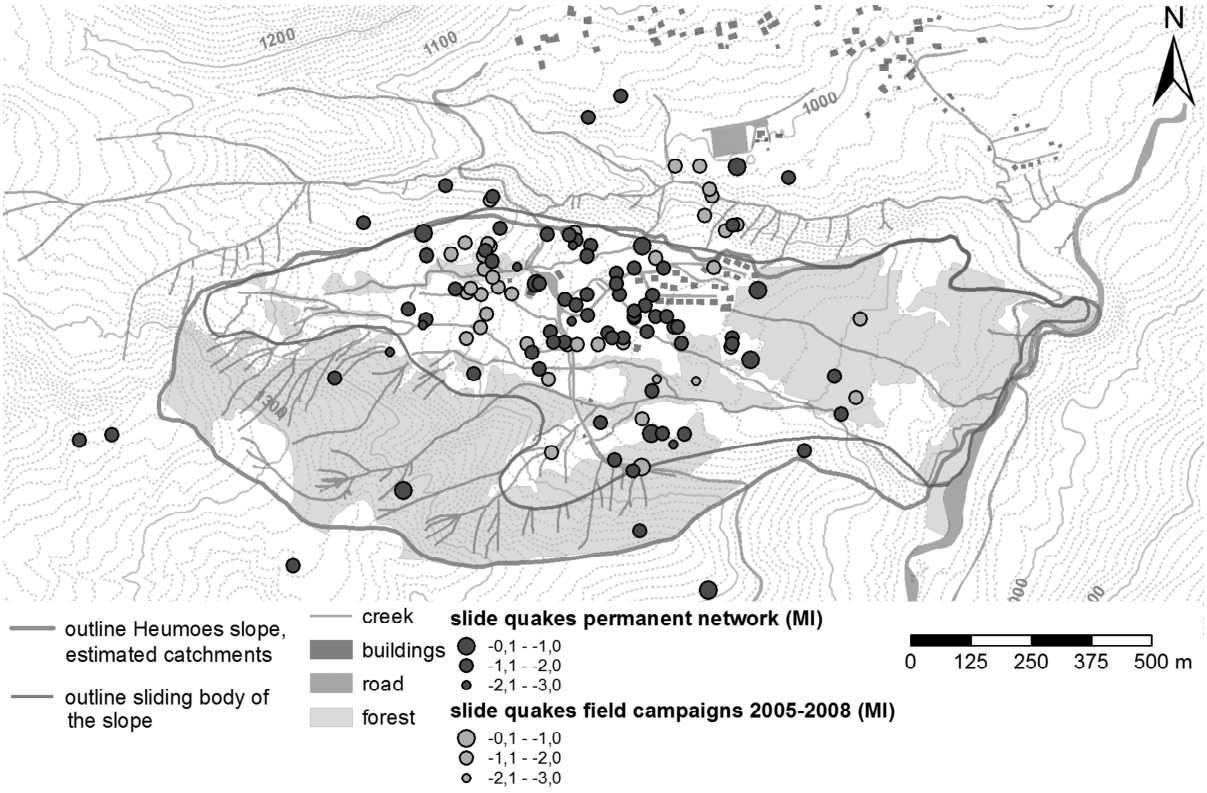

Figure 5. Locations and magnitudes of observed slidequakes at Heumoes slope during field campaigns between 2005 and 2008 (light grey dots) and the permanent seismic monitoring between July 2009 and May 2011 (dark grey dots).

Slidequakes occur at/near the interface between the barrier and slide material (Fig. 6). By contrast, in the most eastern part of the Heumoes slope sediments are thicker and lack

barriers, and no slidequakes or any other seismic signals were observed. In addition, the slope material in the aseismic eastern part of the slope is always water saturated throughout, while the water saturation of the sliding material in the other parts of the Heumoes landslide varies seasonally in depth. Vertical sequences of saturated and unsaturated material are inferred in the center, seismogenic part of the slope, due to the generally low hydraulic conductivity (10^{-7} m/s; Lindenmaier et al., 2005) of its clayey material. The low hydraulic conductivity results in hydrology controlled by surface flow and along preferential water paths at depth rather than by infiltration processes (Lindenmaier et al., 2005). We therefore assume that at Heumoes slope the observed slidequakes were generated in depth.

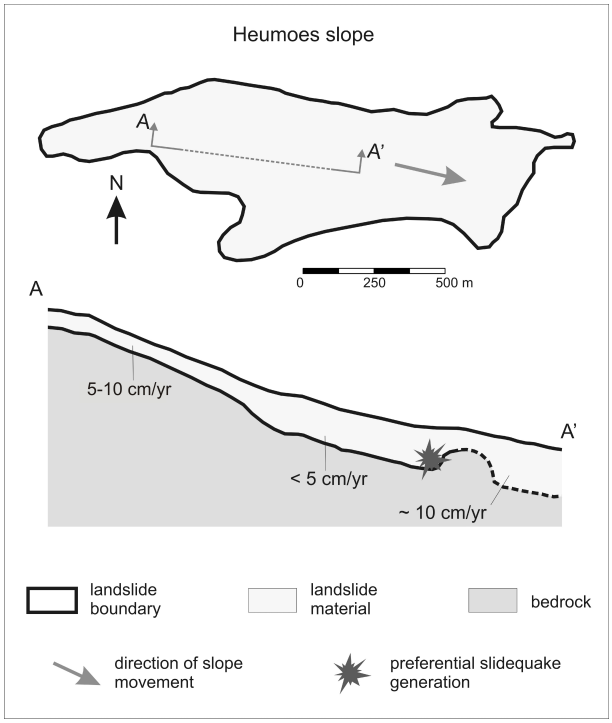

Figure 6. Schematic illustration of preferential slidequake generation at Heumoes slope (landslide and bedrock geometry modified after Walter et al., 2011).

Super-Sauze mudslide

At the mudslide in Super-Sauze, we detected and located 34 events with magnitudes between $-3.2 \leq M_L \leq -1.3$, again clustered in the mid-part of the slope (Fig. 7). Compared to the Heumoes slope, the ambient noise level at Super-Sauze is ~20 dB lower what results in a lower detection threshold so a wider range of magnitudes were observed. A higher rate of slidequakes at Super-Sauze also likely reflects its faster velocity: 83 events in ~22 months at Heumoes slope compared to 34 events in 10 days at Super-Sauze.
At Super-Sauze the cluster of located slidequakes correlates well with the part of the slope showing the highest superficial displacement rates (Fig. 7). Fortunately, there exists an airborne picture from 1956, before the mudslide started to form, and illustrates the bedrock topography of the mudslide. This picture reveals crests that border the entire landslide and channelize the mudslide material in several gullies between. These crests are more or less oriented in direction of slope movement. Figure 7 illustrates that the majority of observed slidequakes are not only generally related to the bedrock crests, but also occur in certain gullies with higher displacement rates. Figure 8 illustrates schematically the interpretation of preferential slidequake generation at the mudslide in Super-Sauze. Figures 7 and 8 show that the majority of slidequakes occurred at the boundaries of two gullies in the mid-part of the slope, which are characterized by higher average displacement rates of 11 m/yr while fewer events were observed in the gullies moving at lower displacement rates.
Only the first metre of the landslide shows material deformation by brittle failure, when drying out in summertime. This is supported by the existence of remarkable fissure structures at the slopes surface (Niethammer et al., 2012). Below, the landslide body is water saturated all the time. We therefore assume that, in contrast to the Heumoes slope, the observed slidequakes at Super-Sauze are generated within this top layer of the landslide.

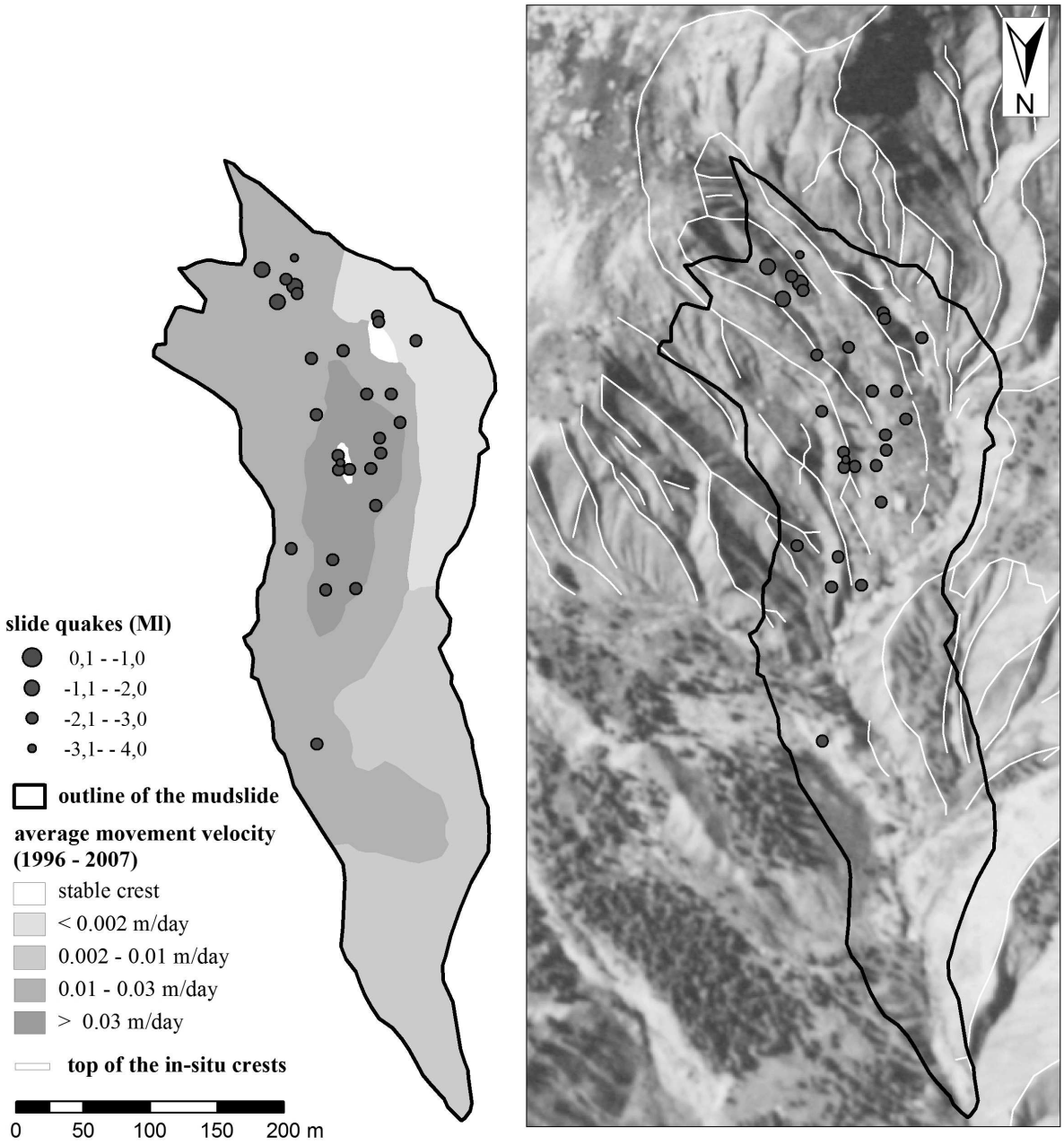

Figure 7. Locations of observed slidequakes at the mudslide in Super-Sauze. Left: Mapped on the average movement velocity of the mudslide (1997–2007) determined by Amitrano et al. (2007). Right: Mapped on an airborne picture from 1956, by courtesy of IGN (Institut Geographique National, Campaign F3139–3639). Highlighted are the tops of the in-situ crests of the bedrock's topography.

DISCUSSION & CONCLUSIONS

The rates and manifestations of deformation are indicative of the underlying processes; e.g. at Super-Sauze aseismic viscous creep likely occurs in areas of lower displacement rates and brittle failure manifest as slidequakes where rates are higher. This dependence of deformation mode on loading rate may be similar to that that inferred for ascending magma, in which fast-rising magma deformed brittle and generated earthquakes while slow-rising magma is characterized by ductile, aseismic deformations (e.g. Tuffen et al., 2003; Ichihara

and Rubin, 2010). The observations at Super-Sauze support this hypothesis of a relationship between loading rate and slidequake generation. However, rate alone does not determine the dominant deformation mechanism since at the Heumoes slope slidequakes cluster where deformation rates are slowest.
At Super-Sauze slidequakes are most common along lateral boundaries, along the boundaries of crests of bedrock (Walter et al., 2008, 2012). Brittle deformation is more likely when sedimentary or softrock materials are less saturated with viscous creep becoming more probable as saturation increases (e.g. Maquaire et al. 2003).

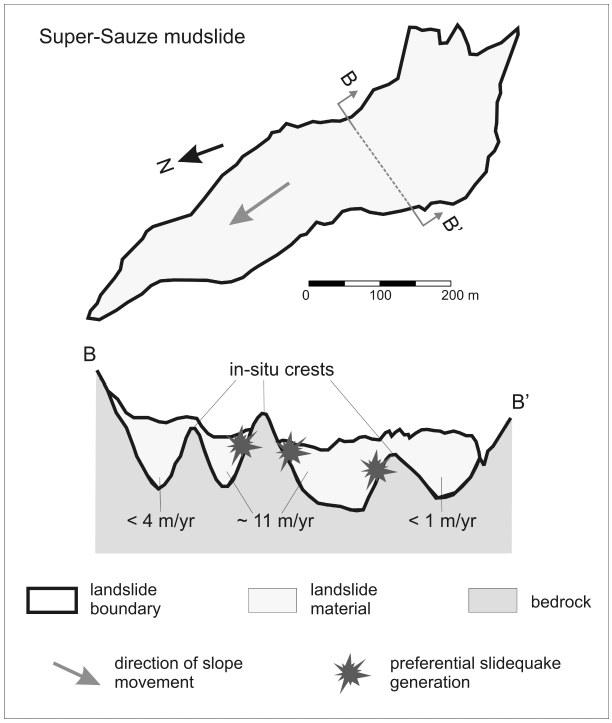

Figure 8. Schematic illustration of preferential slidequake generation at Super-Sauze (landslide and bedrock geometry modified after Malet et al., 2005).

The lateral boundaries and significant bedrock structures at Heumoes slope and at Super-Sauze act as barriers along which slope material becomes more compressed, perhaps promoting draining, lower saturation and brittle failure.
The magnitudes of slidequakes observed at Heumoes slope and at Super-Sauze permits the estimation of possible source parameters. Assuming relationships derived by Wells and Coppersmith (1994) between moment magnitude (M_W) and rupture area dimensions and by Gibowitz et al. (1991) that $M_W \approx M_L$ for $M_W < -2.0$, the observed slidequakes at Heumoes slope and Super-Sauze with magnitudes of $-3.2 \leq M_L \leq -0.5$ correspond to rupture lengths in the range of several meters. The inferred fault plane dimensions and slip rates reasonably match slope extensions and creep rates.
At the Slumgullion landslide, the dilatant properties of the slide material also are key in determining the deformation modes. There the continuous relocation of lateral boundary faults provides them with fresh material, which when sheared rapidly dilates, strengthens and slows the motion. Thus, dilatancy strengthening when displacement rates are highest promotes brittle failure and slidequakes and also keeps the motion in check. The apparently stable location of the basal surface has resulted in steady-state porosity, favoring aseismic slip.
At Super-Sauze, energetic weaker signals with non-impulsive, reverberant character were observed and located at the boundary between the emerging in-situ crest and the mudslide material (Walter et al., 2009, 2012). Similar tremor-like signals were also observed at the Slumgullion landslide (Gomberg et al., 2011), but their source locations have not been determined. Tremor signals have been observed near tectonic faults in the transitional regime between frictionally locked and stably-sliding regions (Rubinstein et al., 2010). The similarity of slope- and crustal-scale seismicity suggests that softrock-landslides may be a useful natural laboratory for testing predictions of specific mechanisms that control fault slip at all scales.
Applying passive seismic monitoring approaches at three different creeping softrock-landslides we were able to infer what conditions led to brittle failure, as evident in episodes of slidequakes along specific boundaries, and to aseismic creep. At the Slumgullion landslide, the majority of slidequakes occurred at the lateral boundaries of the landslide, while no events were detected along the basal surface (Fig.4). Dilatancy-modulated motion along the lateral bounding, strike-slip fault systems is accompanied by stick-slip failure as the active

fault strands continuously rearrange, but also keeps the long-term motion steady. This steady motion over many tens of years has likely lead to basal morphology and porosity that have evolved to stable configurations, favoring steady aseismic sliding (Coe et al., 2009; Gomberg et al., 2011). At Heumoes slope, the slidequakes cluster in the slope area with the lowest surface displacement rates. A significant bedrock rise, oriented perpendicular to the direction of slope movement, divides the landslide geometry in two basins, and probably impedes motion, slows the slide, and leads to slidequakes (Fig.6). At the Super-Sauze mudslide, the slidequakes are preferentially generated in its centre where the deformation rates are highest. There, the slidequake generation is directly linked to in-situ bedrock crests that border several gullies oriented in line to direction of the entire slope movement (Fig.8).
The synoptic comparison of these three different environments of slidequake observations at softrock-landslides provides new explanations for slidequake generation. Regardless the specific observation of the respective landslide, the slidequake generation is generally linked to geometric or rheological heterogeneities along the boundaries between the slide material and the bedrock and/or along lateral boundary faults; these barriers seem to play key roles in slope deformations.

ACKNOWLEDGEMENTS

The authors thank Joan Gomberg, William Schulz, Paul Bodin and Jason Kean for their support for the Slumgullion study. We are thankful to the German Research Foundation (DFG) for their financial support for the studies at Heumoes slope and in Super-Sauze within the research unit FOR-581.

REFERENCES

Amitrano, D., Gaffet, S., Malet, J.-P. and Maquaire, O. 2007. Understanding mudslides through micro-seismic monitoring: the Super-Sauze (South-East French Alps) case study. Bulletin de la Société Géologique de France 178(2), 149-157.

Beroza, G.C. and Ide, S. 2011. Slow Earthquakes and Nonvolcanic Tremor. Annual Review of Earth and Planetary Sciences 39, 271-296.

Brückl, E. and Mertl, S. 2006. Seismic Monitoring of Deep-Seated Mass Movements. Proceedings of INTERPRAEVENT International Symposium "Disaster Mitigation of Debris Flows, Slope Failures and Landslides", Universal Academy Press, Inc. / Tokyo, Japan, 571-580.

Coe, J.A., Ellis, W.L., Godt, J.W., Savage, W.Z., Savage, J.E., Michael, J.A., Kibler, J.D., Powers, P.S., Lidke, D.J. and Debray, S. 2003. Seasonal movement of the Slumgullion landslide determined from Global Positioning System surveys and field instrumentation, July 1998-March 2002. Engineering Geology 68, 67-101.

Coe, J.A., McKenna, J.P., Godt, J.W. and Baum, R.L. 2009. Basal-topographic control of stationary ponds on a continuously moving landslide. Earth Surface Processes and Landforms 34, 264-279.

Depenthal, C. and Schmitt, G. 2003. Monitoring of a landslide in Vorarlberg/Austria. In Stiros, S. and Pytharouli, S (Eds.) Proceedings 11th International FIG Symposium on Deformation Measurements (Publication No. 2). Santorini (Thera) Island, Greece: Geodesy and Geodetic Applications Lab. Dept. of Civil Engineering, Patras University, 289-295.

Diehl, S.F. and Schuster, R.L. 1996. Preliminary geologic map and alteration mineralogy of the main scarp of the Slumgullion landslide, in Varnes, D.J., and Savage, W.Z., eds., The Slumgullion earth flow: A large-scale natural laboratory: U.S. Geological Survey Bulletin 2130, 13-19.

Fleming, R.W., Baum, R.L. and Giardino, M. 1999. Map and description of the active part of the Slumgullion landslide, Hinsdale County, Colorado. U.S. Geological Survey Geologic Investigation Series I-2672, scale 1:1,000, 36 pp.

Gibowicz, S.J., Young, R.P., Talebi, S. and Rawlence, D.J. 1991. Source parameters of seismic events at the underground research laboratory in Manitoba, Canada: Scaling relations for events with moment magnitude smaller than -2. Bulletin of the Seismological Society of America 81(4), 1157–1182.

Gomberg, J., Shedlock, K. and S. Roecker. 1990. The effect of S wave arrival times on the accuracy of hypocenter estimation, Bulletin of the Seismological Society of America 80, 1605-1628.

Gomberg, J., Bodin, P., Savage, W. and Jackson, M. E. 1995. Landslide faults and tectonic faults, analogs?: The Slumgullion earthflow, Colorado. Geology 23(1), 41-44.

Gomberg, J., Schulz, W., Bodin, P. and Kean, J. 2011. Seismic and geodetic signatures of fault slip at the Slumgullion Landslide Natural Laboratory. Journal of Geophysical Research 116, B09404.

Helmstetter, A. and Garambois, S. 2010. Seismic monitoring of Séchilienne rockslide (French Alps): Analysis of seismic signals and their correlation with rainfalls. Journal of Geophysical Research 15(F3), F03016.

Ichihara, M. and Rubin, M.B. 2010. Brittleness of fracture in flowing magma. Journal of Geophysical Research 115, B12202.

Joswig, M. 2008. Nanoseismic Monitoring fills the gap between microseismic networks and passive seismic. First Break 26, 121-128.

Lacroix, P. and Helmstetter A. 2011. Location of seismic signals associated with microearthquakes and rockfalls on the Sechilienne Landslide, French Alps. Bulletin of the Seismological Society of America 101, 341-353.

Levy, C., Jongmans, D. and Baillet, L. 2011. Analysis of seismic signals recorded on a prone-to-fall rock column (Vercors massif, French Alps). Geophysical Journal International 186(1), 296-310.

Lindenmaier, F., Zehe, E., Dittfurth, A. and Ihringer, J. 2005. Process identification at a slow-moving landslide in the Vorarlberg Alps. Hydrological Processes 19, 1635-1651.

Lipman, P.W. 1976. Geologic map of the Lake City caldera area, western San Juan Mountains, southwestern Colorado: U.S. Geological Survey Miscellaneous Investigation Series Map I-962, scale 1:48,000.

Malet, J.-P., van Asch, Th.W.J., van Beek, R. and Maquaire, O. 2005. Forecasting the behaviour of complex landslides with a spatially distributed hydrological model. Natural Hazards and Earth System Sciences 5(1), 71-85.

Maquaire, O., Malet, J.-P., Remaître, A., Locat, J., Klotz, S. and Guillon, J. 2003. Instability conditions of marly hillslopes : towards landsliding or gullying? The case of the Barcelonnette Basin, South East France. Engineering Geology 70, 109-130.

Niethammer, U., James, M. R., Rothmund, S., Travelletti, J. and Joswig, M. 2012. UAV-based remote sensing of the Super-Sauze landslide: Evaluation and results. Engineering Geology (128), 2-11.

Parise, M. and Guzzi, R. 1992. Volume and shape of the active and inactive parts of the Slumgullion landslide, Hinsdale County, Colorado: U.S. Geological Survey Open-File Report 92-216, 29 p.

Peng, Z. and Gomberg, J. 2010. An integrated perspective of the continuum between earthquakes and slow-slip phenomena. Nature Geosciences (3), 599-607.

Roth, M., Dietrich, M., Blikra, L. H. and Lecomte, I. 2005. Seismic monitoring of the unstable rock slope at Åknes, Norway. NORSAR, Report for the International Centre for Geohazards.

Rubinstein, J.L., Shelly, D.R. and Ellsworth, W.L. 2010. Non-volcanic Tremor: A Window into the Roots of Fault Zones. in New Frontiers in Integrated Solid Earth Sciences (eds Cloetingh, S. & Negendank, J.), 287–314.

Schulz, W.H., McKenna, J.P., Biavati, G. and Kibler, J.D. 2009a Relations between hydrology and velocity of a continuously moving landslide – evidence of pore-pressure feedback regulating landslide motion?. Landslides 6, 181-190.

Schulz, W.H., Kean, J.W. and Wang, G. 2009b. Landslide movement in southwest Colorado triggered by atmospheric tides. Nature Geoscience 2, 12, 863-866.

Spillmann, T., Maurer, H., Green, A.G., Heincke, B., Willenberg, H. and Husen, S. 2007. Microseismic investigations of an unstable mountain slope in the Swiss Alps, Journal of Geophysical Research 112, B07301.

Tuffen, H., Dingwell, D.B. and Pinkerton, H. 2003. Repeated fracture and healing of silicic magma generate flow banding and earthquakes?. Geology 31, 1089–1092.

Varnes, D.J. and Savage, W.Z., eds. 1996. The Slumgullion earth flow: A large-scale natural laboratory. U.S. Geological Survey Bulletin 2130, 95 p.

Vidale, J.E. and Houston, H. 2012. Slow slip: A new kind of earthquake. Physics Today 65(1), 38-43.

Walter, M. and Joswig, M. 2008. Seismic monitoring of fracture processes generated by a creeping landslide in the Vorarlberg Alps. First Break 26, 131-135.

Walter, M., Niethammer, U., Rothmund, S. and Joswig, M. 2009. Joint analysis of the Super-Sauze (French Alps) mudslide by nanoseismic monitoring and UAV-based remote sensing. First Break 27(8), 75-82.

Walter, M. and Joswig, M. 2009. Seismic characterization of slope dynamics caused by softrock-landslides: The Super-Sauze case study. In: Malet, J.-P., Remaître, A., Boogard, T. (Eds), Proceedings of the International Conference on Landslide Processes: from geomorphologic mapping to dynamic modelling, Strasbourg, CERG Editions, 215-220.

Walter, M., Walser, M. and Joswig, M. 2011. Mapping Rainfall-Triggered Slidequakes and Seismic Landslide-Volume Estimation at Heumoes slope. Vadose Zone Journal 10(2), 487-495.

Walter, M., Arnhardt, C. and Joswig, M. 2012. Seismic monitoring of rockfalls, slide quakes, and fissure development at the Super-Sauze mudslide, French Alps. Engineering Geology 128, 12-22.

Walter, M., Gomberg, J., Schulz, W., Bodin, P. and Joswig, M. 2013. Slidequake generation versus viscous creep at softrock-landslides: synopsis of three different scenarios at Slumgullion landslide, Heumoes slope, and Super-Sauze mudslide. Journal of Environmental & Engineering Geophysics. 18(4), 269-280. doi:10.2113/JEEG18.4.269.

Wells, D.L. and Coppersmith, K.J. 1994. New empirical relationships among magnitude, rupture length, rupture width, rupture area, and surface displacement. Bulletin of the Seismological Society of America 84(4), 974–1002.

Wienhöfer, J., Lindenmaier, F., and Zehe, E. 2011. Challenges in Understanding the Hydrologic Controls on the Mobility of Slow-Moving Landslides. Vadose Zone Journal 10(2), 496-511.

Fernerkundung zur Detektion und zum Monitoring von Hangrutschungen

Thomas Lege und Michaela Frei

Bundesanstalt für Geowissenschaften und Rohstoffe
Fachbereich „Gefährdungsanalysen, Fernerkundung“
Stilleweg 2
30655 Hannover

E-Mail: thomas.lege@bgr.de; michaela.frei@bgr.de

1. Zusammenfassung

Hangrutsche zählen zu den schwerwiegendsten geologischen Gefahren, die die sozio-ökonomischen Gegebenheiten vieler Länder in Europa und weltweit bedrohen. Der Mensch und die Natur erhöhen gemeinsam die Gefährdung durch Hangrutsche. Die Klimaänderung hat in einigen Regionen die Niederschlagsintensität erhöht, und damit die Häufigkeit von Hangrutschen. Aber auch das Bevölkerungswachstum sowie die Besiedelung und wirtschaftliche Nutzung potentiell gefährdeter- Gebiete erhöhen die katastrophalen Auswirkungen von Hangrutschen.
Rasante Fortschritte der Erdbeobachtungstechniken haben den effektiven Einsatz für das Auffinden, die Kartierung, die Beobachtung und die Gefährdungsanalyse von Hangrutschen stark verbessert. Hangrutschungsanalysen profitieren sowohl von der optischen als auch von der Radar Fernerkundung. Luftbilder in Verbindung mit den neueren Generationen der hochauflösenden optischen Systeme wie World-View, Geo-EYE oder auch die Pliades Serie bieten 0,5 bis 2 m Bodenauflösung, wodurch hochauflösende Bestandsaufnahmen auch in quasi Echtzeit ermöglicht werden. Desweiteren können aus multispektralen optischen Daten die Geologie und Lithologie, Topograpie und Landnutzung abgeleitet werden. Eines der vielversprechendsten Felder der Radar Fernerkundung für das Monitoring von Hangrutschen ist die Entwicklung auf dem Gebiet der SAR Interferometrie zur Erfassung von Bewegungen der Erdoberfläche. Hier sind die differentielle SAR Interferometrie (DInSAR) und die multi-Interferogramme nutzende SAR Interferometrie (z. B.: PSInSAR, SBAS) zu nennen. Für die Detektion und das Monitoring von Hangrutschen werden zunehmend Satelliten gestützte Radardaten eingesetzt. Desweiteren werden für die Erfassung, Kartierung und das Monitoring von Hangrutschen bodengestütztes und flugzeuggetragenes LIDAR, flugzeuggestützte Geophysik und bodengestütztes InSAR (GB-InSAR) operationell eingesetzt. Die hier angesprochenen Fernerkundungsverfahren erweitern und ergänzen die Informationen geologischer Karten, digitaler Höhenmodelle (z.B. LIDAR) und bodenbasierter Datensätze für Hangrutschungsstudien außerordentlich.

2. Einleitung

„Alpentäler aber auch exponierte Landschaftsräume außerhalb des Alpenraumes, sind aufgrund der stark ausgebildeten Morphologie unterschiedlichsten Naturgefahren ausgesetzt. Neben Überschwemmungen, Lawinen und Muren sind vor allem Hangbewegungen wie Rutschungen, Felssturz und Steinschlag sowie Erdfälle zu diesen Gefahren zu zählen. Probleme mit Hangbewegungen treten grundsätzlich in allen Gebieten auf, in denen die geologischen und morphologischen Verhältnisse entsprechende Voraussetzungen bieten“ (STMUG, 2009). Zwischen 2004 und 2011 waren weltweit bei 3059 nicht durch Erdbeben verursachten Rutschungen 35.287 Tote zu beklagen. Werden die

durch Erdbebenverursachten Hangrutschungen hinzugerechnet, sind 84.341 Todesopfer zu zählen. Rutschungen, ausgelöst durch den Bau und Betrieb von Stauanlagen, kosteten 500 Menschenleben zwischen 2003 und 2012 (Petley, 2012; 2013).
Um das Inventar der Hangrutschungen auf europäischer Ebene zu aktualisieren werden neue methodische Ansätze diskutiert. Die Methoden verbinden konventionelle thematische Daten (e.g. topographische -, geologische Karten, Landnutzungskarten, und optische Fernerkundungsdaten) und Geländearbeiten mit Deformationsdaten abgleitet aus PSI (Persistent Scatterer Interferometry) Analysen (Abb. 1 & 2). Die Bearbeitungsskalen liegen im mittleren bis hohen Bereich (z.B. 1:100.000 bis 1:25.000 und 1.25.000 bis 1:5.000). Die Beiträge der PSI Methoden dienen u.a. der Erfassung von geomorphologischen Phänomenen, Veränderungen von Hangrutschgrenzen, Abschätzung der Geschwindigkeiten und Intensitäten (z. B. Bally, 2012; Calò et al., 2014; Cigna et al., 2012).
Das M_S 8.0 Wenchuan-Erdbeben am 12. Mai 2008 in China verursachte mehr als 60.000 Hangrutschungen. Nach Cui et al. (2011) entstanden dadurch 257 Dämme in Flüssen mit z. T. erheblicher Abflussleistung. Eine entsprechende Anzahl von Stauseen mit Wassertiefen von zum Teil über 100 m bildete sich. Um nach dem Beben eine schnelle Übersicht über die Risiken (Überflutung im Staubereich, Blockade von Rettungs- und Versorgungswegen, Stauseeausbruch,…) dieser Ereignisse zu erlangen, war die schnelle Erlangung und Interpretation von Fernerkundungsdaten erforderlich. Insbesondere waren Daten über die Zusammensetzung und die Höhe des Damms sowie die Länge der Stauseen von Bedeutung. Hiermit war das potentielle Überflutungsgebiet im Staubereich wie auch bei einem unkontrollierten Dammbruch abschätzbar. Auch für viele andere Zwecke konnte die umfangreiche fernerkundliche Datenaufnahme nach dem Erdbeben Erkenntnisse liefern, die zum einen die Rettungsmaßnahmen unterstützten und zum anderen zum besseren Verständnis derartiger Ereignisse beitragen. Eine anschauliche Zusammenstellung findet man bei Huadong (2010), der die Ergebnisse der Arbeiten des Projekt Teams „Remote Sensing Monitoring and assessment of the Wenchuan Earthquake“ dokumentiert.
Im folgenden Beitrag werden fernerkundliche Verfahren, die zum Detektieren und Monitoring auch von weniger offensichtlichen Massenbewegungen geeignet sind, vorgestellt. Ein besonderer Schwerpunkt liegt auf der Radarinterferometrie.
Es ist immer notwendig, die mit der Fernerkundung gewonnenen Aussagen am Boden zu verifizieren und zu ergänzen. Im Rahmen dieses „ground truthing“ setzt man verschiedene terrestrische Verfahren zur Vermessung von Hangrutschungen und ihren Bewegungen ein. Auch diese werden vorgestellt. Anwendungsbeispiele veranschaulichen das Einsatzspektrum der vorgestellten Verfahren.

3. Fernerkundliche Verfahren

3.1 Definition der Fernerkundung

Die Fernerkundung (Remote Sensing) liefert Mess- bzw. Beobachtungwerte über Gegenstände, die nicht unmittelbar berührt werden müssen. Diese Information liefert in erster Linie die elektromagnetische Strahlung, die von einem Objekt reflektiert oder abgestrahlt wird. Es sind Definitionen derart zu finden, dass zur Fernerkundung nur Verfahren zählen, deren Messeinrichtungen in fliegendem Gerät (Flugzeuge, Hubschrauber, Raumstationen, Satelliten) installiert sind (Albertz, 2009), andere heben darauf ab, dass das Messgerät sich nicht zwangsläufig in einem Fluggerät jedoch in einer gewissen Entfernung vom Objekt befindet. Letztere Erweiterung ist die hier angenommene Definition. Weitere Variationen dieser Ansätze sind bei Campbell und Wynne (2011) aufgelistet.

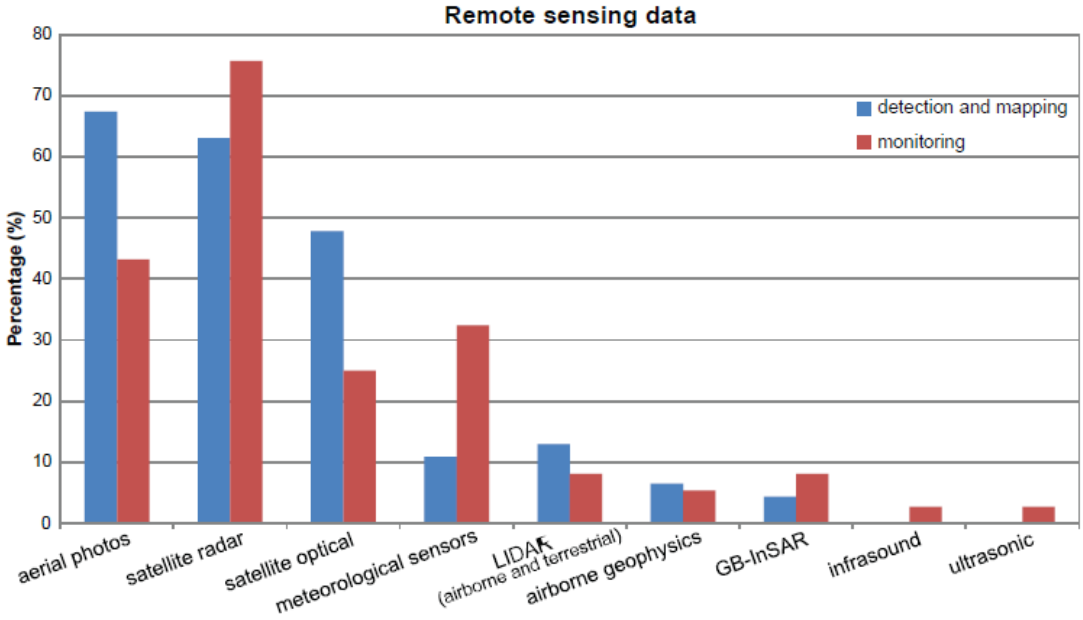

Abbildung 1: Nutzung von Fernerkundungsdaten in Hangrutschungsanalysen (Tofani et al., 2013a)

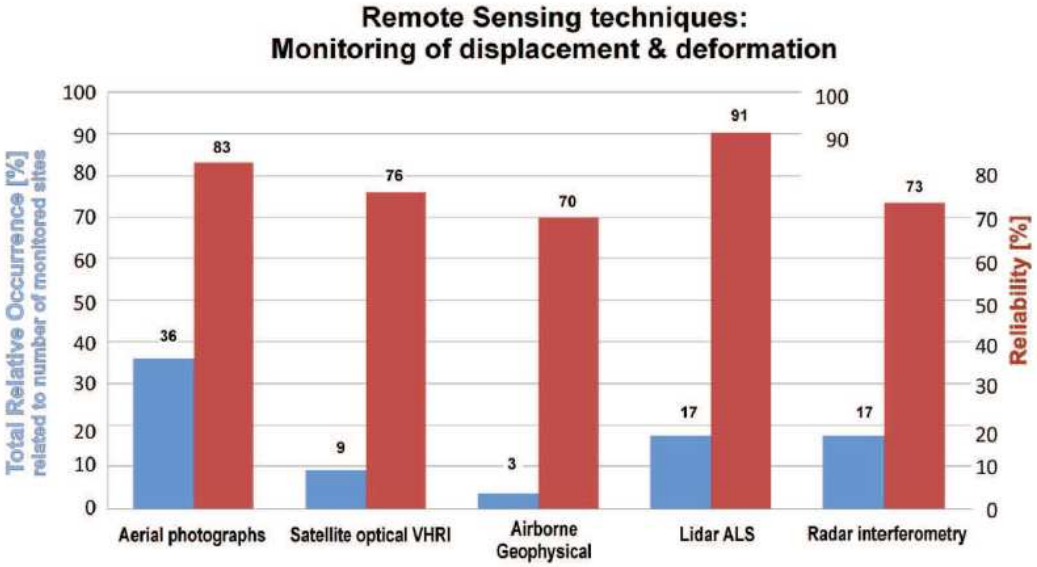

Abbildung 2: Anzahl der untersuchten Hangrutsche und Zuverlässigkeit der Untersuchungsmethoden (Baron und Supper, 2013).

3.2 Luftbildanalyse

Neben den offensichtlichen Narben frischer Rutschungen im Gelände (Huadong, 2010) können nach Wendel und Wehinger (2011), weitere typische Merkmale einer Hangbewegung angegeben werden:

- Morphologische Merkmale: Mulden, Senken, Wülste, Abrisskanten, Verebnungsflächen.
- Hydrogeologische Merkmale: Nassstellen, Quellen.

- Biologische Merkmale: Säbelwuchs und Schiefstellung von Bäumen, Wurzelabrisse.
- Auffälligkeiten an Bauwerken: schief gestellte Mauern, Bordsteine und Pfosten, Risse und Verkippungen von Gebäuden, Absackungen an Straßen.

Viele dieser Merkmale lassen sich bereits an Hand geeigneter, ggf. stereoskopischer Luft- oder Satellitenbilder kartieren (Albertz, 2009) und Hangrutschungsinventare erstellen (z. B.: Moosavi et al., 2014; Couture und Riopel, 2008). Stehen historische Bilder zur Verfügung lässt sich die zeitlich Entwicklung des Untersuchungsgebietes ableiten (z.B. Finkler et al., 2013). Durch photogrammetrische Bearbeitung nacheinander aufgenommener Luft- oder Satellitenbilder werden Geschwindigkeitsfelder der Oberfläche von Hangrutschungen sichtbar (z. B.: Debella-Gilo und Kääb, 2011; 2012). Joswig und Rothmund (2013) setzen hierfür mit Kameras ausgerüstete Drohnen (Unmanned Arial Vehicles: UAV) ein.

3.3 Flugzeuggestütztes Laserscanning (LiDAR)

Die auf dem inzwischen routinemäßig in Befliegungskampagnen mit dem Verfahren Light Detection and Ranging (LiDAR) bzw. flugzeuggestütztem (Airborne) Laserscanning (ALS) aufgenommenen Geländemodelle weisen Rasterweiten von bis zu wenigen Dezimetern bei absoluten Höhengenauigkeiten in der Größenordnung von 10 Dezimeter mit Höhenauflösungen bis zu 1 cm auf. Weitgehend automatisierte Prozesse erlauben die Aufnahme großer Gebiete mit hoher Punktdichte. So existieren von zahlreichen Bundesländern auf der Basis dieses Verfahrens erstellte Digitale Gelände Modelle (DGM). Grundsätzlich ist das Messprinzip dem eines Echolots vergleichbar. Lichtimpulse werden ausgesandt und die Laufzeit bis zur Rückkehr Ihrer Reflexion an der Erdoberfläche gemessen. Aus den genau bekannten Lagekoordinaten des Fluggerätes und der Laufzeit wird die Geländehöhe berechnet. Idealerweise fließen die bekannten Höhen von Kalibrierflächen (z.B. Sportplätze, Parkplätze, Straßen, …) in das resultierende DGM ein. Zum weiteren Studium des Messprinzips kann beispielsweise Campbell and Wynne (2011) zur Hand genommen werden.
Rutschungsgebiete können an typischen morphologischen Merkmalen wie unruhige Oberflächenstrukturen erkannt werden. Abrisskannten und Akkumulationsgebiete sind oft deutlich erkennbar (Bock et al., 2013). Über Differenzberechnungen nach Wiederholungsbefliegungen lassen sich Rutschmassen ableiten (Fredel und Jany, 2013).

3.4 Radarinterferometrie

Das Prinzip des “Synthetic Aperture Radar” (SAR) ist eine Technik die hochauflösende Radardatensätze (Amplitude und Phase), aufgenommen von einem zur Seite schauenden (side looking) Radarsensor vom Flugzeug oder Satelliten, generiert. Die Amplitude eines SAR Bildes stellt die Streuungscharakteristiken der Oberfläche dar, die Phase hingegen ist eher regellos, da sie das gewichtete Mittel der Phasenverzögerung zwischen Senden und Empfangen für alle Streuer am Boden innerhalb der Auflösungszelle beinhaltet. Die Phasenunterschiede zwischen zwei Aufnahmen desselben Objektes aus leicht unterschiedlichen Betrachtungswinkeln können als Änderungen in Range Richtung zwischen Instrument und Oberfläche interpretiert werden, solange die Streueigenschaften der Oberfläche unverändert sind (Kohärenz). SAR Interferometrie ist der Prozess bei dem ein SAR Bild mit den Daten eines zweiten SAR Bildes, aufgenommen zur gleichen Zeit aus unterschiedlichen Orbitpositionen, multipliziert wird. Das Ergebnis ist ein „Interferogram“, dessen Phase die Phasendifferenz zwischen den Eingabebildern repräsentiert. Wie bei der Stereoskopie optischer Bilder dient dieses Ergebnis auch der Erstellung von Digitalen Geländemodellen (DGM). Ist es das Ziel Oberflächenbewegungen zu beobachten müssen Bilder zu unterschiedlichen Zeiten aus derselben Orbitposition aufgezeichnet werden. Das Phasensignal repräsentiert dann die Oberflächenbewegungen in Blickrichtung (line of sight: LOS), die zwischen den einzelnen Aufnahmen aufgetreten sind. Bei der differentiellen SAR Interferometrie (DInSAR) wird die Topographie-Phase vom Interferogram abgezogen um

eine Bewegungskarte zu erhalten (Hooper et al. 2012). Um geringfügige Bewegungen zu erfassen sollten lange Zeitreihen von SAR Datensätzen analysiert werden.
Die grundlegende Begrenzung für InSAR Anwendungen ist für die meisten Sensoren das Rauschen in der Phaseninformation, verursacht durch eine Änderung der Streueigenschaften an der Oberfläche. In einem SAR Bild sind die Amplitude und Phase für jedes Pixel die kohärenten Summenanteile aller Streuer innerhalb der Bodenauflösungszelle. Eine relative Bewegung dieser Streuer oder eine Änderung des Blickwinkels verursacht, dass die Summenanteile der Streuer in den Datensätzen nicht gleich sind, ein Effekt der als Dekorrelation bekannt ist (Hooper et al. 2012). Eine Auswertung von Bewegungsraten ist dann oft nur durch entsprechendes Filtern oder sog. „Multilook" Verarbeitungen möglich, was aber in den meisten Fällen zu Lasten der Auflösung geschieht.
Um die Grenzen der konventionellen InSAR Analysen zu überwinden, wurden Algorithmen für die Zeitreihenanalysen von SAR Daten entwickelt. Die erste Entwicklung in der Reihe der „Persistent Scatterer Interferometrie" (PSI) war der PSInSAR Algorithmus. Dieser zielt darauf kohärente Radar Ziele zu identifizieren, die über den gesamten Beobachtungszeitraum eine hohe Phasenstabilität aufweisen. Radar Zielobjekte, die nur schwach von temporaler und geometrischer Dekorrelation betroffen sind, entsprechen oft punktförmigen Streuern mit hohen Rückstreuwerten etwa durch zweiflächige Reflektion oder deterministische Streuung. Anthropogene Strukturen, aber auch Felsblöcke und Geländeaufschlüsse können gute „Permanent Scatterer" (PS) darstellen. Die für natürliche Objekte abgeleiteten Zeitreihen der Bewegungen, sind allerdings häufig durch eine eher geringe räumliche Verteilung der Messpunkte in diesem Fall (< 10 PS/sqkm) begrenzt, im Vergleich zu den PS Dichten in städtischen Gebieten (> 100 PS/sqkm für multi-temporale C-Band Satelliten Daten) (Ferretti et al., 2011).
Die PSInSAR Technik bietet den Vorteil die Deformation direkt mit einem Streuer zu verbinden, und nicht nur mit einer durch das Radarsystem vorgegebenen Auflösungszelle. Dies ermöglicht eine relativ hohe Beobachtungsauflösung und eine Differenzierung der Deformationen in Abhängigkeit vom jeweiligen PS. Die Genauigkeiten sind abhängig vom Sensor, der Anzahl der Datensätze, dem Zeitraum, der Entfernung vom Referenzpunkt und der Kohärenz der PS. Im Falle einer linearen Deformation kann eine Genauigkeit besser als 1mm/Jahr erreicht werden (Adam et al., 2009). In Regionen ohne Streuer werden Radarreflektoren, sog. Cornerreflektoren, im Gelände installiert und auf den jeweils gewählten Satelliten ausgerichtet (z. B.: Busch und Schäfer, 2013; Singhroy et al., 2010; Froese et al. 2008).
Schäfer (2012a, b) untersucht den Einfluss der Atmosphäre auf die Messungen von Höhenänderungen mit der differentiellen Radarinterferometrie. Busch und Schäfer (2013) zeigen mittels einer technisch herbeigeführten genau definierten Höhenänderung von Corner-Reflektoren in einem Gebiet mit sonst hohen zeitlichen Dekorrelationen, dass auf der Grundlage von ENVISAT-Daten und der PSI-Methode die Erfassung von Höhenänderungen mit einer Standardabweichung von 2 mm möglich ist.
Das Ergebnis einer großangelegten InSAR Validierungsanalyse erbrachte einen mittlerer RMS Fehler für einzelne ERS 1/2 und ENVISAT Messungen der zwischen 4 und 6 mm lag (Strozzi et al., 2010). Singhroy et al. (2011) stellt den Einsatz der satellitengestützten Radarinterferometrie in Kanada inkl. einer Tabelle von Radarsatelliten vor.
Der zweite sehr häufig angewendete PSI Ansatz ist der sogenannte „Small Baseline Subset" SBAS Algorithmus, der es ermöglicht die räumliche und zeitliche Dekorrelation zu reduzieren. Der SBAS wertet zwei DInSAR Datensätze mit kleiner räumlicher und zeitlicher Basis (Baseline) zwischen den einzelnen Satelliten Orbits aus. Es wird eine optimierte Auswahl von zuverlässigen kohärenten Punkten angestrebt um zeitlich dichte Langzeit Deformationsdaten zu erzeugen. Außerdem ist es auf der SBAS Analyse basierend möglich, Deformationsdaten in niedriger und hoher räumlicher Auflösung zu produzieren, also auf lokaler und globaler Skala. Mit SBAS können Multisensor SAR Daten, aufgenommen mit unterschiedlichen Systemen bei gleicher Beleuchtungsgeometrie (ERS-1/2 und ENVISAT), gemeinsam prozessiert werden. Dies eröffnet die Möglichkeit sehr lange Zeitreihen Deformationen aus der Vielzahl der verfügbaren SAR Daten zu berechnen (Casu et al.,

2006). Aktuelle Anwendungen liefern Sansosti et al. (2014) und Bovenga et al. (2012). So lieferte das Prozessing von Daten verschiedener Satelliten mit dem SBAS-Verfahren Deformationsgeschwindigkeitskarten von Rustschungen bei Assisi über einen Zeitraum von 18,6 Jahren (Calò et al. 2014, vgl. Anwendungsbeispiele).
Die satellitengestützte Radarinterferometrie ist unter bestimmten Randbedingungen sehr gut geeignet, durch Hangrutschungen gefährdete Areale zu detektieren und zu monitoren. Einschränkungen in der Anwendbarkeit sind auf die Landnutzung bzw. Landbedeckung, die Neigung des Hanges relativ zur Blickrichtung (LOS) des Satelliten, das verwendete Radar-Band und die Umlaufdauer des Satelliten, d.h. die Wiederholrate der möglichen Aufnahmen und damit die Bewegungsgeschwindigkeit der Rutschmasse zurückzuführen. Insbesondere die Fähigkeit auf regionaler Basis sehr langsame Bewegungen zu messen liefert wertvolle Beiträge in der Prävention von Hangrutschungsgefahren. Diese Bewegungen sind oft zu gering, um sie großräumig mit terrestrischen Methoden aufzuspüren (z. B.: Zhao et al., 2012; Oppikofer, 2012; Singhroy, 2011; Singhroy, 2009; Corsini, 2006). Für gesetzlich und behördlich vorgeschriebene Aufgaben in Deutschland, insbesondere im Bergbau, bietet DMV (2013) Orientierung beim Einsatz von satellitengestützten Verfahren der Radarinterferometrie.

4. Terrestrische Verfahren

Die Interpretation fernerkundlich gewonnener Ergebnisse erfordert Verifizierung, Absicherung und Ergänzung der Datensätze am Boden, das „ground truthing“. Hier kommen neben anderen geologischen und geophysikalischen Verfahren geodätische und bodengestützte fernerkundliche Verfahren zum Einsatz.

4.1 Höhenmessungen; Nivellement

Bei Höhenmessungen werden relative Höhenunterschiede oder absolute Höhen bestimmt. In der Praxis werden abhängig von der Aufgabenstellung unterschiedliche Verfahren bzw. Messsysteme wie Schlauchwaagenmessungen, Nivellierinstrumente, Rotationslaser und Digitalnivelliere eingesetzt. Es lässt sich unterscheiden zwischen einfachen Nivellements mit Genauigkeiten von 5-10 $mm*km^{1/2}$, Ingenieurnivellements mit Genauigkeiten von 2-3,5 $mm*km^{1/2}$ und Feinnivellements 0,3-0,5 $mm*km^{1/2}$ (z. B.: Großmann, 1976; Schneider, 2008; ADV, 2009). In der Markscheiderbergverordnung (MarkscheidBV, 1998) sind die Klassen I, II und III mit Genauigkeiten von 2, 3, und 10 $mm*km^{1/2}$ definiert.
Bei den Nivellements zur Bestimmung der Bewegung der Vulkanflanken des Kilauea zwischen 1983 und 1991 wurden Genauigkeiten durch systematische Betrachtung und Beseitigung von Fehlereinflüssen auf den Messvorgang (vgl. ADV, 2009) von zunächst 7 $mm*km^{1/2}$ im Jahr 1982 auf 2 $mm*km^{1/2}$ im Jahr 1988 reduziert (Delaney et al., 1994).

4.2 Satelitengeodätische Vermessung

GNSS (Global Navigation Satellite Systems) ist der generelle Ausdruck für Satellitennavigationssysteme zur Orts- und Zeitbestimmung und Navigation wie das amerikanische GPS, das russische GLONASS oder das europäische System Galileo. D (differential)GNNSS – bestehen aus Receivern, die an festen Positionen das GPS-Signal empfangen und Rovern, mit denen die Messpunkte aufgenommen werden. Ein Rover bestimmt seine Position mit Hilfe der Receiver und dem GPS-Signal. Grundlegende Informationen zur Funktionsweise von dGNSS finden sich beispielsweise in BfG (2007) oder Korritke (2000). Finkler et al. (2013) nehmen in einer dGPS-Feldkampagne auf einer ca. 15 ha großen Weinbaufläche knapp 6.000 Messpunkte auf. Auf dem entstehenden Mikrorelief werden bei entsprechender Beleuchtung die typischen morphologischen Muster von Massenbewegungen sichtbar. Wiederholungsmessungen über eine geeignete Zeitspanne erlauben die Berechnung von Verschiebungsraten und -richtungen. Nach Oppikofer et al. (2013) kann die Genauigkeit der Positionsbestimmung σ_i bei 1 mm/a in der

Horizontalen und 2 mm/a in der Vertikalen erreichen. Im praktischen Einsatz beim Norwegischen Geologischen Dienst (NGU) werden Werte angenommen, die 2- bis 3-mal höher sind. Böhme et al. (2013) geben für ihre Studie den durchschnittlichen Bewegungsfehler $3\sigma_m$ zwischen 0,6 bis 2,6 mm/a in horizontaler und 1,1 bis 3,9 mm/a in vertikaler Richtung an. Nach Strozzi et al. (2010) beträgt die Standardabweichung in der Positionsbestimmung weniger al 1 cm in der Horizontalen und weniger als 2 cm in der Vertikalen.

4.3 Distanzmessungen

Häufig kommen beim Monitoring von Hangrutschungsarealen Tachymeter (Total Stationen) zum Einsatz. Die Geräte senden einen Laserimpuls (oder andere elektromagnetische Strahlung), der zwischen den Endpunkten der zu messenden Strecke hin- und herläuft. Am Endpunkt der zu messenden Strecke ist ein Reflektor erforderlich. Als Reflektoren werden meist Tripelprismen, Glaskörper mit drei aufeinander senkrecht stehenden Flächen, verwendet. Ein Lichtstrahl, der auf ein Tripelprisma fällt, wird streng parallel zu sich selbst zurückgeworfen, wenn die Achse des Prismas nicht mehr als 10 bis 20 gon von der Lichtrichtung abweicht (Prinzip des Katzenauges) (z. B. Großmann und Kahmen, 1983). Von einem Tachymeterstandort können zahlreiche Reflektorpositionen automatisch vermessen werden (Cardellini und Osimani, 2008, Blikra et al. 2013). Aufgezeichnet werden Laufzeit und zwei Winkel. Die Laufzeit ist das Maß für die durchlaufene Wegstrecke. Delaney et al. (1994) diskutieren Einflüsse des Luftdrucks und der Temperatur entlang langer Messpfade.

4.4 TLS Terrestrisches Laserscanning LiDAR

Im Unterschied zur Tachymetrie, bei dem die Bewegung diskreter Punkte gemessen wird, werden von einem Terrestrischen Laserscanner (TLS) Oberflächen in Form von diskreten Punktwolken erfasst. Innerhalb vergleichsweise kurzer Zeiträume lassen sich Objekte mit hoher Genauigkeit durch Punktraster mit geeigneten Abständen aufnehmen. Das Messprinzip entspricht dem weiter oben dargestellten LiDAR-Verfahren des Airborne Laserscannings. Die kartesischen Koordinaten jedes Messpunkts werden aus den Messwerten von zwei Winkeln und einer Strecke abgeleitet. Darüber hinaus kann die Intensität des reflektiertieren Laserimpulses als Maß für die Reflektivität des vermessenen Objektes aufgenommen werden. Laut Hebel et al. (2013) liegen die 3D-Punktgenauigkeiten aktueller Instrumente für Zielweiten unter 100 m bei ca. 2 mm bis 6 mm. Mit wiederholten Messungen desselben Hangrutsches lassen sich Deformationen detektieren und Volumenbilanzen erstellen (z.B. Ohlmann-Lauber, 2012). Beispielhafte Anwendungen an natürlichen Hangrutschungen finden sich unter anderem bei Kuhn und Prüfer (2014), Travalletti et al. (2013), Haas et al. (2012), Morche et al. (2008) oder Luzi et al. (2006). Erfahrungen praktischer Einsätze im Braunkohletagebau legt Reetz (2013) dar. DMV (2009) bietet Orientierung bei der Verwendung von Laserscann-Messungen für gesetzlich und behördlich vorgeschriebene Aufgaben insbesondere im Bergbau.
LiDAR-Systeme können Erfassungsraten von mehr als einer Million 3D Punkte pro Sekunde erreichen. Sie werden auch auf Land- und Wasserfahrzeugen installiert, so dass Messungen von einer Straße oder einem Gewässer aus durchgeführt werden können. Verwendungen im Zusammenhang mit Hangrutschungen sind den Autoren jedoch (noch) nicht bekannt.

4.5 Bodengestützte Radarsysteme

Die bodengestütze Radarinterferometrie (Ground Based Interferometric Synthetic Aperture Radar: GB-SAR, GB-InSAR oder GB-Radar) wird von einem festen Standpunkt ausgeführt. Grundsätzlich gelten dieselben Mess- und Auswerteansätze wie bei der satellitengestützten Radarinterferometrie. Bewegungen der Oberfläche eines Hangrutsches können über eine Distanz von mehreren Kilometern mit einer hohen Genauigkeit (Standardabweichungen von 1/10 mm bis 1 mm) gemessen werden (Rödelsperger, 2011, Hebel et al. 2013). Beispiele der Messung von Hangrutschungsbewegungen mit GB-SAR sind bei Luzi et al. (2006) und Corsini et al. (2006) zu finden. Noferini et al. (2006) vergleicht die Ergebnisse mit den Daten

von GPS-Stationen. Teza et al. (2008) und Hebel et al. (2013) setzen sowohl TLS wie auch GB-SAR vergleichend ein. Es wird dargelegt, dass die beiden Systeme ein sehr detailliertes geometrisches Modell der Oberfläche eines Hangrutsches liefern können, welches die Basis für weitere Ursachenforschung beispielsweise mit numerischen Modellen sein kann.

4.6 Bohrlochsysteme

Die genannten Systeme liefern (Bewegungs-) daten von der Oberfläche. Die Verteilung der Bewegungen im Rutschkörper kann mit verschiedenen Sensoren in Bohrlochsystemen differenziert aufgenommen werden. Bohrlöcher, die Hangrutschungskörper durchörtern, verformen sich in Abhängigkeit von der Bewegung des Rutschkörpers. Mit speziellen Bohrlochsonden lassen sich diese Verformungen messen.
Die Firma CSG stellt Verlagerungsmodule - sogenannte Differential Mulitparametric Systeme (DMS®) - her, um die Verlagerung bzw. Deformation von Bohrlöchern zu messen. In flexibel miteinander verbundenen, jeweils ca. 1 m langen Bohrlochsonden sind je nach Ausführung Inklinometer, Piezometer, Extensometer, Beschleunigungsaufnehmer, Temperatursonden und digitale Kompasse installiert (vgl. z. B.: Blikra et al., 2013; Cardellini und Osimani, 2008). Ein Gesamtsystem kann bis 120 m lang sein. Crosta et al. (2013) stellen den Zusammenhang zwischen einem Monitoring mit Bohrloch-DMS, GB-InSAR sowie Distanzmessungen und der Modellierung von Hangrutschungsprozessen mit Finite-Elemte-Verfahren dar. Sie gehen dabei auf die verschiedenen Auflösungen und Zeitskalen der unterschiedlichen Messsysteme ein. Sie arbeiten den zusätzlichen Erkenntnisgewinn durch die Beobachtung desselben Bewegungsphänomens an der Oberfläche und im Hangrutschungskörper mit sich ergänzenden Messverfahren heraus. In Calò et al. (2014) werden Modellierungen mit dem oberflächlichem Geschwindigkeitsfeld und den Ergebnissen von Bohrlochinklinometern verifiziert.

5. Anwendungsbeispiele

5.1 Ancona – Living with Landslides

Das Monitoringsystem eines Hangrutsches bei Ancona/Italien besteht aus einer Kombination von acht motorisierten Tachymetern, 34 GPS-Antennen, 33 biaxialen Neigungsmessers und drei 86 m lange in ca. 100 m tiefen Bohrlöchern installierten Verlagerungsmodulen (DMS). Die Tachymeter zielen zur Abstandsbestimmung mehr als 230 festinstallierte Tripelspiegel automatisch an. Alle Messungen werden unmittelbar über ein Netzwerk in eine 24 Stunden besetzte Zentrale übertragen. Im Falle von Messergebnissen, die auf eine Aktivierung des Hangrutsches hinweisen, wird nach Durchlaufen mehrerer Validierungsschritte Alarm ausgelöst und innerhalb von 30 Minuten der Evakuierungsplan in Gang gesetzt (Cardellini und Osimani, 2008 und 2012; Cardinaletti et al. 2011).

5.2 Aknes und Mannen Felsrutschungen in West Norwegen

Das Risiko großer Hang- oder Felsrutschungen ist in Norwegen sowohl für Dammprojekte und als Auslöser für Tsunamis in Fjorden ein lange diskutiertes Thema. Die Erfassung, das Monitoring und die Frühwarnsysteme für die Hang- und Felsrutschgebiete sind vor diesem Hintergrund in nationalen Normen festgelegt. So liegen z.B. die Vorwarnzeiten bei unter 72 h und die Evakuierungszeit bei max. 12 h. Es muss ein tägliches kontinuierliches Monitoring gewährleistet sein, durch die Messung von Bewegungsraten mit an ein Echtzeit Monitoring gekoppeltes Frühwarnsystemen. Die Gebiete Aknes und Mannen sind mit 4 Bohrlöchern mit DMS Systemen versehen (Differential Monitoring of Stability). Die Systeme sind 100 bis 120 m lang und mit bis zu 245 Sensoren versehen, bestehend aus biaxialen Inklinometern, Temperatursensoren, sowie Piezometern und digitalen Kompassen, um die internen Deformationen der Rutschungsmassen, den Wasserdruck und die Temperaturbedingungen zu dokumentieren. Diese Daten sind die kritischen Parameter in einer Akzelerations Phase (Blikra et al., 2013).

5.3 Verbicaro Nord Calabrien (Italien)

Die Gemeinde von Verbicaro ist als ein Gebiet mit sehr hohem hydrogeologischem Risiko klassifiziert, ermittelt auf der Basis der Auswirkungen für die Siedlungen, die Gewerbebetriebe und die Bevölkerung, was nach dem italienischem Gesetzes Dekret 180/89 eine dringende Maßgabe für Risiko Prävention bedeutet. Innerhalb des Gebietes sind 24 Hangrutsche kartiert. Die wichtigsten Rahmenparameter für den Einsatz der Persistent Scatterer Interferometry (PSI) Methode sind die Erfassung der Aktivitäten und Intensitäten dieser langsamen bis sehr langsamen Bewegungen dieser Hangrutsche. Die Herausforderung in dieser Region liegt u.a. im Fehlen von eindeutigen PS Objekten innerhalb der Hangrutschgrenzen. Es wurden ERS-1/2 und RADARSAT-1/2 PSI Daten von 1992-2011 ausgewertet, die auf die maximale Hanglänge hochgerechnet wurden. Die Methode erlaubt es den Status der Aktivität und die Intensitäten für 13 der 24 kartierten Hangrutsche zu bewerten. Derzeitige Grenzen liegen in der Charakteristik und räumlichen Abdeckung der PSI Daten. Es konnten jedoch 2 neue Phänomene in den Jahren 2010 und 2011 aufgezeigt werden. Für die restlichen Hangrutsche konnten die in 2007 erfassten Aktivitäten bestätigt werden. Die Intensitäten der Bewegungen können in „sehr langsam“, „langsam“ und „zu vernachlässigend“ klassifiziert werden. Die wichtigsten Ergebnisse dieser Untersuchung waren die Erfassung der Haupteinflussfaktoren auf die PSI Auswertung, wie das Fehlen von PS Objekten innerhalb der Hangrutschgrenzen, die zeitliche Abdeckung der verfügbaren Daten und die Notwendigkeit der Geländeuntersuchungen und die Validierung, ebenso wie die operationellen Prozeduren um die Schwellwerte zu definieren, die mit ±5 mm/Jahr für die Aktivitäten und für die Intensitäten zwischen extremen und sehr langsamen Phänomenen bei 16 mm/Jahr liegen. Letztere wurden um 20% reduziert, um den zeitlichen und räumlichen gemittelten Bewegungsraten Rechnung zu tragen, und den einzelnen Hangrutschen repräsentative Geschwindigkeiten zuzuweisen. Räumlich und zeitlich hochauflösende Daten der neuen Satellitengenerationen ebenso wie weitere Entwicklungen in der PS Prozessierung werden die Einsatzmöglichkeiten der PSInSAR Daten für die hier diskutierten Hangrutschanalysen weiter verbessern (Cigna et al., 2012).

5.4 Aletschwald Region (Schweiz)

Im Rahmen diese Anwendung werden unterschiedliche Verfahren für das Hangrutsch Monitoring im Überblick beschrieben und ihre Genauigkeit diskutiert.
Im Aletschwald wurden die Verlagerungen innerhalb eines instabilen Hanges zwischen 1976 und 2008 mit Hilfe von Luftbildern, SAR Interferometrie und dGPS beobachtet. Die Beobachtungsreihe beruht auf Daten der ERS‐1, JERS, ERS‐2, Envisat, ALOS und TerraSAR‐X Satelliten, differentialen GPS Messungen, die im Vergleich mit wiederholten Luftbildbefliegungen und Interpretationen ausgewertet wurden. In der ersten Phase (2002) wurden InSAR Daten zur Erfassung der instabilen Hänge mit einer groben Abgrenzung des Ausmaßes und der Bewegungsgeschwindigkeiten ausgewertet. Nachdem sich die detektierten Bewegungsraten in den InSAR Daten erhöhten (2007), wurde die zeitliche Entwicklung der Bewegungen mit DGPS und ADP (Airborne Digital Photogrammetry) zusätzlich zu InSAR evaluiert. Für die zukünftige Beobachtung der Massenbewegungen im Aletschwald werden jährlich DGPS Daten und Luftbilder im Bereich der Großen Aletsch Gletscherzunge, zusammen mit Envisat ASAR, ALOS PALSAR, and TerraSAR‐X InSAR Daten ausgewertet. Sollten zeitlich dichtere Beobachtungsreihen aufgrund einer Intensivierung der Bewegungen notwendig werden, werden zusätzlich Extensiometer oder GB-InSAR Messungen eingesetzt (Strozzi et al., 2010).

5.5 Ivancich Hangrutsch/ Assisi (Italien)

Der Hangrutsch in der Region Assisi ist durch Untersuchungen vor Ort gut bekannt. Es wurde untersucht in wieweit sich DInSAR Techniken für Erfassung, das Monitoring und die Modellierung der Bewegungsabläufe eines sich langsam bewegenden aktiven Hangrutsches in urbaner und sub-urbaner Umgebung eignen. Für die Langzeitbeobachtung wurden große Serien von SAR Daten herangezogen: C-Band Daten des ERS-1/2 und Envisat (April 1992 bis November 2010) und X-Band SAR Daten des Cosmo-SkyMed (CSK) (Dezember 2009 bis Februar 2012). Als DInSAR Technik für diesen multisensoralen Datensatz wurde SBAS verwendet um die Bewegungsdaten in voller Auflösung zu berechnen. Durch die hohe Auflösung der Daten und die lange Zeitreihe von über 18 Jahren konnte das Verhalten des Hangrutsches und seine interne Dynamik sehr genau erfasst werden. Die CSK Daten sind durch eine hohe Wiederholungsrate und höhere Auflösung gegenüber den ERS und Envisat Daten gekennzeichnet, und diese Parameter resultieren in einer 15 Mal höheren PS Punktdichte. Zusammen mit den traditionellen geologischen und geotechnischen Informationen konnten die Bewegungscharakteristiken und -entwicklungen des Hangrutsches sehr genau erfasst werden. Die DInSAR Messungen wurden mit den Messungen an zwei Inklinometern ergänzt und ergaben ein quasi lineares Verhalten für die Hangrutschbewegungen über den Zeitraum von mehr als 18 Jahren. Die Geschwindigkeiten überschritten lokal 8 mm/Jahr. Durch den Einsatz der DInSAR Bewegungsdaten konnten die Bewegungscharakteristiken über einen sehr langen Zeitraum detailliert erfasst und modelliert werden (Calò et al., 2014).

6. Zusammenfassung

Zusammenfassend wird festgestellt, dass die hier vorgestellten Boden-, Luft- und Weltraum-gestützten Verfahren für die Detektion und das Monitoring von Hangrutschungen sehr gute, sich ergänzende Datensätze liefern (Strozzi et al., 2010). Zurzeit zeichnen einige Radar Satelliten Daten auf, die Bewegungsdaten, basierend auf u.a. DInSAR, PSInSAR und SBAS Auswertungen, liefern können. Dies sind der Envisat der ESA, der kanadische Radarsat-1 und 2, der deutsche TerraSAR-X und der italienische Cosmo-SkyMed, sowie die im März 2014 startenden Missionen der Sentinel Serie (Hooper et al., 2012).
Die Beurteilung von Oberflächenveränderungen an Hangrutschen ist oftmals die effektivste Methode um die Bewegungsmuster, aber auch die auslösenden Faktoren zu erfassen. PSI Datensätze sind ein schlagkräftiges Instrument um Bewegungsraten in Hangrutschen zu messen, da sie einen synoptischen Blick und eine Wiederholung in unterschiedlichen Zeitintervallen und unterschiedlichen Skalen erlauben. In vielen Fällen, hier sind u.a. Italien, Norwegen und die Schweiz zu nennen, sind PSI Daten schon in die Beobachtungsstrategien aufgenommen, da die gemeinsame Nutzung von Satelliten- und Bodendaten die Entdeckung und geologische Interpretation von Hangrutschen erleichtert und ein besseres Verständnis der Hangrutschgeometrien und Bewegungsabläufe erlaubt (Tofani et al., 2013b).

7. Literatur

Adam, N., Parizzi, A., Eineder, M., Crosetto, M., 2009: Practical persistent scatterer processing validation in the course of the Terrafirma project.- Journal of applied Geophysics, 69, 59-65.

ADV, 2009: Feldanweisungen für die Präzisionsnivellements zur Erneuerung und Wiederholung des Deutschen Haupthöhennetzes (DHHN) im Zeitraum 2006 bis 2011.- AK Raumbezug, 3. überarbeitete Fassung vom 1.8.2009, 47 S. (www.adv-online.de)

Albertz, J., 2009: Einführung in die Fernerkundung, 4., aktualisierte Auflage.- WBG, Darmstadt, 254 S.

Bally, P., Ed., 2012: Scientific and technical Memorandum of The International Forum on Satellite EO and Geohazards.- ESA, 21-23 May 2012, Santorini, Greece, 164 S. http://esamultimedia.esa.int/docs/EarthObservation/Geohazards/esa-geo-hzrd-2012.pdf, doi:10.5270/esa-geo-hzrd-2012,

Baron I., Supper, R., 2013: Application and reliability of techniques for landslide site investigation, monitoring and early warning – outcomes from a questionnaire study. - Nat. Hazards Earth Syst. Sci., 13, 3157-3168.

Bovenga, F., Wasowski, J., Nitti, D.O., Nutricato, R., Chiaradi, M. T., 2012: Using COSMO/SkyMed X-band and Envisat C-band SAR interferometry for landslide analysis.- Remote Sensing of Environment 119, 272-285, doi:10.1016/j.rse.2011.12.013.

BfG, 2007: Höhenmessungen mit GPS – Status quo und Entwicklungstendenzen.- Kolloquium am 16. November 2006, Koblenz, 87 S.

Blikra, L., H., Kristensen, L., Lovisolo, M., 2013: Subsurface monitoring of large rockslides in Norway: A key requirement for early warning.- IJEGE, 13, 307-314; doi: 10.4408/IJEGE.2013-06.B-28.

Böhme, M., Hermanns, R. L., Oppikofer, T, Fischer, L., Sunkholt, H. S. S., Eiken, T., Pedrazzini, A., Derron, M.-H., Jaboyedoff, M., Blikra, L. H., Nilsen, B., 2013: Analyzing complex rock slope deformation at Stampa, western Norway, by integrating geomorphology, kinematics and numerical modeling.- Engineering Geology, 154, 116-130.

Bock, B., Wehinger, A., Krauter, E., 2013: Hanginstabilitäten in Rheinland-Pfalz - Auswertungen der Rutschungsdatenbank Rheinland-Pfalz für die Testgebiete Wißberg, Lauterecken und Mittelmosel.- Mainzer geowiss. Mitt., 41, Mainz, 103-122.

Busch, W., Schäfer, M., 2013: Integration von satellitengestützter Radarinterferometrie und Nivellement zum Monitoring von Höhenänderungen an Corner-Reflektor-Standorten.- in: Sörgel, U., Schack, L., (Hrsg.): Tagungsband GeoMonitoring 2013, 14./15.3.2013 in Hannover, 113 – 132.

Calò, F., Ardizzone, F., Castaldo, R., Lollino, P., Tizzani, P., Guzzetti, F., Lanari, R., Angeli, M.-G., Pontoni, F., Manunta, M., 2014: Enhanced landslide investigations through advanced DInSAR techniques: The Ivancich case study, Assisi, Italy.- Rem. Sens. of Envir., 142, 69-82, http://dx.doi.org/10.1016/j.rse.2013.11.003.

Campbell J., B., Wynne, R., H., 2011: Introduction to Remote Sensing, 5th Edition.- The Guilford Press, New York, 667 S.

Cardellini, S., Osimani, P., 2008: Living with landslide: the Ancona case history and early warning system.- Proc. 1st World Landslide Forum, 18th-21st Nov. 2008, Tokyo.

Cardellini, S., Osimani, P., 2012: Living with landslides: the Ancona case.- in 7th EUREGEO, Bologna, Italy, 12th-15th June 2012: Proceedings; European Congress on Regional Geoscientific Cartography and Information Systems; sustainable geo-management,- 1. Opening papers: 46-47.

Cardinaletti, M., Cardellini, S., Ninivaggi, A., 2011: The integrated landslide managing System of Ancona.- http://www.preventionweb.net/applications/hfa/lgsat/en/image/href/512 am 3.2.14

Casu, F., Manzo, M., Lanan, R., 2006: A quantitative assessment of the SBAS algorithm performance for surface deformation retrieval from DInSAR data.- Rem. Sens. of Envir., 102, 3-4, 195-210.

Cigna, F., Bianchini, S., Casagli, N., 2012: How to assess landslide activity and intensity with Persistent Scatterer Interferometry (PSI): the PSI-based matrix approach.- Landslides, 10, 267-283.

Cui, P., Han, Y., Chao, D., Chen, X., 2011: Formation and Treatment of Landslide Dams Emplaced During the 2008 Wenchuan Earthquake, Sichuan, China.- in Evans, S., G., Hermanns, R. L., Strom, A., Scarascia-Mugnozza, G., eds., Natural and artificial Rockslide Dams. Lecture Notes in Earth Sciences, 133, Springer Verlag: Berlin Heidelberg, S. 295-321.

Corsini, A., Farina, P., Antonello G., Barbier, M., Casagli, N. et al., 2006: Space-borne and ground-based SAR interferometry as tools for landslide hazard management in civil

protection.- International Journal of Remote Sensing - 27, 12/14, 2351-2369, doi:10.1080/01431160600554405

Couture, R., Riopel, S.. 2008: Regional landslide susceptibility mapping and inventorying in the Mackenzie Valley, Northwest Territories.- in Locat, J., Perret, D. Turmel, D., Demers, D., Leroueil, S., Proceedings of the 4th Canadian Conference on Geohazards: From Causes to Management. Presse de l`Université Laval, Québec, 594 p., http://www.geohazards.ggl.ulaval.ca/alea/couture.pdf.

Crosta, B., G., Imposimato, S., Roddeman, D., 2013: Monitoring and Modelling of Rock Slides and Rock Avalanches.- IJEGE Bookseries (6), p. 3-14; doi:10.4408/IJEGE.2013-06.B-01

Debella-Gilo, M., Kääb, A., 2011: Sub-pixel precision image matching for measuring surface displacements of mass movements using normalized cross-correlation.- Remote Sensing of Environment 115, 130-142, doi:10.1016/j.rse.2010.08.012.

Debella-Gilo, M., Kääb, A., 2012: Measurements of Surface Displacement and Deformation of mass movements using least squares matching of repeated high resolution satellite and aerial amages.- Remote Sensing, 4, 43-67; doi:10.3390/rs4010043.

Delaney, P. T., Miklius, A., Arnadottir, T., Okamura, A. T., Sako, M. K., 1994: Motion of Kilauea Volcano during sustained eruption from the Puu Oo and Kupaianahe vents, 1983-1991.- supplemental information: USGS Open-File Report 94-567, 23 p.

DMV, 2009: Grundsätze zum Einsatz von luftgestützten und terrestrischen Laserscanneraufnahmen im Bergbau, Deutscher Markscheiderverein e.V., Herne 2008; Ausgabe 13.11.2009; 9 S. (www.dmv-ev.de)

DMV, 2013: Grundsätze zum Einsatz von satellitengestützten Verfahren der Radarinterferometrie zur Erfassung von Höhenänderungen.- Deutscher Markscheiderverein e.V., Herne 2013; Ausgabe 18.11.2013; 9 S. (www.dmv-ev.de)

Ferreti, A., Fumagalli, A., Novali, F., Prati, C., Rocca, F., Rucci, A., 2011: A new algorithm for processing interferometric data-stacks: SqueeSAR.- IEEE Trans. on Geosc. and Rem. Sens., 49, 9, 3460-3470.

Finkler, C., Emde, K., Vött, A., 2013: Gravitative Massenbewegungen im Randbereich des Mainzer Beckens: Das Fallbeispiel Roterberg (Langenlonsheim, Rheinland-Pfalz).- Mainzer geowiss. Mitt., 41, Mainz, 51-102.

Fredel, A., Jany, S., 2013; Die Anwendung von Airborne Laser Scanning auf rutschungsgefährdetem Terrain, Fallbeispiel: Kliffküsten der Halbinsel Jasmund/Rügen. – in: In Sörgel, U., Schack, L., (Hrsg.): Tagungsband GeoMonitoring 2013 – 14./15.3.2013 in Hannover, 171 – 185.

Froese, C., R., Poncos, V., Skirrow, R., Mansour, M., Martin, D., 2008: Characterizing complex deep seated landslide deformation using corner reflector InSAR (CR-InSAR): Little Smokey landslide, Alberta.- in Locat, J., Perret, D. Turmel, D., Demers, D., Leroueil, S., Proceedings of the 4th Canadian Conference on Geohazards: From Causes to Management, Presse de l`Université Laval, Québec, 287-294.

Großmann, W. 1976: Vermessungskunde I, de Gruyter, Berlin, New York, 196 S.

Großmann, W., Kahmen 1983: Vermessungskunde II, de Gruyter, Berlin, New York, 294 S.

Haas, F., Heckmann, T., Hilger, L., Becht, M., 2012: Quantification and modelling of debris flows in the proglacial area of the Gepatschferner, Austria, using ground-based LiDAR.- IAHS Publ. 356, Proceedings of the Symposium “Erosion and Sediment Yields in the Changing Environment”, CAS-Chengdou, China, 11.-15. Oct. 2012, 293-302.

Hebel, H.-P., Linke, J., Busch, W., Wujanz, D. Neitzel, F. 2013: Radarscanner und Laserscanner – zwei Systeme, die sich ergänzen.- In Sörgel, U., Schack, L., (Hrsg.): Tagungsband GeoMonitoring 2013 – 14./15.3.2013 in Hannover, 113 – 132.

Hooper, A., Bekaert, D., Spaans. K., Arikan, M., 2012: Recent advances in SAR interferometry time series analysis for measuring crustal deformation.- Tectonophysics, 514-517, 1-13.

Huadong, G., ed., 2010: Atlas of Remote Sensing of the Wenchuan Earthquake.- CRC Press Boca Raton, 244 S.

Joswig, M., Rothmund, S., 2013: Erfassung von Rissstrukturen und rutschungsinduzierter Bruchprozesse an Lockergesteinshangrutschungen durch hochauflösende Fernerkundung und Nanoseismic Monitoring.- in: Sörgel, U., Schack, L., (Hrsg.): Tagungsband GeoMonitoring 2013, 14./15.3.2013 in Hannover, 143 – 155.

Kuhn, D., Prüfer, S., 2014: Coastal cliff monitoring and analysis of mass wasting processes with the application of terrestrial laser scanning: a case study of Rügen, Germany, Geomorphology, 13 p., in press, http://dx.doi.org/10.1016/j.geomorph.2014.01.005.

Korritke, N., 2000: Grundsätze zum Einsatz von satellitengeodätischen Verfahren im Bergbau.- http://www.dmv-ev.de/images/stories/uploads/gps_grundsatze_00_06_06a_deu.pdf (7.2.14)

Luzi, G., Pieraccini, M., Mecatti, D., Noferini, L., Macaluso, G., Galgaro, A., Atzeni, C., 2006: Advances in ground-based microwave interferometry for landslide survey; a case study.- International Journal of Remote Sensing, 27, 12/14, 2331-2350, doi:10.1080/01431160600554975

MarkscheidBV, 1998: Markscheider-Bergverordnung vom 19.12.1986 (BGBl. I S. 2631), zuletzt geändert durch Artikel 4 der Verordnung vom 10.8.1998 (BGBl. I S. 2093).

Noferini, L., Pieraccini, M., Mecatti, D., Macaluso, G., Luzi, G., Atzeni, C., 2006: Long term landslide monitoring by ground-based synthetic aperture radar interferometer.- International Journal of Remote Sensing 27, 9-10, 1893-1905, doi:10.1080/01431160500353908

Moosavi, V., Talebi, A., Shirmohammadi, B., 2014: Producing a landslide inventory map using pixel-based and object-oriented approaches optimized by Taguchi method.- Geomorphology 204, 646-656, http://dx.doi.org/10.1016/j.geomorph.2013.09.012.

Morche, D., Schmidt, K.-H., Sahling, I., Herkommer, M., Kutschera, J., 2008: Volume changes of Alpine sediment stores in a state of post-event disequilibrium and the implications for downstream hydrology and bed load transport.- Norsk Geografisk Tidsskrift - Norwegian Journal of Geography, 62, 2; 89–101.

Ohlmann-Lauber, J., 2012 Filterungsansätze zur Bestimmung flächenhafter Deformationen aus TLS-Daten.- In Niemeyer, W., Riedel, B., Lehmann, M., (Hrsg.): Tagungsband GeoMonitoring 2012 – 8./9.3.2013 in Braunschweig, 127-142.

Oppikofer, T., Saintot, A. Otterå, S., Hermanns, R. L., Anda, E., Dahle, H., Eiken, T., 2013: Investigation on unstable rock slopes in Møre og Romsdal – status and plans after field surveys in 2012.- NGU Report No.: 2013.014, Geological Survey of Norway, 323 p.

Petley, D., 2012: Global pattern of loss of life from landslides.- Geology 40 (10), 927-930.

Petley, D., 2013: Global Losses from Landslides associated with dams and reservoirs.- IJEGE Bookseries (6), p. 63-72; doi:10.4408/IJEGE.2013-06.B-05.

Reetz, F.-P., 2013: Geomonitoring im Braunkohletagebau – Praktische Anwendungen – Erfahrungen und Ausblicke.- In Niemeyer, W., Riedel, B., Lehmann, M., (Hrsg.): Tagungsband GeoMonitoring 2012 – 8./9.3.2013 in Braunschweig, 189-205.

Rödelsperger, S., 2011: Real-time Processing of Ground Based Synthetic Aperture Radar (GB-SAR) Measurements. Schriftenreihe Fachrichtung Geodäsie, Fachbereich Bauingenieurwesen und Geodäsie, Technische Universität Darmstadt Heft 33, http://tuprints.ulb.tu-darmstadt.de/2755/ 98 S.

Sansosti, E., Berardino, P., Bonano, M., Calò, F., Castaldo, R., Casu, F., Manunta, M., Manzo, M., Pepe, A., Pepe, S., Solaro, G., Tizzani, P., Zeni, G., Lanari, R., 2014: How second generation SAR systems are impacting the analysis of ground deformation.- International Journal of Applied Earth Observation and Geoinformation 28, 1-11, http://dx.doi.org/10.1016/j.jag.2013.10.007.

Schäfer, M. 2012a: Atmosphäre als Phasenbestandteil der differentiellen Radarinterferometrie und ihr Einfluss auf die Messung von Höhenänderungen.- Dissertation, TU Clausthal, 127 S., Clausthal-Zellerfeld. Siehe auch http://radar.signale.de/diss.

Schäfer, M. 2012b: Der Einfluss der Atmosphäre bei der Erfassung von Höhenänderungen mit differentieller Radarinterferometrie.− In: Seyfert, E. (Hrsg.): Erdblicke – Perspektiven für die Geowissenschaften, 32. Wissenschaftlich-Technische Jahrestagung der

Deutschen Gesellschaft für Photogrammetrie, Fernerkundung und Geoinformation e.V. (DGPF), Bd. 21, 14.-17.03.2012 in Potsdam, 418-427.

Schneider, K.-J., 2008: Bautabellen für Ingenieure mit Berechnungshinweisen und Beispielen.- Werner Verlag.

Singhroy, V., 2009: Satellite Remote Sensing Applications for Landslide Detection and Monitoring.- in Sassa., K, Canuti, P. (eds.), 2009: Landslides – Disaster Risk Reduction, Springer Verlag, Heidelberg 2009, 143-158.

Singhroy, V., Murnaghan, K., Couture, R., 2010: InSAR monitoring of a retrogressive thaw flow at Thunder River, lower Mackenzie.- 63rd Canadian Geotechnical Conference and the 6th Canadian Permafrost Conference, 12.-16. Sept. 2010, Calgary, Canada, 1317-1322, http://pubs.aina.ucalgary.ca/cpc/CPC6-1317.pdf.

Singhroy, V., Charbonneau, F., Froese, C., Couture, R., 2011: Guidelines for InSAR Monitoring of Landslides in Canada.- 14th Pan-American Conference on Soil Mechanics and Geotechnical Engineering, 5 S, http://geoserver.ing.puc.cl/info/conferences/PanAm2011/panam2011/pdfs/GEO11Paper968.pdf.

STMUG, Bayerisches Staatsministerium für Umwelt und Gesundheit, 2009: Projekt Georisiken im Klimawandel, Vorhaben: „Gefahrenhinweiskarte Bayerische Alpen Steinschlag – Felssturz – Rutschung – Hanganbruch Alpenanteil Landkreis Miesbach“, Abschlussbericht Umwelt Spezial, 80 S.

Strozzi, T., Delaloye, R., Kääb, A., Ambrosi, C., Perruchoud, E., Wegmüller, U., 2010: Combined observations of rock mass movements using satellite SAR interferometry, differential GPS, airborne digital photogrammetry, and airborne photography interpretation.- J. Geophys. Res., 115, F01014, 1-11, doi:10.1029/2009JF001311.

Teza, G., Atzeni, C., Balzani, M., Galgaro, A., Galvani, G., Genevois, R., Luzi, G., Mecatti, D., Noferini, L., Pieraccini, M., Silvano, S., Uccelli, F., Zaltron, N., 2008: Ground-based monitoring of high-risk landslides through joint use of laser scanner and interferometric radar.- International Journal of Remote Sensing, 29, 15/16, 4735-4756, doi:10.1080/01431160801942227.

Travalletti, J., Malet, J.-P., Samyn, K., Grandjean, G., Jaboyedoff, M., 2013: Control of landslide retrogression by discontinuities: evidence by the integration of airborne- and ground-based geophysical information.- Landslides, 10, 37-54, doi:10.1007/s10346-011-0310-8

Tofani, V., Segoni, S., Agostini, A., Catani, F., Casagli, N., 2013a: Technical Note: Use of remote sensig for landslide studies in Europe.- Nat. Hazards Earth Syst. Sci., 13, 299-309.

Tofani, V., Raspini F., Catani, F., Casagli, N., 2013b: Persistent Scatterer Interferometry (PSI) technique for landslide characterization and monitoring.- Remote Sens., 5, 1045-1065.

Wendel, M., Wehinger, A., 2011: Ingenieurgeologische Aufnahme der Hangrutschung in Löllbach (Landkreis Bad Kreuznach).- Mainzer geowiss. Mitt., 39, Mainz, 105-142.

Zhao, C., Lu, Z., Zhang, Q., de la Fuente, J., 2012: Large-area landslide detection and monitoring with ALOS/PALSAR imagery data over Northern California and Southern Oregon, USA.- Remote Sensing of Environment 124, 348-359.

Landslide hydrology – understanding and quantifying the influence of hydrological processes in unstable slopes

Bogaard, T.A. (Delft University of Technology, Water Sources Section,Chair of Hydrology)
t.a.bogaard@tudelft.nl

Hydrological processes in landslides: lessons from experiments

ABSTRACT: Much research attention is nowadays focussed on improving our hydrological process understanding of landslides. The objective of this paper is to discuss and generalise results on the complex hydrological behaviour in landslides. The work is based on the experiments performed in 2007 and 2008 at landslides in the French Alps. Preferential flow paths and perched water bodies are very important instable slopes but even more in active landslides. However, the dual permeability system increases not only infiltration but also drainage. There are distinct differences of hydrological processes across a landslide area. Infiltration, drainage and temporarily storage of water within the parts of the landslide are in delicate balance and that determines to a large extend the pore pressure build up.

1. Introduction

Hydrologically triggered or re-activated landslides are important from societal point of view. The prediction and/or mitigation of these hazards are daily practice for engineering companies and civil protection agencies. These can be strongly hampered by the lack of hydrological understanding of the study site. The study of hydrological processes deals with stocks and fluxes of water in the earth system. Also in landslide studies, the importance of understanding the hydrological processes and their complexity is recognized. To be able to quantify hydrological behaviour we have to assess the soil hydraulic characteristics, what we do via sampling and laboratory measurements like porosity, (un)saturated permeability and so on. In addition, hydrological experiments can be designed and performed in order to assess insight in processes underlying the observed behaviour of a system, in our case the hydrological triggering of landslides.

This paper aims to discuss the lessons learned from several on-site sprinkling experiments designed to improve our understanding the hydrological behaviour on active landslides. In this discussion the focus will be on experiments performed in the framework of the French research project EcouPref in southern France initiated to study the role of preferential flow in landslides in weathered clay shales.

In addition, the derived insight can also be compared with other recently performed large scale experiments on hydrologically triggered landslides. The small and large scale experiments will briefly be summarized. The discussion of the results will be in the context of improved understanding of hydrological behaviour of landslides and landslide prone areas. This contribution ends with conclusions and recommendations for experimental investigations.

2. Experimental designs

In 2007 two 100 m^2 sprinkling experiments which lasted several days were designed and performed: one at the Super-Sauze active mudslide in the Ubaye valley, southern France (Debieche et al, 2011) and at the Laval landslide near Draix, southern France (Garrel 2011;

Fressard et al, 2009). The main objective was to unravel the complex hydrological behaviour of preferential flow through the abundant fissure network on two active, moving slopes. Moreover, these experiments were a kind of open-air laboratory to use different (experimental) field methods such as geophysical monitoring and combined hydrological and hydrochemical monitoring. As a follow up, 'downscaled' sprinkling tests were performed in 2008 at the Super-Sauze mudslide (Ubaye valley, southern France) using a limited set of measurements in order to assess the spatial heterogeneity of the studied processes (Ponton et al, 2008; Krzeminska et al, 2009; Krzeminska et al, submitted).

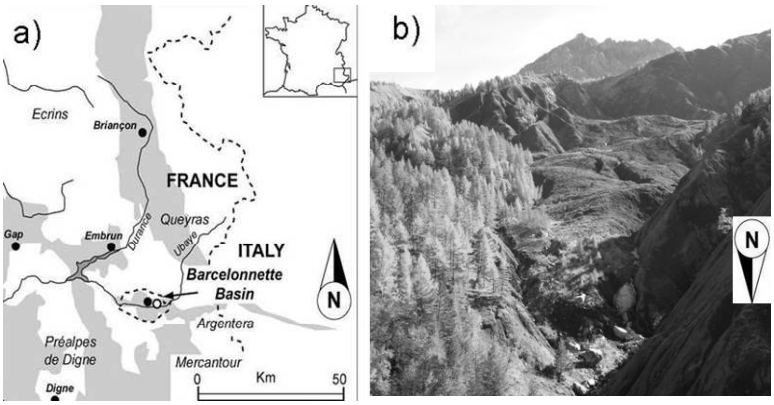

Figure 1. (a) The location of Barcelonnette basin and (b) the Super-Sauze mudslide.

The core of these experiments was tracing of infiltrated water using Cl^- and Br^- over two periods for the duration of 3 days or 7-8 hours. The water in the experiments was taken from a local upslope spring draining towards the active landslides and Cl^- and Br^- salt was added. Both elements are conservative tracers with low background concentration.

The hydrological response was monitored using geophysical methods like seismic surveys and 2D Electric Resistivity Tomography and abundant nested soil moisture sensors and open standpipe piezometers distributed within and outside the sprinkling area. The water quality was determined using Electric Conductivity meters in piezometers and regular water sampling of the groundwater system.

3. Hydrological interpretation of the Results

The results were extensively described in the specific papers which will not be repeated here. However, some basic numbers necessary for this discussion will be presented. The applied rainfall intensity was around 8-10 mm/hr for the large scale experiments. This resulted in an infiltrated volume of 280mm of water in two times three days, Super-Sauze (Debieche et al, 2011) and around 400mm of water which accumulated in three days at Laval, Draix (Garel, 2010). The small-scale experiments used approx. 40-50 mm/hr (summer storm intensity) for 7 to 8 hours of which between 80 mm and 420mm infiltrated depending on the exact location on the Super-Sauze landslide. The infiltration rates are much higher than could be expected from matrix permeability characteristics alone and show high infiltration capacity resulting from secondary porosity due to fissure network. However, except for one small scale test, these large infiltration fluxes did not result in full saturation of the subsurface.

The three experiments all used artificial tracers to establish pre-event and event water contribution in the groundwater (subsurface water) system. In case of the Super-Sauze experiments, after a dry period a second tracer was applied to separate the event water of the first sprinkling phase from the second sprinkling period. This dry recession phase allowed the groundwater system to

reset. By using two sprinkling periods one mimics the dynamic behaviour with dry or wet initial conditions.

The chemical response is as variable as the hydrodynamic response; the event sprinkling water can contribute between negligible to 90% of the groundwater. No conclusive generalisation of this event and pre-event mixing is possible, but shallow piezometers seem to show slightly higher event water contributions then the deeper observations and the event water contribution tends to increase with time as pre-event water is displaced. Most interestingly, the event – pre-event water ratio does not necessarily coincide with the observed responses of the hydrodynamics.

It is the combination of these two sources of information which helps unravelling the hydrological processes in hillslopes. The dual porosity system is dominating most landslides and unstable slopes and can act and react in several ways. The dual porosity system consists of a high porosity compartment of macropores (e.g. fissures due to displacement of parts of the slopes) and a low porosity matrix compartment. In case both compartments are hydrologically active the term dual permeability system is used. In the following a generalised interpretation is discussed.

Fast responding systems.
Here the availability of large fissures facilitates much more infiltration then could be expected based on the (small-scale) soil hydraulic properties. During several sprinkling experiments large fluxes of water infiltrate the landslide exceeding precipitation statistics. When the precipitation has infiltrated the residence time seems rather limited, the saturated water layer that builds up drains quickly and often full saturation is not reached. In other words, there is only a potential build-up of pressure in case the rainfall intensity is larger than drainage capacity. In the majority of the cases we see a large percentage of pre-event water in the observation piezometers, indicating well mixing (and with time displacement) of pre-event groundwater with event sprinkling water.

The fissures facilitating the infiltration also act as important drains rapidly moving the water. In some cases towards the bedrock, sometime laterally and potentially exfiltrate towards incised surface gullies. The influence of water flowing from the bedrock system towards the landslide has been mentioned in literature (e.g. Wilson and Dietrich (1987). Interestingly, the large scale Wiler slope experiments in 2007 and 2008 to trigger a landslide in Swiss in framework of the TRAMM project (http://www.cces.ethz.ch/projects/hazri/tramm/) showed almost infinite infiltration (8 times annual precipitation in 5 consecutive sprinkling days) but could not reach saturation. Here, the interpretation was a large drainage capacity via the underlying bedrock. In many landslide hydrological model approaches the increased infiltration rate is taken into account but not a kind of transient draining capacity of the system.

Water storing systems.
When the drainage is less fluid as is observed in several occasions, we encounter a system with high storage capacity but limited drainage and thus results in longer duration build-up of positive pressure. These systems will reach saturation and remain well saturated for a considerable time. These systems will lead to saturation overland flow or subsurface storm flow via pipes, drains and so on. The event - pre-event water mixing depends on the available storage capacity at the onset of the precipitation input. Geotechnically, such systems will be very prone to mass movement, slides or flows can develop in case enough gravitational energy is available.

Less hydrological active systems.
Also parts of a hillslope or landslide can show infiltration rates, which resemble the documented range of matrix infiltration rates but clearly lower then the very high infiltration rates of the fissure dominated slopes. Here experiments show larger overland flow fluxes as response to the relatively high sprinkling rates. These systems are more dominated by pre-event water as limited event water infiltrates and mixes with the subsurface water system. However, also here, some preferential flow can exist and locally result in higher event water concentration. These are the systems with surface water erosion, rills and possible gully development, but also with shallow

landslides or soil slips, were detailed soil hydrological research can be necessary (soil moisture, tensiometer information, etc).

Groundwater versus perched water systems.
Another very interesting feature is the development of layered pore pressure build up: i.e. there is no continuum of pore water pressure. This has limited influence on the deeper slope stability. In the same way as that fissures or refilled fissures can result in distinct hydrological zones (laterally), the presence of blocks of unweathered material such as clay shales in the Ubaye examples or local regions with clear permeability differences will lead to important local hydrological response. Debieche and co-workers (2011) identify this as the most likely explanation for the observed pattern in vertical pore pressures observed in nested piezometers at different depths. Also at Laval (Fressard et al., 2009; Garrel 2010) the influence of fresh marls blocks within the deforming slope material seemed very important for the distribution of infiltrating water. Geotechnically, this has the advantage that a system still remains stable while storing the water. The drainage of this perched water is not straightforward depending on local conditions. However, as these perched water bodies are surrounded by unsaturated soil, it seems not unlike to conclude that the drainage is often quite slow only taking place via evaporation or slow lateral drainage. Clearly, prolonged rainfall can result in saturation of the entire soil profile. Soils with manifold, scattered permeability differences then are less prone to destabilization of singular intensive rain events but more likely to be affected by prolonged, accumulated precipitation infiltration.

This would mean that highly heterogeneous deposits are more stable than we could expect from the analysis of their components. They hinder a continuous build-up of a groundwater table, fragmenting the water distribution.

4. Conclusions

Field and laboratory results often criticized for the idiosyncrasy of results. Every location is different and so it is almost impossible to generalise the findings. However, the basic question is whether we do learn something outreaching the very specific field site where the experiments were performed? Note that the experiments are not designed to assess spatial difference of soil hydraulic variables but to assess the spatial differences in hydrological processes! Well-thought of experiments are not performed to obtain one or two parameters for a pre-defined numerical model. Experiments are no expensive replacements for parameter measurements. They are designed to better grab the underlying processes. The same is advocated by Kleinhans et al (2010) for designing laboratory experiments in hydrological research.

The different experiments show interesting similarities, especially in relation to the occurrence of preferential flow via fissure flow paths. The importance of the experiments seems to be in the (combined) infiltration and drainage processes that can be identified. It suggest that getting grip on the combined infiltration and drainage capacity and the possible transient aspects of these two during crises phases could help us forward in better understanding the complex landslide behaviour. In such a dynamic environment as landslides the dual permeability system will not be static but also change over time: an open research field.

A second conclusion that emerged was the importance of development of perched water tables due to local differences in hydraulic characteristics. This leads to water storage in the vertical profiles while the pore pressure development at the slipsurface is reduced increasing the overall stability.

The use of conservative tracers in sprinkling experiments is an important asset to sprinkling experiments and is highly recommended. The sources of the water can be quantified and more knowledge is gained on the subsurface flow paths and mixing.

Looking at the results of the large and small scale experiments in the clay shales of southern France it becomes clear that flow processes differ enormously across landslides. A clear spatial differences in hydrological process of groundwater recharge and drainage in the clay-shale unstable slopes comes forward, suggesting the use of the small-scale 'downscaled' sprinkling experiments such as described by Ponton et al, (2008), Krzeminska et al (2009) and Krzeminska et al (submitted) could be a good step forward quantifying hydrological spatially across research sites.

5. Acknowledgements

The experiments used for this paper were financed by the ANR-ECCO Programme 'Ecosphère Continentale': Project ECOU-PREF 'Ecoulements préférentiels dans les versants marneux fracturés' (2005-2008) for the French Ministry of Research and the French Research Agency. The experiments were performed by a large group of colleagues and should be regarded as a collaborative achievement. The continuous discussion about how to interpret these results has been very stimulating. A special thanks to Dr. J-P Malet for being the driving force behind this project. However, any mistakes, (mis-)interpretations or omissions are solely the responsibility of the author.

6. References

Debieche, T.-H.,T.A. Bogaard, C. Emblanch, V. Marc, D.M. Krzeminska, J.-P. Malet 2011 Hydrological and hydrochemical processes observed during large scale infiltration experiment in initial saturated conditions: the Super-Sauze mudslide experiment. Hydrological Processes. DOI: 10.1002/hyp.7843

Fressard,M., O. Maquaire, J.-P. Malet, S. Klotz & G. Grandjean 2009. Morpho-structure and triggering conditions of the Laval landslide developed in clayshales, Draix catchment (South French Alps). Pp. 107-110. Proceeding conference on Landslide Processes Analyses, Strasbourg Feb 2009

Garel, E. 2010. Etude des processus de recharge des nappes superficielles et profondes dans les versants marneux fortement heterogenes. Cas des Terres Noires des Alpes du Sud de la France _ ORE Draix. PhD Thesis Université d'Avignon et des pays de Vaucluse

Kleinhans, M.G., M. F. P. Bierkens, and M. van der Perk 2010. On the use of laboratory experimentation: "Hydrologists, bring out shovels and garden hoses and hit the dirt", Hydrol. Earth Syst. Sci. 14, 369-382

Krzeminska, D.M., T.A. Bogaard T.-H. Debieche, V. Marc, J. Ponton & J.-P. Malet 2009. Quantitative analysis of preferential flow during small scale infiltration tests on an active mudslide, French Alps. Pp. 151-156. Proceeding conference on Landslide Processes Analyses, Strasbourg Feb 2009

Krzeminska, D.M., T.A. Bogaard T.-H. Debieche, F. Cervi, V. Marc, & J.-P. Malet 2011. On-site investigation of fissure flow with small-scale sprinkling tests on active mudslide. Submitted to and in review with ESPL.

Ponton, J, D.M. Pradzynska, T.-H. Debieche, T.A. Bogaard, J.-P. Malet, V. Marc, J. Travelletti, 2008. Suivi hydrogéophysique d'écoulements hydriques sur des glissements-coulées argileux par expérimentations d'infiltration provoquée. 8pp. 1e Journees 'Alea Gravitaire', 17-18 Novembre 2008, Orleans, France.

Wilson, C.J. & W.E. Dietrich 1987. The contribution of bedrock groundwater flow to storm runoff and high pore pressure development in hollows. Proceedings of the Corvallis Symposium: Erosion and Sedimentation in the Pacific Rim. IAHS Publications 165, pp. 49-59.

Landslide hydrology

understanding and quantifying the influence of hydrological processes in unstable slopes

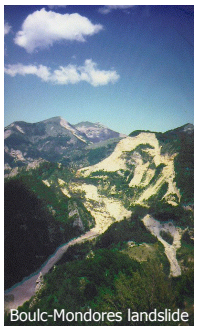

Boulc-Mondores landslide

Thom Bogaard
t.a.bogaard@tudelft.nl

TU Delft
Delft University of Technology

Research Thom Bogaard

http://scholar.google.nl/citations?user=ECH3uCwAAAAJ&hl=nl

The main focus of my research is to understand and quantify the hydrological processes in mountainous areas, relate it to landdegradation and assess the impact for society
The second focus is on innovative hydrometeorological observation methods and tracer techniques

Landslide and hillslope hydrology

- *Influence preferential flow, feedbacks deformation-slope hydraulics, influence long term vegetation development, coupled hydrological-slope deformation modelling*

Hydrometeorological observations and tracers in hydrology

- *Water quality, stable water isotopes*
- *Usage of synthetic DNA in stream water tracing*
- *Field based data collection, network analysis*
- *Testing innovative measurement techniques such as Fibre Optic Cable*

Natural risk management

- *Evaluate visualisation techniques in risk communication*

Thom Bogaard

Landslide hydrology

understanding and quantifying the influence of hydrological processes in unstable slopes

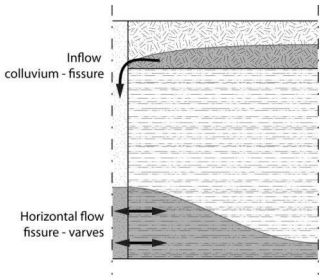

Special thanks to: Theo van Asch, Rens van Beek, Jean-Philippe Malet, Dominika Krzeminska, Martijn Westhoff, Roberto Greco, Mark Bakker, Joanne van der Spek, Shao Wei, and many many others

TU Delft
Delft University of Technology

Outline of my presentation

Background and motivation

Examples of complex hillslope hydrology

From concepts to models

Discussion

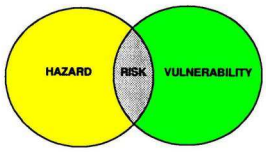

What is the role of hydrology in landslides?

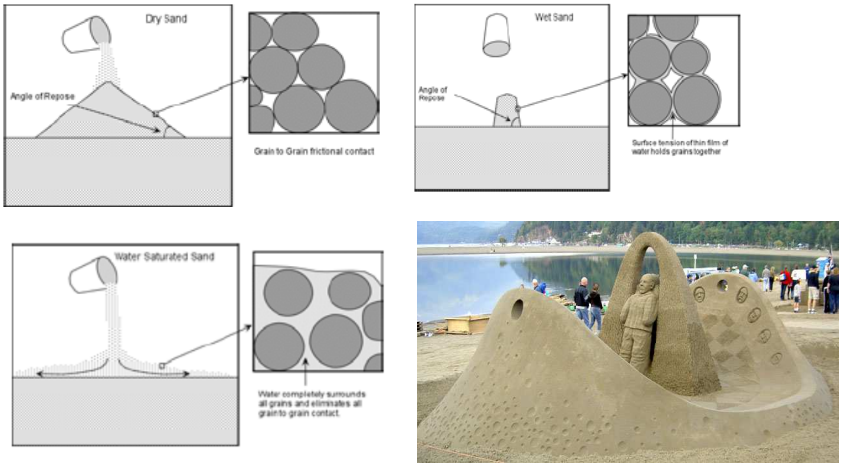

What is the role of hydrology in landslides?

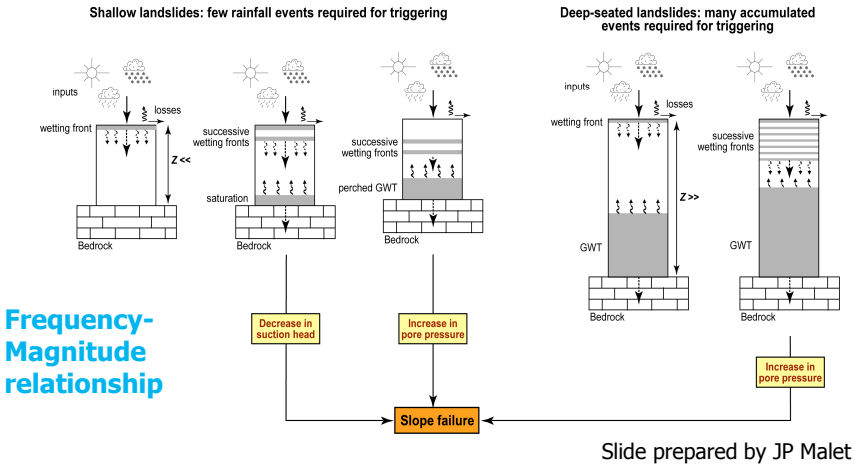

Frequency-Magnitude relationship

Slide prepared by JP Malet

What is the role of hydrology in landslides?

The hillslope and its unsaturated zone is part of the hydrological cycle

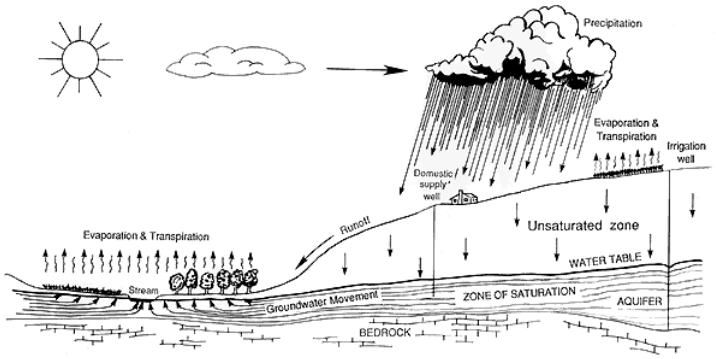

My motivation?

What can landslide research learn from hillslope hydrology (vv)?

Improving process understanding causing slope instability.

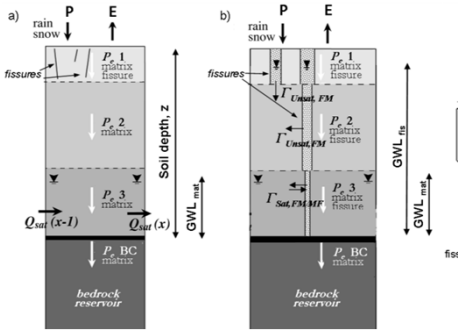

Origin of water: Heumos slope

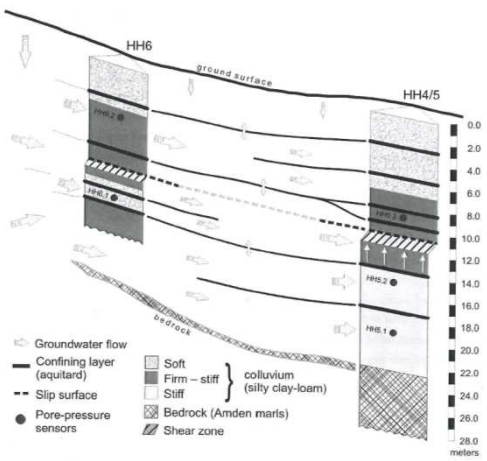

Wienhofer et al, 2010

Origin of water: La Clapière

Elevation dependent isotopic signal in water

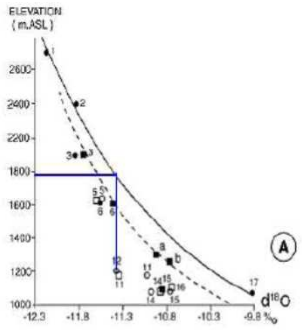

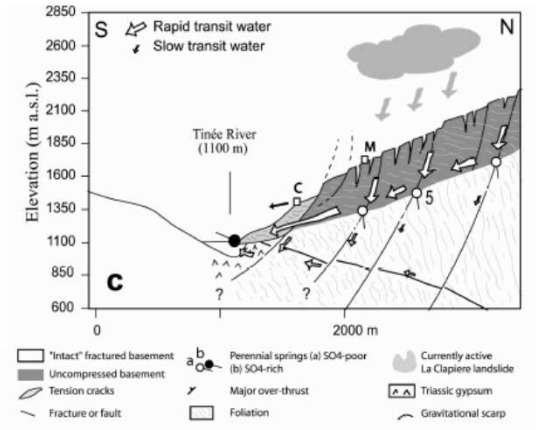

Guglielmi et al, 2002

Origin of water: Ca'Lita Landslide

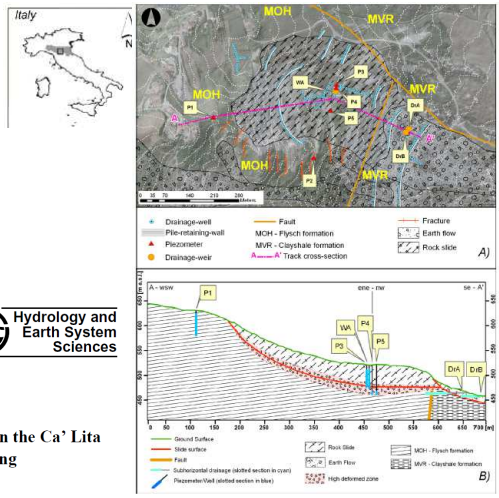

Hydrol. Earth Syst. Sci., 16, 4205–4221, 2012
www.hydrol-earth-syst-sci.net/16/4205/2012/
doi:10.5194/hess-16-4205-2012

Hydrology and Earth System Sciences

Origin and assessment of deep groundwater inflow in the Ca' Lita landslide using hydrochemistry and in situ monitoring

F. Cervi[1], F. Ronchetti[1], G. Martinelli[3], T. A. Bogaard[2], and A. Corsini[1]

Local flow path:
TRAMM project
Wiler, Swiss

- Sprinkling experiment
- 8 · P_{year} in 5 days
- No failure

- Underlying fractured bedrock with high permeability
- Dead wood acting as stabilizers or fast water pathways
- A stone skeleton connected with root system.

Local flow path: Draix

Large scale infiltration experiment Draix
Monitoring the electric resistivity

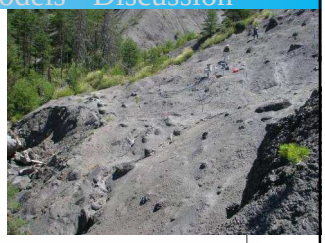

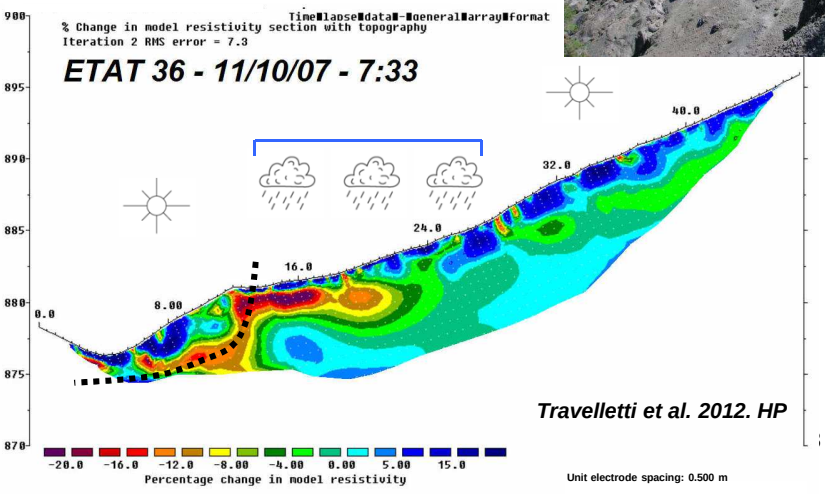

Travelletti et al. 2012. HP

Background – Examples – Concepts and models - Discussion

Origin of water and flow path: Super-Sauze

Hydrochemical synthetic cross-section Super Sauze showing spatially distributed hydrological processes and water sources

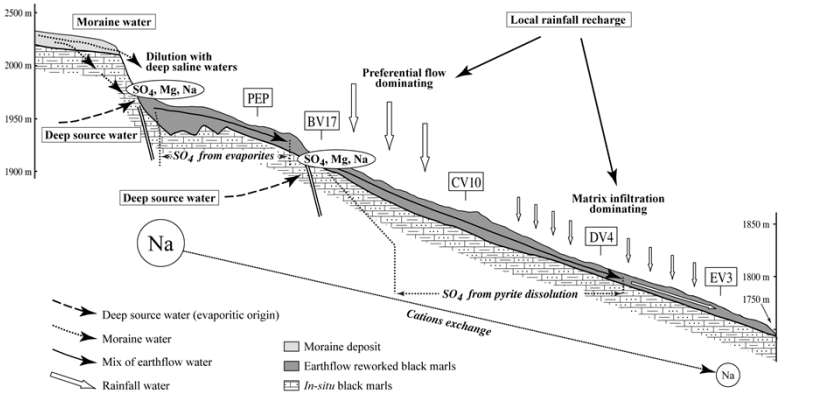

De Montety et al., 2007

Thom Bogaard

Conceptual model infiltration in the Super-Sauze mudslide

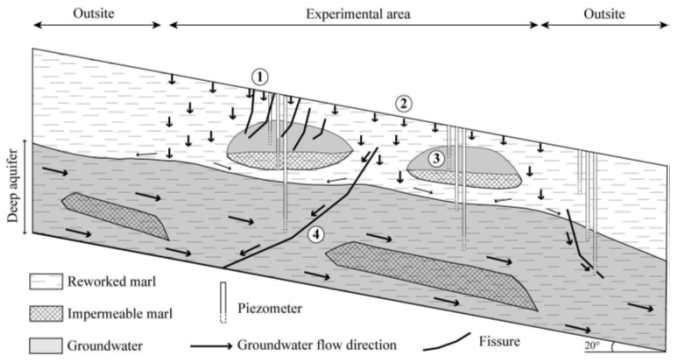

Debieche et al 2012

1) Preferential infiltration
2) Matrix infiltration
3) Perched water bodies preventing deeper pore pressure build up;
4) Lateral preferential flow draining the groundwater system

Thom Bogaard

Background – Examples – Concepts and models - Discussion

How does water flow in hillslopes according to 'catchment hydrologists'?

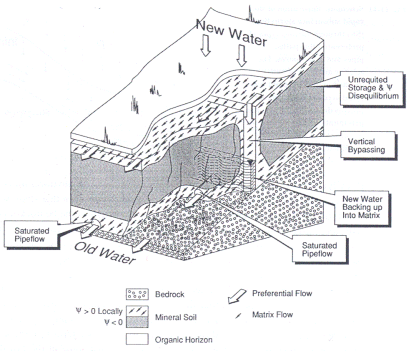

McDonnell, 1990

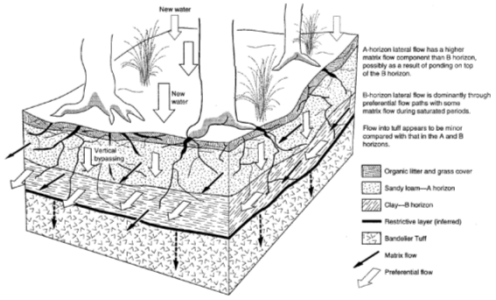

Newman, 1998

Thom Bogaard

How does water flow in hillslopes according to 'catchment hydrologists'?

'Fill and spill' hypothesis (Tromp van Meerveld and McDonnell, 2006 ,WRR)

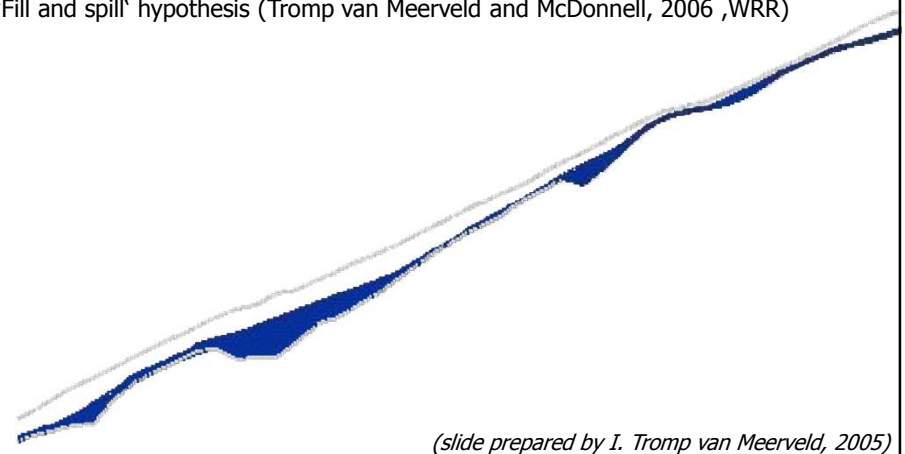

(slide prepared by I. Tromp van Meerveld, 2005)

Background – Examples – Concepts and models - Discussion

Subsurface flow at hillslope scale: preferential flow is the rule not the exception

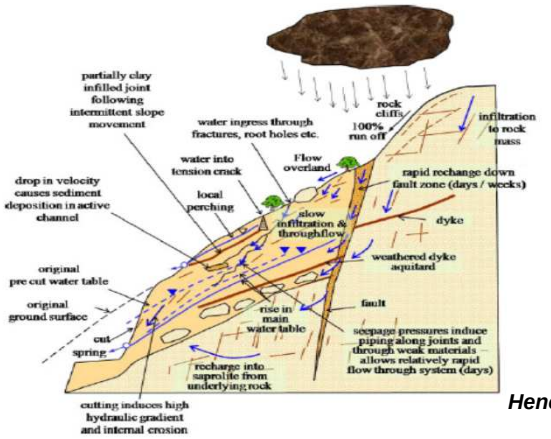

Hencher, 2010

Thom Bogaard

Subsurface flow at soil scale: preferential flow is the rule not the exception also in a 'homogeneous' soil

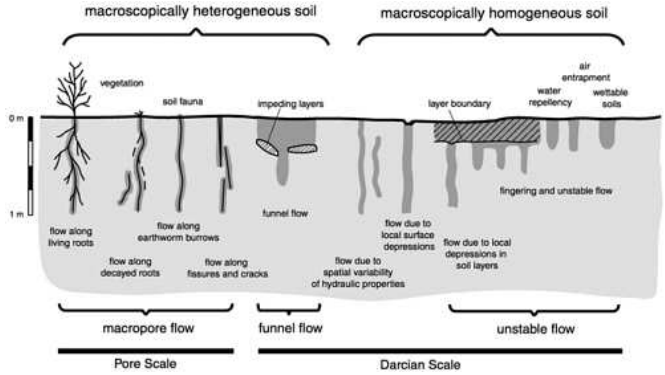

Hendrickx and Flury, 2001

Subsurface flow at soil scale: Preferential flow examples using blue dye

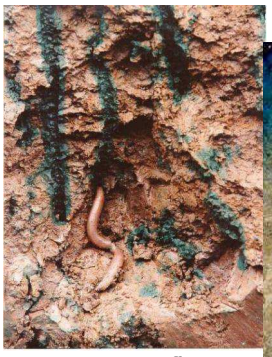

Macropore flow

Fingered flow

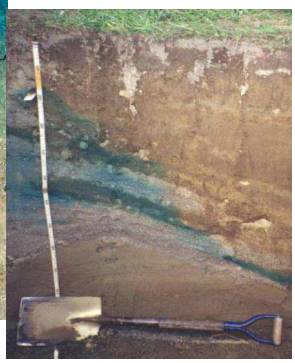

Funneled flow

Slide prepared by Loes van Schaik

From concepts to models

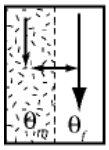

Physical deterministic

Dual permeability model

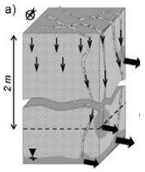

> Simplified dual permeability: PCRaster

Conceptual

Water balance in fissure

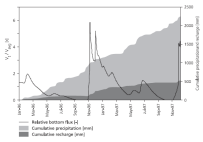

Empirical

preferential flow ~ P_{eff}, θ

Empirical

GW recharge via pref. flow ~ P_{eff} and θ

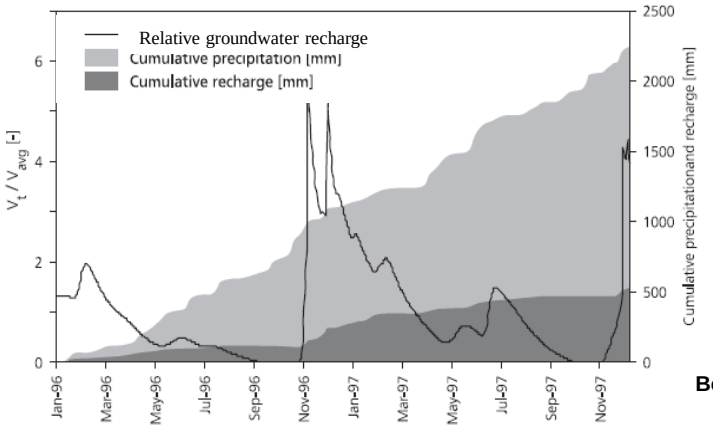

Bogaard, 2001

Dual permeability modeling in COMSOL
Testing of hypothesis, concepts

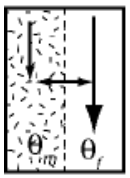

$$\begin{cases} \left[C_f(h_f)+S_e(h_f)S_s\right]\dfrac{\partial h_f}{\partial t}=\nabla\left[K_f(h_f)\left(\nabla h_f+1\right)\right]-\dfrac{\Gamma_w}{w_f} \\ \left[C_m(h_m)+S_e(h_m)S_s\right]\dfrac{\partial h_m}{\partial t}=\nabla\left[K_m(h_m)\left(\nabla h_m+1\right)\right]+\dfrac{\Gamma_w}{w_m} \\ \Gamma_w=\alpha_w\dfrac{K_f(h_f)+K_m(h_m)}{2}(h_f-h_m) \end{cases}$$

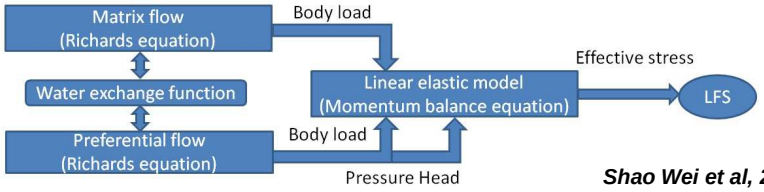

Shao Wei et al, 2013

Dual permeability modeling in COMSOL
Testing of hypothesis & concepts

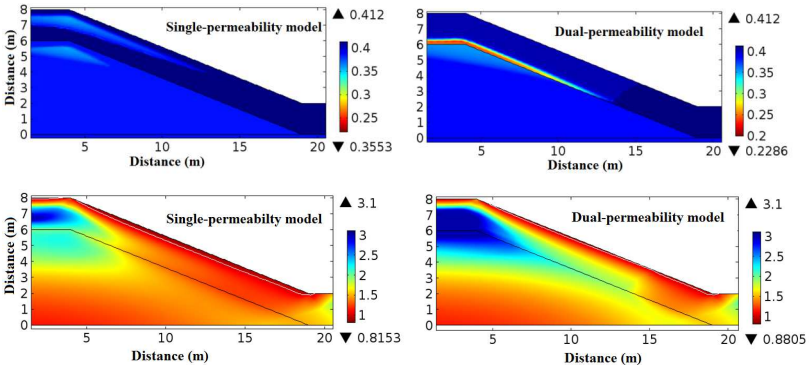

Shao Wei et al., 2013

Open question: Which system is determining the slope pore water pressure at the slipsurface? Preferential or matrix system?

From concepts to models

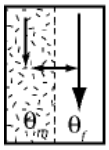

Physical deterministic

Dual permeability model

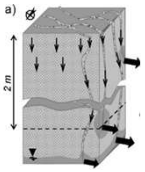

Simplified dual permeability: PCRaster

Conceptual

Water balance in fissure

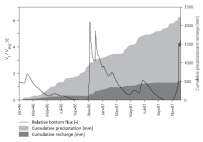

Empirical

preferential flow ~ P_{eff}, θ

Coupled hydrological systems: fissure water balance

Varved clays: (refilled) fissures act as storage and transfer pathway

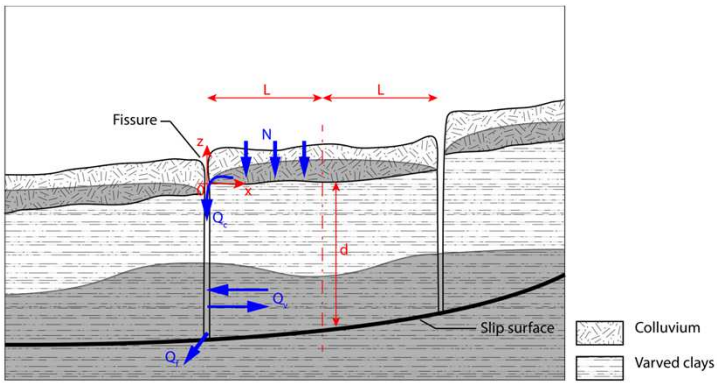

Van der Spek et al. 2013. HESS

Coupled hydrological systems: fissure water balance

How does pore pressure develop in a varved clay landslide?

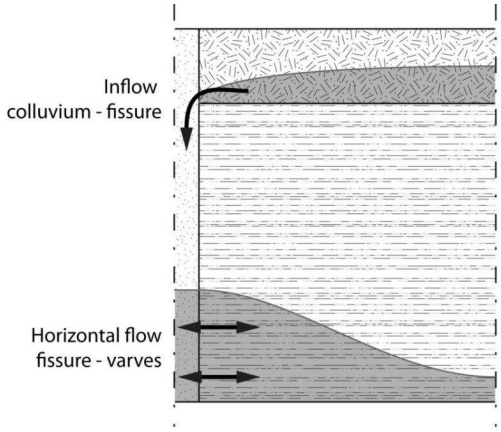

Two subsystems:

- Varved clays
- Colluvium
- Connected by fissure

Van der Spek et al. 2013. HESS

Background – Examples – Concepts and models - Discussion

Results

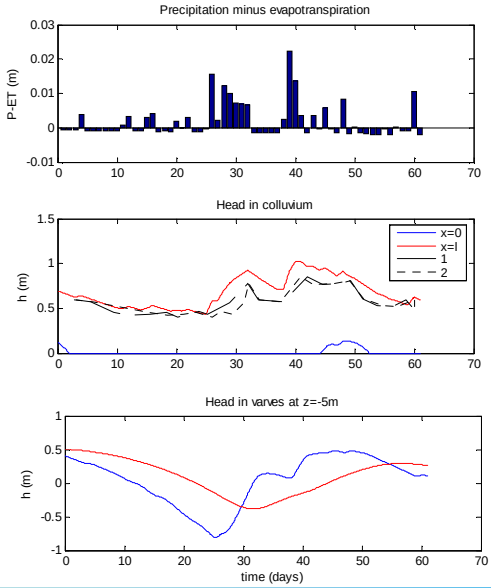

Calibration on La Mure landslide (fissure depth 5m, L=5m)

Colluvium

X=L; Halfway 2 fissures in varve

X=0; Fissure/Varve boundary

Varve

Van der Spek et al. 2013. HESS

Thom Bogaard

Results

Colluvium

Varve

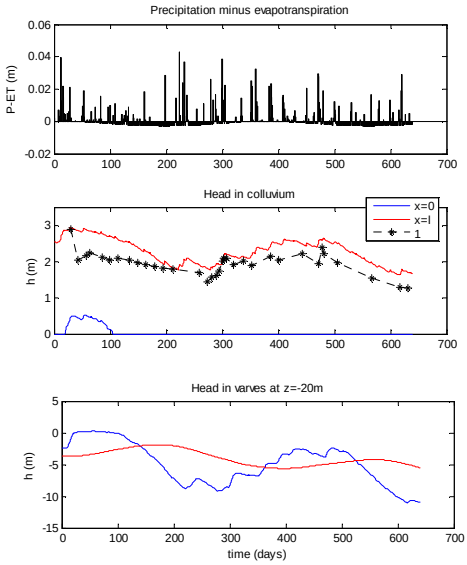

Calibration on Avignonet landslide (fissure depth 20m, L=20m)

X=L; Halfway 2 fissures in varve

X=0; Fissure/Varve boundary

Van der Spek et al. 2013. HESS

Background – Examples – Concepts and models - Discussion

From concepts to models

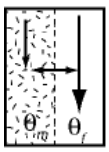

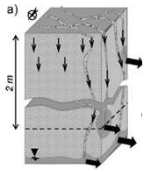

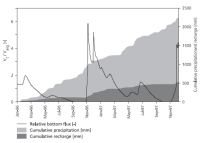

Physical deterministic

Dual permeability model

> Simplified dual permeability: PCRaster

Conceptual

Water balance in fissure

Empirical

preferential flow ~ P_{eff}, θ

Thom Bogaard

Sprinkling and geophysical experiments at Super-Sauze mudslide

Sprinkling tests using water and chemical tracers, 2D ERT

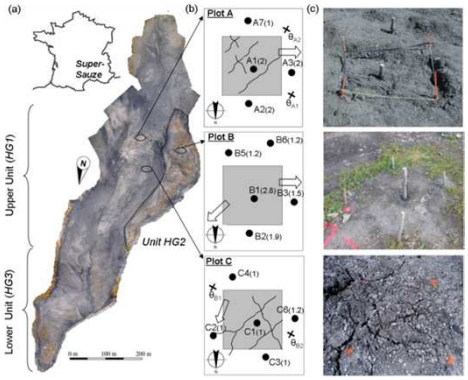

Krzeminska et al. (ESurfD_D, 2014 in review), Debieche et al. 2012 (HP), Grandjean et al, 2012 (HP), Traveletti et al, 2012 (HP)

Thom Bogaard

Background – Examples – Concepts and models - Discussion

Spatial distribution of hydrological processes

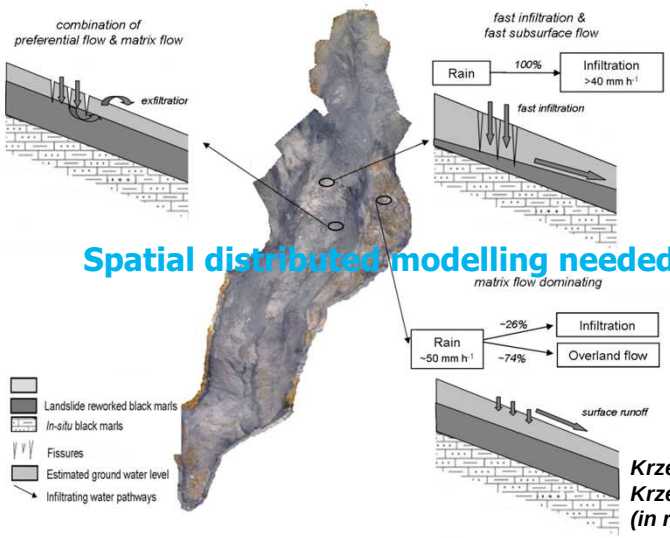

Spatial distributed modelling needed…

Krzeminska et al, 2013
Krzeminska et al, 2014 (in review)

Thom Bogaard

Simplified dual permeability in STARWARS

Spatially-distributed hydrological-stability model extended with fissure flow (Van Beek, 2002)

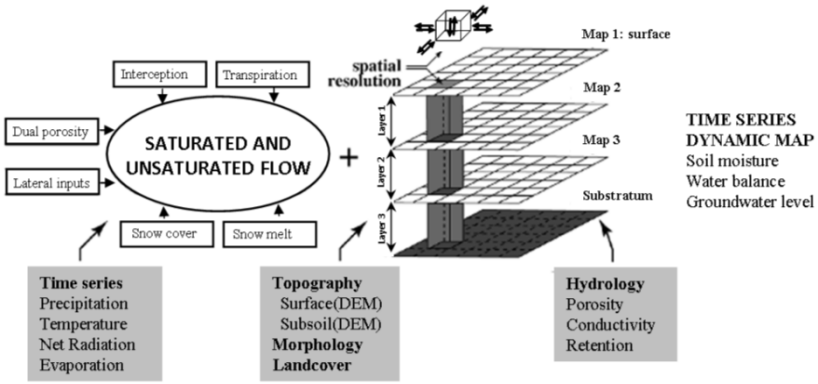

Van Beek, 2002;
Krzeminska et al. (2013, HESS)

Simplified dual permeability in STARWARS

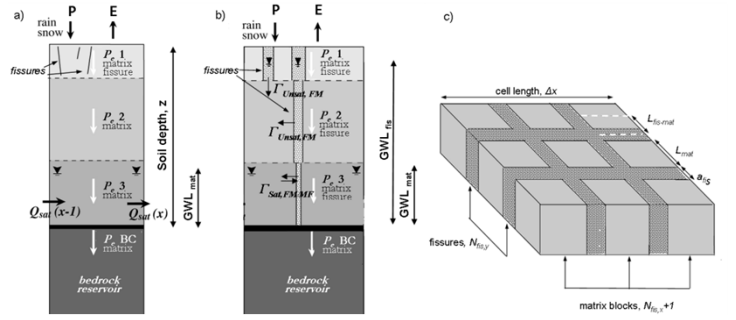

FISSURES

Highly pervious zones: Characterized by mean aperture, distribution and lateral connectivity.

No lateral exchange between unsaturated fissures and matrix.

Lateral exchange between fissure and matrix based on potential distribution.

Krzeminska et al. (2013, HESS)

To make it more complex… the landslide is moving!

Traveletti et al. 2010

Simplified dual permeability in STARWARS + dynamic fissure feedbacks

Relationship Factor of Safety with Fissure density

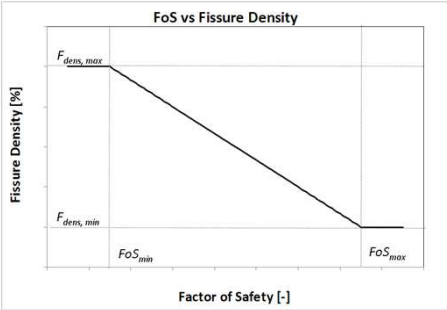

Mapping, lab tests

Relationship between soil moisture content and Fissure Connectivity

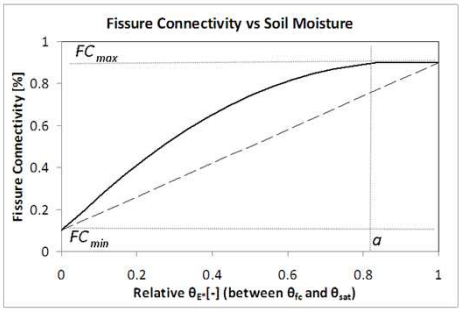

Sprinkling tests

Krzeminska et al. (2013, HESS)

Results: model runs using synthetic geometry

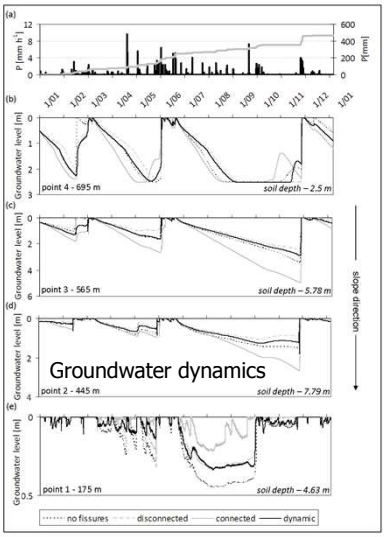

INFLUENCE OF FISSURES – dynamic approach
An example of hydrological feedback between fissure connectivity and soil moisture content

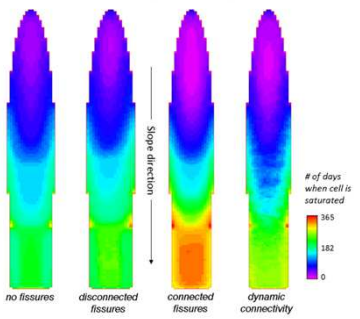

Number of days of saturation

Krzeminska et al. (2013, HESS)

To conclude and discuss…

Preferential flow rules
- both fast infiltration & drainage
- is dynamic, spatially distributed
- links to displacement which feeds back to soil hydraulic properties

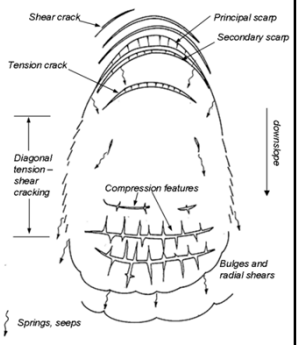

-> Does this means we have to built more complicated models?
No, it means we have to look for the right level of simplification (Zehe and Sivapalan, 2009)

To conclude and discuss…
Where does geophysics comes in?

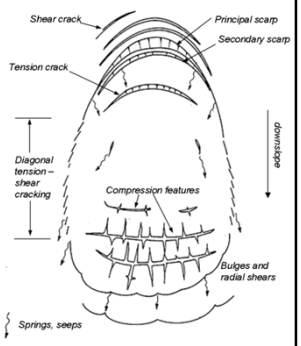

Preferential flow rules
- both fast infiltration & drainage
- is dynamic, spatially distributed
- links to displacement which feeds back to soil hydraulic properties

-> Does this means we have to built more complicated models?
No, it means we have to look for the right level of simplification (Zehe and Sivapalan, 2009)

Landslide hydrology: outlook

Cross-disciplinary and multi-technological

HYDROLOGICAL PROCESSES
Hydrol. Process. 26, 2067–2070 (2012)
Published online in Wiley Online Library
(wileyonlinelibrary.com) DOI: 10.1002/hyp.9454

Preface

Hydrological behaviour of unstable clay-shales slopes: the value of cross-disciplinary and multitechnological research at different scales

Bogaard, Malet, Schmittbuhl, HP, 2012

Engineering Geology 128 (2012) 1
Contents lists available at SciVerse ScienceDirect
Engineering Geology
journal homepage: www.elsevier.com/locate/enggeo

'Integration of technologies for landslide monitoring and quantitative hazard assessment'

Malet and Bogaard, Engineering Geology 2012

Landslide hydrology

Hydrology in hillslopes is more than water infiltration and water pressure distributions. The reality is much more complex and still too poorly understood and quantified.

- The influence of preferential flow paths, feedbacks with displacement
- The quantification of the origin of water in a slope section
- The exact role of vegetation on the water balance of a slope

Thom Bogaard

DGG-Kolloquien
1988 - 2014

1988	Köln	Feldtechniken in der Landseismik
1989	Stuttgart	Unterstützung der seismischen Interpretation durch Bohrlochmessungen
1990	Leoben	Umweltgeophysik
1991	Bochum	Integrierte Interpretation in der Angewandten Geophysik
1992	Leipzig	Ingenieurgeophysik
1993	Kiel	Ausgewählte Themen aus der Marinen Geophysik
1994	Münster	Nichtseismische Verfahren in der Angewandten Geophysik
1995	Hamburg	Geophysikalische Bohrlochmessverfahren
1996	Freiberg	Fernerkundung - Remote Sensing
1997	Potsdam	Kolloquium ersetzt durch den "Internationalen Tag"
1998	Göttingen	Angewandte Geothermie
1999	Braunschweig	Satellitengeophysik
2000	München	Magnetik
2001	Frankfurt	Interpretation reflexionsseismischer Messungen
2002	Hannover	Neue Aspekte der Explorations- und Produktionsgeophysik
2003	Jena	Interdisziplinärer Einsatz geophysikalischer Methoden
2004	Berlin	Aerogeophysik
2005	Graz	Geophysik zur Vorerkundung von Tunneln
2006	Bremen	Georadar
2007	Aachen	NMR
2008	Freiberg	Geophysikalisches Monitoring
2009	Kiel	Polare Geophysik
2010	Bochum	Entwicklung geophysikalischer Messgeräte
2011	Köln	Induzierte Seismizität
2012	Hamburg	Angewandte Gesteinsphysik
2013	Leipzig	Stimulation & Fracking
2014	Karlsruhe	Geohazards – Landslides